Extreme Design Events of Non-Gaussian Stochastic Processes

by

Samuel J. Edwards

A dissertation submitted in partial fulfillment
of the requirements for the degree of
Doctor of Philosophy
(Naval Architecture and Marine Engineering)
in The University of Michigan
2021

Doctoral Committee:

Professor Armin W. Troesch, Co-Chair
Associate Professor Matthew Collette, Co-Chair
Assistant Professor Yulin Pan
Associate Professor Seymour Spence

Samuel J. Edwards
sjedw@umich.edu
ORCID iD: 0000-0002-7512-1742

To my family,

Acknowledgments

When I look back on my eight years at the University of Michigan, I can't help but think of how lucky I am. Sure, the football team didn't win a Big Ten championship during my time here and my last 1.5 years were interrupted by a pandemic but alas, the connections I've made here and the opportunities the university has provided have been life changing.

I would like to start off by thanking my family and friends for the continual support and laughs throughout the years. You all have motivated me to keep going and to work harder. I would like to give a special thanks to my parents for always being there for me and encouraging my many interests.

My co-chairs Professor Armin Troesch and Professor Matthew Collette have been instrumental in my development as a student and researcher. I regret not being able to spend hours in Professor Troesch's office discussing new and exciting ideas due to the pandemic but I am thankful for his flexibility and ideas over Zoom. I am very thankful for the willingness to help and focus on academic skill development from Professor Collette.

I would also like to thank my committee members Yulin Pan, Seymour Spence, and the late Charlie Doering. I appreciate your input, flexibility, and the collaboration we were able to have.

All of the staff in the NAME department deserve my thanks as well for their desire to help and making things simple so that I only really had to focus on schoolwork and research.

I would also like to acknowledge the support by the Office of Naval Research (ONR) through the Probabilistic Assessment of Design Events for Complex Systems Subject to Stochastic Input project (program manager Kelly Cooper) and the SMART scholarship.

Table of Contents

List of Figures

List of Tables

Abstract

The nature of the ocean is chaotic and, as a result, marine structures face extreme, non-linear load effects. It follows that the prediction of these rare events is a challenge. Attempts to predict extreme loads on offshore structures are generally probabilistic in nature. These purely probabilistic approaches involve a considerable amount of conjecture when enforcing distributions to the process and deciding which single probability of exceedance is suitable. In an attempt to remove these conjectures, a method is developed and proposed in this thesis. Employing the known extreme Gaussian behavior as a foundation, non-Gaussian processes with Gaussian input are transformed into the Gaussian space where extreme characteristics and realizations of extreme events of the transformed non-Gaussian process are produced. This thinking is first applied in the Stochastic Gaussianization Iteration Method (SGIM) where a Gaussian transform is applied to the non-linear process of interest to use Gaussian extreme event prediction tools. The progress and development of this method is discussed and applications in predicting extreme accelerations in hull slamming and estimating extreme tower base bending moments in offshore wind turbines will be shown.

The SGIM provided the platform for the key method developed in this dissertation: the Matched Upcrossing Equivalent Linear System (MUELS) method. In the MUELS method, the Design Loads Generator (DLG) runs through linear systems that share a mean-upcrossing period with the non-linear system of interest. The DLG provides an ensemble of input time series realizations that lead to extremes of said linear systems, which can then be used as input into the non-linear system of interest. The development of the MUELS method with subsequent applications follow in this dissertation. It is shown that the MUELS method can estimate extreme characteristics, most notably extreme time series realizations, of most non-linear processes tested in this dissertation. The MUELS method also shows the capability of discovering previously unknown dynamics of a stochastically forced Duffing

oscillator.

Chapter 1

Introduction

1.1 Estimation of Extreme Ocean Events

The stochastic nature of the ocean environment leads to rare events that are unpredictable in both timing and magnitude. It follows that improving models and methods to aid in the prediction of extreme event characteristics is a wide and active area of research. Over the years, many different methods and techniques have been developed which approach these problems in a variety of ways. Of course, it is impossible to perfectly model anything, and these approaches must always make assumptions to reduce the problem into a more manageable one. As these methods are further developed, the assumptions are becoming less and less restrictive.

In the marine environment, it is commonly assumed the elevation of the 1-D ocean surface can be reasonably modeled as a Gaussian process. In this dissertation, and in the other methods discussed throughout, that assumption will be kept. With the assumption of a Gaussian wave elevation, many powerful and widely accepted results can be used. In Lindgren (1972), it was found that the ensemble average of realizations containing a maximum value at time t_0 approximates the scaled autocorrelation function of the process centered at time t_0. The assumption of a Gaussian sea surface means this result can be applied to find the expected extreme wave profile for a certain exposure time. To characterize these maxima and determine the rarity, another powerful result can be taken from Rice (1944) and Leadbetter (1966). In these papers, the upcrossing rate of different levels for Gaussian processes is derived. The upcrossing rate can be used to describe how rare or extreme different levels are. It is clear that extreme events in Gaussian processes are well studied, but what about non-Gaussian processes?

Systems that operate in the marine space respond in different ways to the as-

sumed Gaussian waves. These responses, however, are not always linear and therefore may not be represented by a Gaussian distribution. How, then, can the extreme and rare events be determined? The first instinct to estimate extreme responses of ocean structures may be to apply the corresponding extreme wave in the specified time period. Often times this does not produce the corresponding extreme response due to the complexity of the structure and how it responds to different excitation frequencies. The complexity is sometimes simplified by entering the probability domain and estimating extreme loads using Extreme Value Theory. For non-Gaussian, and often times not closed form, probability distributions, it follows that for extreme loads, the tail of the distribution must be known. When probability distribution functions are generated from collected data, probabilities of extreme events are often unknown. Hence, tail extrapolation is often used where a curve is fit to the pdf or cdf near large values so that the large, extreme values have an estimated probability associated with them. The fitted tail has no real physical basis and is purely mathematical so it is difficult to say which fit curve or line best represents the real system.

1.2 Objective of Current Research

The objective of this research is to provide a tool to aid in the estimation of extreme characteristics of non-linear systems through a physics-based model approach. In particular, the research in this thesis is meant to rapidly produce ensembles of short time series realizations of extreme values as well as the inputs that led to those extremes using the Design Loads Generator (Alford, 2008, Kim, 2012). These inputs are extremely valuable for investigating the behavior of an entire system when a particular degree of freedom is undergoing an extreme event. While the Design Loads Generator (DLG) was developed for linear system with Gaussian input, non-linear applications of the DLG have been researched and developed in Kim (2012), Seyffert (2018). In both of these approaches, a linear related process was used as a sort of surrogate for the non-linear process of interest e.g., relative velocity used for hull slamming. In Seyffert (2018), the surrogate process is further developed to investigate combined loading based on the combination property of these (possibly independent) Gaussian surrogate processes.

The research presented in this thesis continues the development of the DLG, specifically for non-linear processes. It has been shown in Kim (2012), Seyffert (2018)

that the surrogate approach is effective and powerful. That being said, what if knowledge of non-linear process of interest is incomplete? In this dissertation, a surrogate searching tool called the Matched Upcrossing Equivalent Linear System (MUELS) method using the DLG is developed and applied.

While a Monte Carlo approach remains a valid technique for studying non-linear systems, the computational cost for extremely rare events is usually prohibitive. With the MUELS method, a large quantity of conditional extreme time series realizations of shorter length i.e., 100 seconds or less, can be produced and used to study the response of a system during an extreme event. The rapidity and flexibility of this method are huge advantages and allow for interesting studies from both academic and design standpoints. The MUELS method has the capability to estimate extreme inputs to various non-linear systems, including "black box" systems where the model may be unknown.

1.3 Literature Review

1.3.1 NewWave

NewWave theory was introduced in Tromans et al. (1991) as an approach to generate extreme responses using the most probable wave profile surrounding an extreme crest. The wave profile is described as in Equation 1.1:

$$\eta^* = \alpha\rho(\tau) + g(\tau) \tag{1.1}$$

where α is the crest height, $\rho(\tau)$ is the auto-correlation function of the wave elevation, and $g(\tau)$ is a Gaussian process with zero mean and standard deviation that changes from zero at the extreme crest to the standard deviation of the wave field at a certain distance away from the extreme crest.

NewWave was developed into Constrained NewWave in Taylor et al. (1997). In Constrained NewWave, the essential idea is inserting the NewWave profile into a random realization of the wave elevation so that the system has a load history before interacting with the extreme wave train. The addition of the profile generally doesn't affect the underlying statistics of the wave elevation given the localization of the extreme crest, but could with certain conditions. Using the Constrained NewWave method, the authors found good agreement with the extreme response of a simplified jack-up platform as derived by convolving the conditional distribution of extreme

response on wave crest height and the distribution of wave crest height.

Many applications involving Constrained NewWave are from experimental setups due to the short wave elevation time series formed (Göteman et al., 2015, Hann et al., 2018, Santo et al., 2017). These experiments generally found success in estimating extreme responses using NewWave approaches. NewWave, or at least extreme response applications, is largely based on the belief that large waves lead to large responses. The search for extreme responses shouldn't necessarily be limited to these extreme waves but rather sets of waves that lead to extreme responses. The maximum wave amplitude in this set of rare waves is generally less than the extreme wave amplitude for the same exposure period. The inputs that lead to extreme responses are useful to have for study into other degrees of freedom. While there are applications that could find success with the NewWave methods, the approach for estimating these extreme responses could be viewed from the opposite perspective. Instead, the search for an ensemble of input wave profiles that lead to extreme responses could be searched for. With this approach, the statistics of other degrees of freedom during an extreme event of a particular degree of freedom could be estimated and more informed design choices could be made.

1.3.2 Linearization Techniques

The basic idea of linearization is to find a linear surrogate for a non-linear process so that linear analysis can be used. The simplest method to linearize a non-linear system[1] is shown in Equation 1.2.

$$\min_{a,b} \epsilon = g(x) - ax_0 - b \tag{1.2}$$

Here, the sum $ax_0 + b$ represents the candidate equivalent linear system involving the mean-removed system input $x(t)$ and $g(x)$ is the non-linear system of interest. The sum ax_0+b is considered an equivalent linear system given that ϵ is appropriately minimized (Roberts and Spanos, 1990). Of course, additional criteria to minimize have been discussed and studied to obtain better equivalent linear systems such as minimizing ϵ^2 or to match the root mean square between the equivalent linear system and the non-linear system of interest (Roberts and Spanos, 1990). An even more robust equivalent linear system is shown in Equation 1.3 (Roberts and Spanos,

[1]Without hysteresis effects.

1990).

$$\min_{h(u)} \epsilon = g(x) - \int_{-\infty}^{t} h(t-u)x(u)\,du + b \tag{1.3}$$

Here, the impulse response function, $h(u)$ that minimizes the difference between the equivalent linear system and non-linear system of interest is selected.

In Ismaili and Bernard (1997), these methods were applied to a two-wells Duffing oscillator under white noise forcing. The two-wells Duffing oscillator is represented by Equation 1.4.

$$\ddot{x}_t + c\dot{x}_t + k(-x_t + \lambda x_t^3) = \sigma\dot{W}_t \tag{1.4}$$

Here, c is the linear damping coefficient, k is the linear stiffness, λ is the cubic stiffness parameter, σ is the forcing coefficient, and $\dot{W}_t$ is the white noise. To obtain the minimum ϵ, a system of equations was solved to generate the equivalent linear system of the Duffing oscillator presented in Roberts and Spanos (1990), which is shown in Equation 1.5.

$$\ddot{x}_t + c\dot{x}_t + k_{eq}(x_t - m) = \sigma\dot{W}_t \tag{1.5}$$

Here, k_{eq} and m are the linearization parameters. In the application presented, the authors extended the linearization principle to account for the two domains of attraction present in the two-wells system. For a weakly forced system, the "locally" linearized method was able to recover the bimodal pdf to a good degree of accuracy. The authors also reiterated the flaws in basic linearization, namely in that linearizing a non-Gaussian, non-linear system that is forced by a Gaussian process will result in a Gaussian response. While this is addressed in Roberts and Spanos (1990) with the idea of Gaussian closure, the authors took a different approach that was more specific to the system.

Many different linearization techniques have been developed and applied over the years. The approaches to the main linearization process of non-linearly stiff systems are reviewed and discussed in Elishakoff and Crandall (2017). The authors reduce the approaches into two main camps reliant on approximations made, as shown in Equations 1.6-1.7.

$$\frac{dE}{dk_{eq}} = -2\int_{-\infty}^{\infty}[f(x) - k_{eq}x]x\psi(x, k_{eq})\,dx + \int_{-\infty}^{\infty}[f(x) - k_{eq}]^2\frac{d\psi}{dk_{eq}}\,dx = 0 \tag{1.6}$$

$$\frac{dE}{dk_{eq}} = 2\int_{-\infty}^{\infty}[f(x) - k_{eq}x]x\phi(x)\,dx = 0 \tag{1.7}$$

In both of these methods, the idea is to minimize the mean square error between the equivalent linear stiffness, k_{eq} and the non-linear stiffness, $f(x)$. As such, the expected value of the squared difference requires the pdf of the displacement, $\phi(x)$. It is here that the two methods diverge. In many situations, access to this pdf is limited. In cases where estimations to the pdf is unreliable or impossible, as in Equation 1.6, the pdf of the linearized system, $\psi(x, k_{eq})$, which also depends on the equivalent stiffness, is used. Of course, the results using Equation 1.6 are less accurate due to this but are of course easier to obtain.

In Zhang and Spanos (2020), multiple non-linear systems were linearized using a novel approach involving harmonic averaging and statistical linearization for a system that is both deterministically and stochastically forced. The authors were able to recover the magnitude of the response spectra quite well as well as the average mean square value. However, insights into the transfer function phase relationships as well as time series comparisons would be helpful for any extreme value analysis. This paper provides a solid resource for linearization, but it would be of academic and design interest to compare time series of the responses as well as extreme characteristics.

In Fujimura and Kiureghian (2007), the linearization scheme is focused on the tail of distribution of the non-linear system stochastically forced by a Gaussian process. The combinations of Gaussian random variables that define a certain response level are linearized at the most probable combination. The linearization defines the tail equivalent linear system (TELS) and can yield the response characteristics of the non-linear system through an iteration scheme using different, specified threshold levels. The tail-equivalent linearization method was also extended for multi-component systems in Broccardo and Kiureghian (2016). While this method has been shown to provide good results in predicting rare events when compared to Monte Carlo simulations, the user still must have enough knowledge of the system to choose the design points, or at least the domain of the design points.

1.3.3 FORM and SORM

First and Second Order Reliability Methods (FORM and SORM) are two techniques that can be used to estimate extreme responses. When considering Gaussian processes, the system, $R(t)$ is decomposed as:

$$R(t) = \mu(t) + \sum_{i=1}^{n} u_i s_t(t) \tag{1.8}$$

where $\mu(t)$ is a time varying mean function, u_i is a standard Gaussian random variable, $\mathbf{s}(t) = [s_1(t)...s_n(t)]$ is a vector of deterministic basis functions that depend on the process, and n is the effective resolution of the decomposition (Kiureghian, 2000).

In the non-Gaussian case, additional steps must be taken. For a non-Gaussian process excited by a Gaussian process, one possible method to determine the non-Gaussian extreme realization is to first decompose the input process as in Equation 1.8 (Grigoriu, 1995). To generate a solution, a design point, r, must first be specified. Then, the optimization problem shown in Equation 1.9 generates the most probable input that leads to an extreme output of level r.

$$\begin{aligned} &\text{minimize } \tfrac{1}{2}||\mathbf{u}||^2 \\ &\text{subject to } g_0(\mathbf{u}) = r - R(\mathbf{u}, t_0) = 0 \end{aligned} \tag{1.9}$$

Here, $\mathbf{u}$ is the vector of standard normal random variables, g_0 is the limit state surface, and t_0 is the time at which the design event will occur.

Within this optimization is where FORM and SORM diverge. In FORM, the limit state surface, g_0, is linearized at the design point $\mathbf{u}^*(r, t_0)$. The optimized response at this design point is an equivalent Gaussian response with a probability of exceedance of:

$$P(R(t_0) \geq r) = \Phi(-\beta(r, t_0)) \tag{1.10}$$

$$\beta(r, t_0) = ||\mathbf{u}^*(r, t_0)|| \tag{1.11}$$

where β is the distance from the origin to the hyperplane created by the linearization and also known as the reliability index. It should be reiterated that the linearization of the limit-state surface results in the set of input components that lead to an extreme event for an equivalent Gaussian response. Of course, the response that is used is the result of inputting the optimized components, $\mathbf{u}^*$, into the non-Gaussian model, resulting in an "extreme" non-Gaussian event. The equivalent Gaussian response may be an acceptable approximation for the non-Gaussian response, such that the optimized input components lead to a non-Gaussian extreme of the desired level, but it really depends on how non-Gaussian the output is.

In SORM, a parabolic surface is fit to the limit state at $\mathbf{u}^*$. The optimized response here is not an equivalent Gaussian response, but can be represented by a 2^{nd} order polynomial of Gaussian processes.

For both FORM and SORM, it should be noted that the solution provided is the most probable one. That is to say, both FORM and SORM result in a single realization containing the most probable extreme event at the given design level.

Given the ability of FORM and SORM to produce extreme realizations of non-Gaussian processes with Gaussian input, there is a clear potential for use in the marine field. Jensen (2009) applied FORM to produce realizations of extreme mid-ship longitudinal bending moments on a container ship. The wave elevation, $H(x,t)$ was a Gaussian process and was broken down in the following form:

$$H(x,t) = \sum_{i=1}^{n} (u_i c_i(x,t) + \bar{u}_i \bar{c}_i(x,t)) \tag{1.12}$$

where $u_i, \bar{u}_i$ were uncorrelated standard Gaussian random variables and $c_i, \bar{c}_i$ were orthogonal sinusoids with coefficients proportional to the square root of the input spectrum at the corresponding frequency.

For the sake of computational efficiency when performing optimizations, the number of frequency components, n, is generally limited. A structural/hydrodynamic model was built and represented by $R(t|u_1, \bar{u}_1, u_2, \bar{u}_2, \ldots, u_n, \bar{u}_n)$. The limit surface, G, was defined as in Equation 1.13 and the reliability index, β, associated with the design level of interest, r, is given in Equation 1.14.

$$G(u_1, \bar{u}_1, u_2, \bar{u}_2, \ldots, u_n, \bar{u}_n) \equiv r - R(t_0 | u_1, \bar{u}_1, u_2, \bar{u}_2, \ldots, u_n, \bar{u}_n) = 0 \tag{1.13}$$

$$\beta = \sqrt{\sum_{i=1}^{n} (u_i^{*2} + \bar{u}_i^{*2})} \tag{1.14}$$

It should be noted that the threshold, r, can be arbitrarily chosen, but generally methods to select values of r can be employed. The underlying distribution is not always straight forward, however, and using FORM and the associated exceedance levels from different values of r to potentially develop this would be tedious. In Jensen et al. (2014), the suggestion of using FORM results and Monte Carlo simulations to inform a fit to a Gumbel distribution is made. In this case, the use of a Poisson model or order statistics is necessary which implies conditions on R. These assumptions help break down the model and allow for the use of powerful results, but ultimately limit the versatility.

As noted before, with the limited amount of frequencies, the amount of time needed to remove memory effects, t_0, must be balanced by the time it takes for a limited amount of frequency components to repeat themselves in the time domain. The limited amount of components also lead to a wave profile that is somewhat restricted in terms of expressiveness. Within the bounds of repetition, however, the solutions to Equation 1.13, $\mathbf{u}_i^*$, provide a single wave profile that can be used as input into R to produce a conditional, non-Gaussian response at the specified design level.

While the single, most probable maximum response is useful, there are many applications that require a large number of realizations at a certain design level or exposure time without making any assumptions on an extreme distribution to draw the threshold point from.

In applications of FORM by Jensen et al. (2014), the most probable wave set that leads to a predetermined extreme response, such as bending moment, is produced. While certainly useful, FORM is limited in the specification of the design level. If the distribution of the system is not well defined, the extreme value or design level cannot be found without assuming an extreme distribution. There is also the issue of having only a single realization. If multiple realizations are sought, different

predetermined values must be generated and FORM must be applied again for each value. In design, knowledge of the system's behavior in different conditions over various time horizons is necessary. To determine multiple realizations of extreme responses of a system with an unknown, non-Gaussian distribution, and therefore unknown extreme distribution, a new approach must be taken. As mentioned before, the extreme events in the Gaussian space are well-studied and mostly agreed upon. If one were to use these Gaussian-derived methods for a non-Gaussian process, the results would be unreliable. But if a rational transformation was applied to this non-Gaussian process, the results in the Gaussian space could potentially be taken advantage of.

1.4 Overview of Thesis

The research proposed in this dissertation involves using Gaussian extreme value theory and applying it to a surrogate for a non-Gaussian process with Gaussian input. First, the Stochastic Gaussianization Iteration Method (SGIM) which involves the transformation of a non-Gaussian process into the Gaussian space through the normal score transformation (Deutch and Journel, 1998, Johnson, 1987) is introduced and developed. Realizations of extreme events of the transformed non-Gaussian process are determined using the Design Loads Generator (Kim, 2012), along with the Gaussian input that leads to those extremes. The Gaussian input that led to the extreme transformed non-Gaussian events can then be used as input into the non-Gaussian process. The SGIM is developed and applied to estimate extreme characteristics of an impact oscillator as well as the bending moment of an offshore wind turbine. Limitations of the SGIM are also identified and discussed. Second, the Matched Upcrossing Equivalent Linear System (MUELS) method, which builds off of the SGIM, is introduced and developed. The MUELS method generates a set of two-parameter linear systems with the same upcrossing rate as the non-linear system of interest for a given input spectrum. These linear systems are entered into the Design Loads Generator where inputs that lead to extreme linear events are generated. These inputs from all of the candidate linear systems are then used to force the non-linear system of interest to search for an equivalent linear system best matching the extreme behavior of the non-linear system. The use of these linear systems is a different approach to linearization and is also a systematic surrogate search method. It should also be noted that the non-linear extreme behavior identified is

conditioned on the zero-upcrossing period estimated from the non-linear process as well as the input into the two-parameter surrogate process giving the largest most probable non-Gaussian maximum. Systems with unknown dynamics, like some non-stationary systems, could be investigated with this method as presented without knowledge of a surrogate that could represent the system of interest. The MUELS method is developed and applied to Duffing oscillators and the same impact oscillator as the SGIM. The objective of this research is to develop a process in which results for prediction of extreme Gaussian events can be applied to a transformed non-Gaussian process in order to identify the conditional extreme behavior of the non-Gaussian process.

Chapter 2

Background

2.1 Introduction

Methods to estimate extreme values, specifically in the marine environment, have been developed and used as the basis for new methods throughout the years. In this section, a theoretical and mathematical background is presented to better understand the advances and disadvantages of existing methods and techniques. The approaches presented below range from complete probabilistic approaches to processes that determine the most likely sea surfaces at the time of extremes.

2.2 (Gaussian) Extreme Value Theory

The behavior of any system can in part be described in a probabilistic sense through its probability distribution function (pdf) and consequently its cumulative distribution function (cdf). Furthermore, if multiple trials of this system in a certain state can be assumed to be independent and identically distributed (i.i.d.), the extreme value pdf or cdf for the system's behavior during said state can be described. The extreme value cdf describes the distribution of largest values out of a specified number of trials. If N trials have been observed, then the extreme value cdf, $F_e(x)$, of a process with a cdf $F(x)$ can be described as:

$$F_e(x) = F(x)^N \tag{2.1}$$

It follows that, through the chain rule, the extreme pdf is:

$$f_e(x) = Nf(x)F(x)^{(N-1)} \tag{2.2}$$

While important, these equations alone do not inform a design. From here,

assumptions and decisions must be made in terms of safety factors or how to include the chosen response level into the design with other competing factors. With the selection of a single number, the system's behavior near the extreme is missed and, if the original cdf is lacking information that was not observed, can be erroneous. There is also the issue of combining that single number with other numbers, say multiple loads, to estimate a failure event. Lastly, coming up with the exact N can be a challenge.

In Ochi (1990a), this basic theory was incorporated into estimating extreme wave amplitudes. It should be noted that it is generally considered that the instantaneous elevation of the 1-D ocean surface is narrow banded and can be defined by a Gaussian random variable and the distribution of the positive maxima of the ocean surface (e.g. the wave amplitudes,) can be described by a Rayleigh distribution with a parameter equal to the root mean square of the wave elevation. Ochi describes the pdf of maxima of the wave amplitudes in a given, not necessarily narrow banded, sea state using the following expressions:

$$f_X(x) = \frac{2}{1+\sqrt{1-\epsilon^2}}\left[\frac{\epsilon}{\sqrt{2\pi}}e^{-x^2/(2\epsilon^2)} + \sqrt{1-\epsilon^2}\,x\,e^{-x^2/2}\,\Phi\left(\frac{\sqrt{1-\epsilon^2}}{\epsilon}x\right)\right] \tag{2.3}$$

$$\epsilon = \sqrt{1-\frac{m_2^2}{m_0 m_4}} \tag{2.4}$$

$$m_k = \int_{-\infty}^{\infty} \omega^k S(\omega)\,d\omega \tag{2.5}$$

where $S(\omega)$ is the spectral density function of the given sea state, $\Phi(\cdot)$ is the cdf of the Gaussian distribution, and ϵ is the bandwidth parameter of the sea state.

From there, using Equations 2.2 & 2.3, he found that the maximum wave amplitude corresponding with the peak value of the extreme pdf, $\hat{x}$, in m cycles is the solution of:

$$\frac{1}{m} \approx 1 - F_X(\hat{x}) \text{ as } m \text{ approaches } \infty \tag{2.6}$$

Equation 2.6 describes the most probable maximum of the 1-D ocean surface in

m cycles. Note that this m characterizes the number of independent waves observed. If one were to instead begin with describing the instantaneous elevation of the ocean surface instead of the positive maxima, a different number of cycles would be used to find an equivalent most probable maximum.

It should also be noted that strictly speaking, extreme characteristics of ocean processes viewed as time series cannot be done using extreme value theory due to dependence between peaks. As such, Leadbetter and Rootzen (1988) discusses extreme value theory as related to stochastic processes taking into account dependence between peaks and changes in parameters over time.

2.3 (Non-Gaussian) Extreme Value Prediction Techniques

When a process is not so easily described by a closed form or well-known pdf, alternative methods using General Extreme Value Theory can be used. In General Extreme Value Theory, it is can be approximated that any set of random variables that are independent and identically distributed will eventually converge to one of three extreme value distributions: the Gumbel distribution, the Fréchet distribution, or the Weibull distribution.[1] From here, different methods can be used to estimate the shape parameters of one of the aforementioned distributions, as done in Razola et al. (2016). Razola et al. fit a Weibull distribution to acceleration peaks of a high speed craft model. The Weibull distribution is described by two shape parameters, a and b, and is defined as follows:

$$F(x) = 1 - e^{-(x/a)^b} \tag{2.7}$$

To determine the shape parameters for the acceleration peak process, they took samples of acceleration peaks and performed an optimization problem on the R^2 statistic. Performing the same exercise in Equation 2.6, the most probable maximum acceleration, $\hat{x}_e$, in the expected amount of cycles in a given number of cycles, n, was estimated to be:

$$\hat{x}_e = a[log(n)]^{1/b} \tag{2.8}$$

[1]Assuming that the distribution function of the random variables is max stable (Leadbetter et al., 1983).

Another fitting method for an arbitrary process is to estimate the distribution of the "tail" of the process. The positive tail of a process describes the values in the upper limit of process' distribution. Properly estimating the tail of a process is of interest because the extreme value sought is in the tail somewhere. One method to estimate the tail distribution and the most probable maximum is the Peaks Over Threshold approach. In this method, a threshold, u, is selected and the parameters of the Generalized Pareto distribution, σ and ξ, are fit to the tail through maximum likelihood estimation. It can be shown (Coles, 2001) that the cdf of the peak distribution, $F_{peaks}(x)$ and the most probable maximum in m observations, $\hat{x}_m$ are:

$$F_{peaks}(x) = 1 - (\xi_u(1 - F(x)_{POT})) \tag{2.9}$$

$$\hat{x}_m = \begin{cases} u + \frac{\sigma}{\xi}[(m\xi_u)^{\xi} - 1] & \text{if } \xi \neq 0 \\ u + \sigma log(m\xi_u) & \text{if } \xi = 0 \end{cases} \tag{2.10}$$

where $F_{POT}(x)$ is the distribution of peaks over the threshold, u, and ξ_u is the probability that any global peak exceeds u. In Michelen and Coe (2015), POT is compared with other methods, including tail fitting, in estimating the short-term extreme force on the power conversion chain of a wave energy converter. However, in the marine environment, it is often difficult to accurately estimate the tail of a distribution due to the rarity of events and changing conditions, making it difficult to justify the use of POT in conjunction with a GPD (Pipiras, 2020). Still, efforts made to describe the tail of the distribution, even in a marine environment, are made. In Belenky et al. (2019), the extreme response of a piece-wise linear oscillator, which has ship stability applicability, was investigated. The behavior of the tail was found to be dependent on various factors but was more or less defined under the set of circumstances examined in this paper. While this paper provides an excellent derivation and study, it is limited in that the solution is specific to the model and the results are not necessarily usable outside of a piece-wise linear oscillator.

While specifically estimating the tail structure can be useful, it does not give a complete picture of the system when it is experiencing an extreme event. To properly consider the failure modes of the system, the response of all (or at least related) degrees of freedom must be considered when experiencing an extreme event.

The consideration of multiple, possibly correlated, loads and responses increases the complexity even more. To simplify the issue, there are guidelines and rules that apply constant factors to loads when one specific load is considered extreme (Lloyd's Register, 2020), but even these were shown to not be reliable, mostly due to the fact that the load combination factors are static, when in reality it is more likely that they would follow a distribution (Seyffert, 2018).

The problem is that, generally, there is not enough information on the model to build out a full statistical or practical estimate of the different degrees of freedom and how they all relate. There are certainly ways to accomplish this, as in Naess (1994), but many idealizations must be made or conditions must be met, namely belonging to a certain set of oscillators and having white noise forcing. For the most part, we cannot say for certain how one degree of freedom will react when another is experiencing an extreme response. Of course, Monte Carlo simulations (MCS) can be performed to study the extreme responses. While MCS can reveal a lot about a system, they are generally time consuming. Even so, they are popular and methods to improve efficiency have been implemented. In Chai et al. (2016), an efficient MCS system was developed by understanding that the mean upcrossing rate of the system when it is in the tail of the distribution (i.e., experiencing an extreme event) is generally regular, and by fitting parameters to the equation that describes this upcrossing rate, an extrapolation on the extreme response can be performed. Techniques like this can be highly useful but are limited in that they are generally specific to the problem at hand.

In Echard et al. (2011), the Kriging method (Matheron, 1973) was combined with Monte Carlo simulations to estimate probability of failure. By using the interpolation characteristics of the Kriging method, a population of Monte Carlo points, say n_{MC}, can be classified by calling the true performance function of the system an amount of times less than n_{MC}. The iterative nature of this method involves active learning where the design of experiments, or the sampled input from the initial population of Monte Carlo simulations, is updated and improved through the Kriging method. Using this method, the authors were able to accurately estimate the probability of failure for a spring-mass-dashpot system with parameters characterized by random variables using significantly less calls to the performance function. While the initial population of Monte Carlo simulations can be updated if the probability of failure

is not sufficient, the estimation and probability of failure is still limited to what lies in that population. Any unknown or rare behavior not represented in this sampling space could be ignored leading to poor estimations.

A slightly different approach to the extreme value estimation problem is the idea of critical wave groups. In Anastopoulos and Spyrou (2019), the authors use the critical wave group approach to estimate the probability that the roll angle of a ship a greater than some critical value. Essentially, a law of total probability set up is assumed where the probability of extreme roll angles given the presence of mutually exclusive wave groups and certain initial conditions is used in conjunction with the probability that those wave groups and initial conditions actually occur. Another point of interest is the use of Markov chains to construct realistic wave groups. The Markov chain approach generates the expected wave groups with periods that exist in a range of critical periods given a sea state. The method is applied to a small ocean surveillance ship to estimate the probability of exceedance for a number of roll angle thresholds. Monte Carlo simulations were used to estimate the moderate thresholds i.e., in the linear regime, and were not used for comparison in the larger critical roll thresholds where roll is expected to be more nonlinear. In the irregular wave setup, results for the critical wave method using mean-stationary initial conditions were shown along with two other rare solution types with initial conditions. While the solutions with initial conditions appear contiguous with the Monte Carlo probability of exceedance curve, it is difficult to assess the accuracy without Monte Carlo results in the nonlinear regime.

Another method that involves special attention to the tail of the distribution is the sequential sampling strategy developed in Mohamad and Sapsis (2018). In Mohamad and Sapsis (2018), the authors use observations of the randomness and uncertainty within the model e.g., stochastic forcing or system parameters, along with observations of a response interest, which may be a mapping function based off of the randomness and uncertainty, to learn the pdf of the observation of interest. The learned pdf then uses an optimal set of inputs, or the uncertainty and randomness in the system, to minimize the difference between the learned pdf and actual pdf of the response of interest. This approach naturally provides special interest to the tails of the distribution. The method also uses a surrogate of the mapping function to reduce complexity and also does not require the actual pdf of the quantity

of interest. Instead of using the actual pdf, upper and lower confidence intervals of the surrogate mapping function are used to calculate distance from the learned pdf. Sequential samples in this fashion are used to learn more about the tail statistics of the response of interest. The method was applied to estimating the pdf of forces and moments acting on an offshore platform. After 15 iterations, the authors found good agreement between the actual and learned forcing pdfs. That being said, the least "confident" area of the learned pdf i.e., the area where there was the widest band of confidence interval, was near the tail. Again, while the hydrodynamic forcing application is a complex one, the uncertainty regarding the tail area could lead to poor estimation of extremes. In Gong et al. (2020), the sequential sampling strategy was again used to estimate extremes in a hydrodynamic context. The authors used a different objective function more focused on extreme responses as opposed to responses with low probability. The method provided an estimated extreme pdf that closely approximated the true extreme pdf.

Unlike Gaussian processes, it should also be noted that non-Gaussian processes are not stationary by default. Without the guarantee of the system of interest being stationary, prediction of extreme events and characteristics becomes much more difficult. Referring back to Leadbetter and Rootzen (1988), the main focus is on stationary processes so while it provides a good starting point, derivations made and theories stated are not directly applicable to non-stationary processes. Investigating non-stationary extremes is important to ensure safety and proper design of any structure. That being said, there may not be knowledge that the system can exhibit this type of behavior due to limited data or modeling simplifications.

In the techniques described above, a considerable amount of data and knowledge is needed to ensure good and reliable fits. While they are more flexible compared to set and assumed extreme value distributions, the computational expense may hinder design processes, especially when considering different operating conditions or cases with multiple loads that lead to failure. Furthermore, specific care and finesse must be taken to account for potential non-stationary behavior.

2.4 The Design Loads Generator

It was mentioned in Section 2.3 that the general extreme value distributions were limits and there is a possibility that either the wrong extreme distribution is chosen

or the process that is being dealt with may not even converge to one of the three types. So in lies the question: how can ensembles of extreme realizations of processes with unknown extreme distributions be generated? A major building block towards developing a technique to answer the question at the end of the previous section lies in the Design Loads Generator (DLG) ((Alford, 2008, Kim, 2012). The DLG is a tool that generates extreme realizations of a Gaussian process with a Gaussian input at the Target Extreme Value (TEV) of interest. The TEV is simply an indicator of how the magnitude of the expected maximum increases with the number of observed trials, n, is of the form:

$$TEV = \sqrt{2log(n)} \tag{2.11}$$

It can be noted that for a Gaussian process, the most probable maximum value is n cycles is the product of the TEV and the rms of the process, which is also the standard deviation, σ, in Gaussian processes. As such, in this thesis, the rarity of events will be classified according to the TEV, in the fashion of the number of standard deviations, e.g. 3σ. A 3σ event indicates a TEV of 3, which suggests an extreme event with a most probable maximum that is 3 standard deviations above the mean.

The DLG works by using creating a response spectrum[2] of the Gaussian process from an input spectrum and transfer function, and then randomly sampling phases from optimized, modified Gaussian distributions which lead to extreme values at $t = 0$ via the following equation:

$$x_0 = \sum_{j=1}^{N} a_j cos(\epsilon_j) \tag{2.12}$$

where x_0 is an extreme response, a_j are Fourier amplitudes of the response of interest, and ϵ_j are phases that are randomly sampled from optimized phase pdfs.

It should be noted that the modified Gaussian distribution for each phase ϵ_j used by Alford was:

[2]Note that for each frequency component, the response spectrum $S_R(\omega_i j = \frac{a_j^2}{2d\omega}$. The vector $\mathbf{a} = [a_1, \ldots, a_N]$ populates the same coefficients in Equation 2.12.

$$f_{\epsilon'_j}(z) = \frac{1}{\lambda_j\sqrt{2\pi}}e^{-z^2/2\lambda_j^2} + \frac{1}{2\pi}(1 - erf(\frac{\pi}{\lambda_j\sqrt{2}})) \tag{2.13}$$

where each λ_j was a variable to be solved for. Here, the distributions of the phases were said to be independent but not identically distributed due to the λ_j parameter.

To find the parameters of the modified Gaussian distribution, λ_j, Alford equated the pdf of the random variable shown in Equation 2.12, which is a summation of modified Gaussian pdfs with different parameters λ_j, to that of the extreme Gaussian distribution. In the pdf space, however, this is a daunting task. Instead, Alford moved into the characteristic function space where she was left with the following equation to be solved:

$$\int_{-\infty}^{\infty} \frac{m}{\sigma\sqrt{2\pi}}e^{isx}e^{-x^2/2\sigma^2}(\Phi(\tfrac{x}{\sigma}))^{m-1}\,dx =$$
$$\prod_{j=1}^{N}\int_{-1}^{1} e^{ia_j sy}\frac{\sqrt{2\pi}e^{-(arccos\,y)^2/2\lambda_j^2} - \lambda_j erf(\frac{\pi}{\lambda_j\sqrt{2}}) + \lambda_j}{\pi\lambda_j\sqrt{1-y^2}}\,dy$$

where m is the number of cycles in the specified time period and σ is the standard deviation of the process.

Still left with N unknowns, a subplex optimization was introduced with the cost function, f, chosen as:

$$f = \sum_{k=1}^{N_s} |\psi_{x_m}(s_k) - \prod_{j=1}^{N}\psi_{Y_j}(s_k)| \tag{2.14}$$

where $\psi_P(s_k)$ is the characteristic function of pdf, P = theoretical extreme Gaussian (x_m) or modified Gaussian (Y_j), at s_k and N_s is the number of discrete values of s that were used.

After the optimization, the phase pdfs Alford came up with did not quite line up with those of the theoretical extreme Gaussian distribution. In Kim (2012), Kim introduced a standard Monte Carlo rejection sampling scheme of the phase modified Gaussian distribution, which he called the Acceptance-Rejection Algorithm. The algorithm improved upon the discrepancy between the theoretical extreme Gaussian distribution and the extreme distribution from the optimization of phase sets.

To increase the DLG's versatility in predicting extreme responses, in Seyffert (2018), the idea of surrogate processes was introduced. As mentioned before, the DLG provides ensembles of realizations of extreme *Gaussian* processes. The entire solution structure of the DLG is geared towards Gaussian processes and so it cannot reliably produce extreme realizations of extreme non-Gaussian processes. However, there are Gaussian processes that can be considered "indicators" for extreme non-Gaussian processes. Seyffert considered a failure surface which is a function multiple non-linear processes, which are transformations of a linear, Gaussian input. The "indicator" linear functions, which are also Gaussian and linear functions of the input, that best define each of the non-linear processes can be considered in a weighted sum and a new linear process is formed. The weighted sum can be used to explore the failure space, determine different maxima clustering configurations, and how it all impacts system failure.

To continue the expansion of the DLG into the non-Gaussian, non-linear domain, the idea of moving those non-Gaussian, non-linear processes into the Gaussian domain is explored.

Chapter 3

Building Blocks

3.1 Introduction

In this section, the development of the Stochastic Gaussianization Iteration Method (SGIM) is discussed along with applications. The SGIM is a major building block in developing the method detailed later in this thesis. It is important to detail the structure and application methods of the SGIM to provide a foundation for the method discussed later.

First, the methodology behind the SGIM is described. Second, a study testing the limits of the SGIM is performed using a Duffing oscillator to toggle the non-linearity (and non-Gaussianity) of the system. Third, two applications of the SGIM will be presented in which differing levels of non-Gaussianity are displayed: determining extreme acceleration characteristics near hull slams; and developing wind and wave environments that lead to extreme tower base bending moments in an offshore wind turbine. The results in the hull slamming application have been published and presented in the Practical Design of Ships and Other Floating Bodies (Edwards et al., 2019b) and the results in the offshore wind turbine tower base bending moment have been published and presented in OCEANS (Edwards et al., 2019a).

3.2 The Stochastic Gaussianization Iteration Method

In the marine environment, different reactions and relationships between forces or degrees of freedom may lead to responses that are highly non-Gaussian and/or non-linear. Many analyses rely on a linear transfer function between the (assumed) Gaussian wave elevation and the resulting Gaussian output. While these assumptions may be valid for some cases, they simply cannot provide meaningful results when discussing these highly non-Gaussian, non-linear (NGNL) responses. This is

unfortunate, as the methods developed to estimate extreme responses of Gaussian processes with Gaussian input have proven to be powerful. As mentioned in Section 2.4, the use of surrogate processes may be a solution. But, when there is not a clear and/or highly correlated "indicator" function, an alternative method must be taken to estimate realizations of non-Gaussian extreme events. To take advantage of the proven Gaussian process extreme response prediction methods in the NGNL domain, the Stochastic Gaussianization Iteration Method (SGIM) was developed.

The SGIM is an iterative process which relies on the normal score transformation and the Design Loads Generator (DLG). The normal score transformation is a one-to-one mapping of the non-Gaussian random variable to a Gaussian random variable in the probability space. In the normal score transformation, the cdf of a random variable is used to transform said random variable into a Gaussian random variable as shown below:

$$\begin{aligned} Y: &= F_X(x) \rightarrow \\ F_Y(y) &= P(Y \leq y) = P(F_X(x) \leq y) = \\ P(X \leq F_X^{-1}(y)) &= F_X(F_X^{-1}(y)) = y \rightarrow \\ F_Z(z) &= F_Y(y) = y \\ z &= F_Z^{-1}(y) \\ z &= \mu + \sqrt{2}\sigma erf(2 * y - 1) \end{aligned}$$

where X is the random variable of interest, Y is a uniform random variable, and Z is a Gaussian random variable with mean, μ and standard deviation σ. In the following studies and applications, the standard Gaussian random variable ($\mu = 0, \sigma = 1$) was used. The intermediate step of transforming X into a uniform random variable, Y, is shown to better illustrate how the normal score transformation can be repurposed as a simple inversion sampling scheme with an initial transformation.

This technique can be used as a sampling scheme to transform a non-Gaussian random process into a pseudo-Gaussian process. The "pseudo" tag is used here because while the transformed process has a Gaussian distribution, it is not necessarily a true Gaussian process. It is difficult to say if the transformed process is a Gaussian process due to the implicit nature of the transformation and the fact that the cdf of

the non-Gaussian process is a spline generated using a computer. The spline is a fit to the distribution of the non-Gaussian process and therefore once the gaussianization is applied, the estimation involved in the distribution fitting leads to a realization of a process that is not purely Gaussian, but reasonably close enough to call it a pseudo-gaussian process. Going forward, however, the transformed pseudo-gaussian process will be treated as a Gaussian process for use in the DLG.

As mentioned in Section 2, the DLG is a tool that generates an ensemble of extreme realizations of a Gaussian process. For use in the SGIM, the DLG provides extreme realizations of the pseudo-gaussian process as well as the input that leads to each extreme realization. These inputs are valid realizations of the input spectrum and can be used as input into the non-Gaussian model. The resulting non-Gaussian outputs are conditioned on the previous pseudo-gaussian process being extreme. These conditioned non-Gaussian outputs belong to the set $\Omega = \{\omega : X'(\omega)_{i+1,NG} | X(\omega)_{i,G} \geq \hat{X}_{i,G}\}$ where the subscript NG identifies X as a non-Gaussian time series, the subscript G identifies a Gaussian time series, and $\hat{X}_{i,G}$ is some minimum threshold for the TEV of iteration i. The non-Gaussian time series of iteration $i+1$ are conditioned on the Gaussian time series of iteration i being extreme realizations at iteration i. The inputs that lead to the extreme pseudo-gaussian events are simply a function of said pseudo-gaussian events, and the set Ω can be alternatively represented as $\Omega = \{\omega : X'(\omega)_{i+1,NG} | z_{i,G}(t) \in Z_{i,G}\}$ where $z_{i,G}(t)$ is a realization of the input that leads to an extreme value in the Gaussian space on iteration i and $Z_{i,G}$ is the set containing all such realizations. By gaussianizing the non-Gaussian outputs again, transfer functions between the now Gaussianized outputs and the inputs that led to the previous pseudo-gaussian extremes can be generated, averaged over the ensemble, and put into the DLG, forming an iteration scheme. It is possible that the continued iterations will result in overlap between realizations in the set $Z_{i,G}$ and the set Z_{NG}, which contains all realizations of input that lead to extreme non-Gaussian events in the given exposure period. The iterations continue until a level of convergence is reached, either with a known extreme non-Gaussian cdf or when the extreme cdf between iterations does not change. The process is further outlined in the flowchart shown in Figure 4.2.

The idea here is that by continuing to effectively condition the current non-Gaussian simulation on the previous pseudo-gaussian simulation being extreme, the

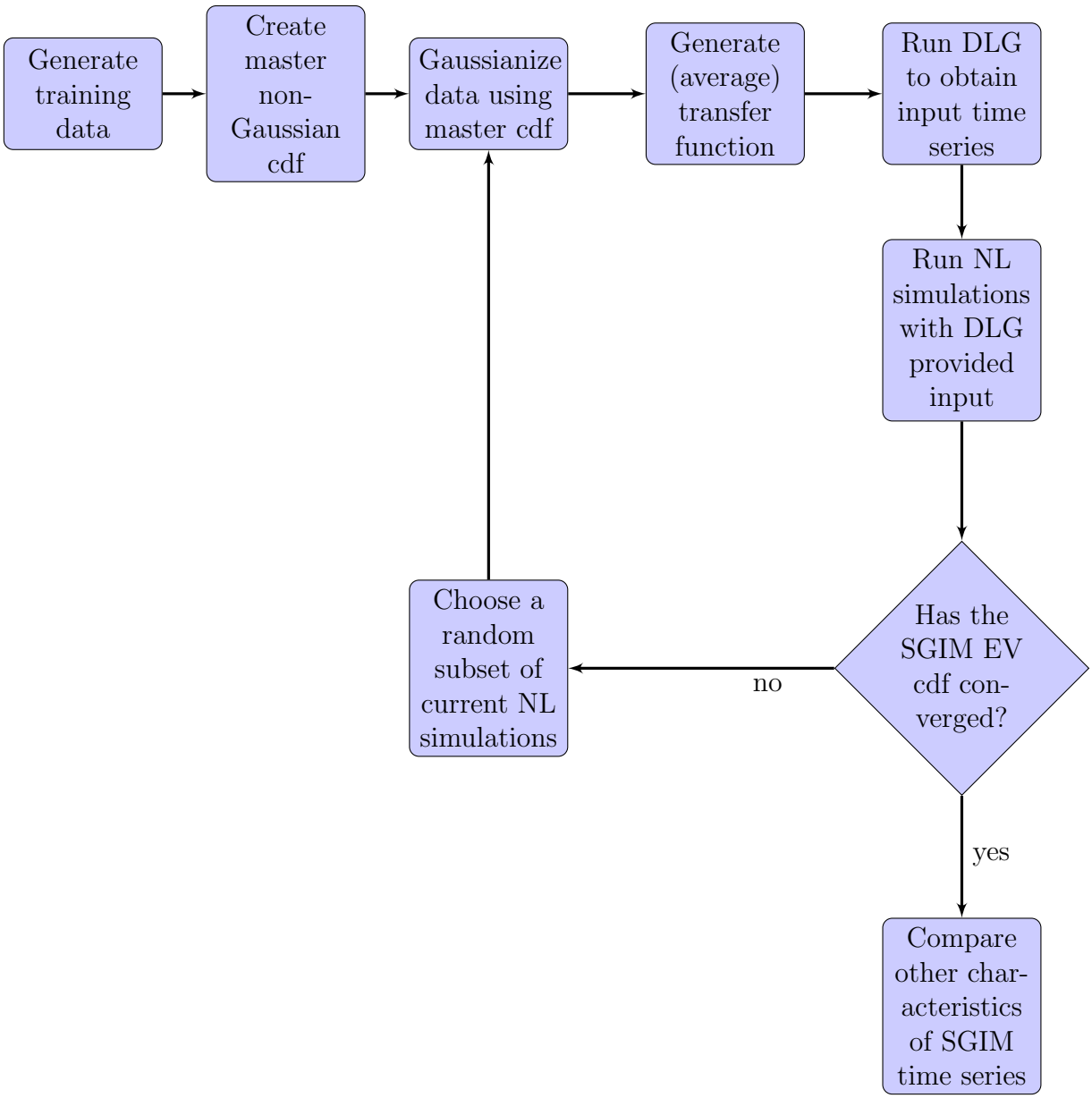

Figure 3.1: The Stochastic Gaussianization Iteration Method (SGIM) flowchart

non-Gaussian extreme cdf will be recovered. Since there is a one-to-one probability mapping between the non-Gaussian process and the Gaussianized process, there is potential for the conditional non-Gaussian process to converge with the extreme non-Gaussian process. Of course, since the model and the Gaussianized transfer function have different phase relationships with the input, there is no guarantee that the convergence will occur. There is also the fact that when the transformation occurs, it is unknown how the time scales change. When entering the DLG, a target extreme value (TEV) is required. The TEV, in the Gaussian space, is entirely dependent on the amount of cycles expected in the exposure time (Equation 2.11). It is not clear how the exposure time changes when moving from the non-Gaussian space to the Gaussianized space. As a result, there is additional uncertainty added each iteration.

There are alternative ways to recover a non-Gaussian extreme cdf, but in this method, an unlimited amount of realizations of the non-Gaussian extreme cdf will be accessible without making assumptions about the time between peaks or the behavior of the process leading up to and following the extreme response. For use in applications that require additional information about the process near the extreme, this is clearly important. While the information near extremes could be collected in Monte Carlo simulations, the SGIM has the potential to reduce run time and change exposure time on the fly.

3.3 The Duffing Oscillator: A Variable Non-Linear Test for the SGIM

Given the analytical nature of the SGIM, the allowable non-linearity/non-Gaussianity in which the SGIM will eventually recover the extreme cdf is unknown. To begin to explore this limit, a well studied non-linear model with the ability to toggle the amount of non-linearity in the system was required. The Duffing oscillator, which is represented by Equation 3.1, was chosen as it is a well studied problem with marine applications (Naess (1994)) and the non-linearity in the system can be easily changed by altering the value of the β parameter.

$$\ddot{x} + \delta\dot{x} + \alpha x + \beta x^3 = gE(t) \tag{3.1}$$

where δ is the effective linear damping constant, α is the effective linear stiffness constant, β is the cubic stiffness constant, g is a scaling factor to match the rms of the excitation to that of a unit amplitude sine wave, and $E(t)$ is the excitation time

series and is drawn directly from an ITTC wave spectrum (ITTC, 2002).

In the study, Duffing oscillators with various β values underwent waves from an ITTC spectrum. Note that realizations of the ITTC spectrum are Gaussian and since any linear combination of Gaussian processes is Gaussian, the input $E(t)$ is a Gaussian process. Table 3.1 lists the parameters of the system and the input spectrum.

Parameter	**Value**
δ	0.1
α	1
g	$\sqrt{2}$
H_s	3
T_m	$\frac{4\pi}{3}$

Table 3.1: Parameters used for the Duffing oscillator SGIM study along with the parameters used for the ITTC spectrum. Note that all parameters are dimensionless for simplicity.

The β values selected for these analyses were 0.00, 0.01, 0.04, and 0.08. The β value of 0.00 results in a linear, Gaussian Duffing oscillator and served as a control for the study. It also served as an "identity test" for the SGIM as a process; that is to say, given the ability of the DLG to provide extreme realizations of Gaussian processes, a Duffing oscillator with $\beta = 0.00$ in the SGIM should provide convergence, as it would without the use of SGIM, due to the DLG.

To test the limits of the SGIM, the extreme value cdf from the method was compared with that of 500, 7000 s Monte Carlo simulations for each β case. In the SGIM, 500, 500 s realizations of extreme pseudo-gaussian events were produced each iteration and 50 of those realizations were used to generate a new transfer function for the following iteration. To decompose the Gaussianized response and the associated input time series, a combination of *MATLAB*'s Welch's (Welch (1967)) power spectral density estimate function, `pwelch`, and the Fast Fourier Transform function, `fft`, was used with default parameters. The relationship, described by Equation 3.2, between the response spectrum, input spectrum, and transfer function was used to estimate the transfer function for use in the DLG.

$$S_{out}(\omega) = |H(\omega)|^2 S_{in}(\omega) \tag{3.2}$$

Here, $S_{out}(\omega)$ is the response spectrum as a function of radial frequency, ω, $H(\omega)$ is the transfer function, and $S_{in}(\omega)$ is the input spectrum. The SGIM was continued

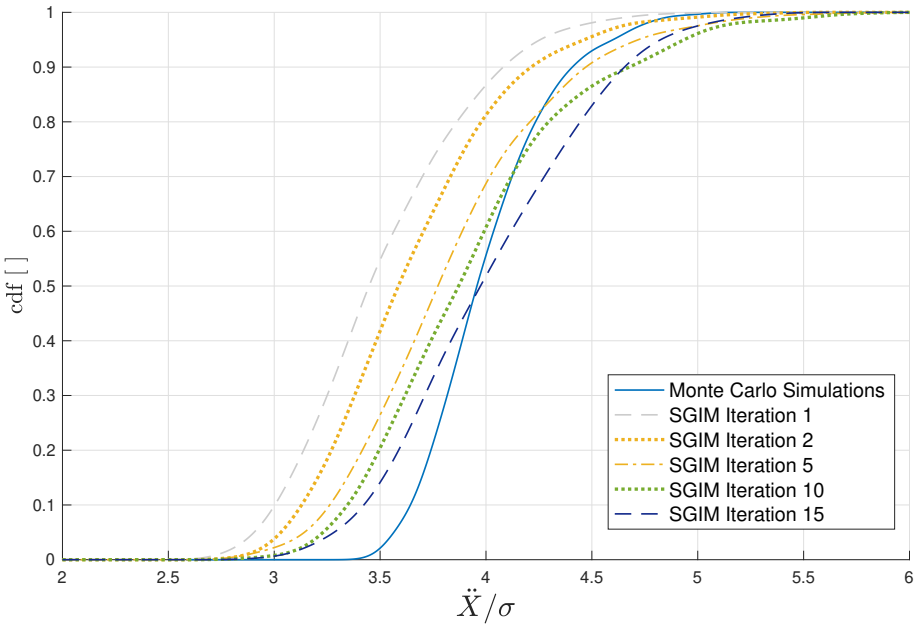

Figure 3.2: The Monte Carlo and SGIM extreme value cdfs in the Duffing oscillator with a non-linearity constant of 0.00.

until a visual convergence was reached; either with the Monte Carlo extreme cdf or between the extreme cdfs of multiple concurrent iterations.

For each case, the rms of the process will be used to normalize the response of interest: the acceleration. The rarity of these events is indicated by the number of standard deviations above the mean, as discussed in Section 2.4. Also, note that for a zero-mean process, the standard deviation and the rms are equivalent.

As shown in Figure 3.2, the SGIM on a Duffing oscillator with $\beta = 0.00$ was able to closely reproduce the extreme value cdf from the Monte Carlo simulations in terms of median. The variance in the SGIM extreme cdfs is relatively large (2.5x larger) compared to that of the Monte Carlo extreme cdf.

In Figure 3.3, in the extreme cdf recovered by the SGIM for a Duffing oscillator with $\beta = 0.01$, convergence was reached slightly faster than in the Duffing oscillator with $\beta = 0.00$. That being said, the median value of the visually converged SGIM extreme cdf was about 8% lower than that of the Monte Carlo simulations. The SGIM extreme cdf retained the relatively large variance as well.

In Figure 3.4, for $\beta = 0.04$, the convergence of the SGIM extreme cdfs between concurrent iterations took longer than in the previous two cases, but the median value of the final SGIM iteration extreme cdf was closer to the Monte Carlo simulation

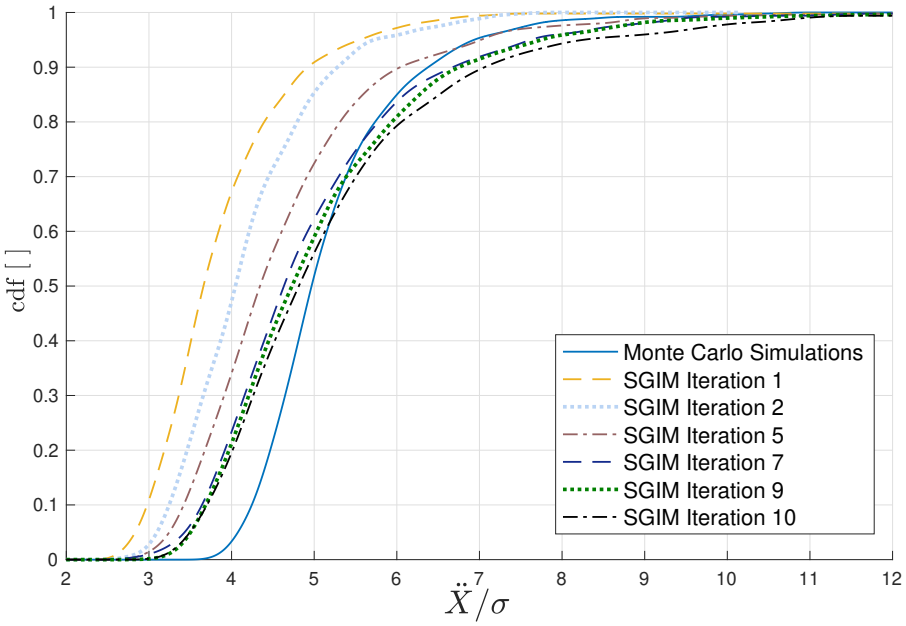

Figure 3.3: The Monte Carlo and SGIM extreme value cdfs in the Duffing oscillator with a non-linearity constant of 0.01.

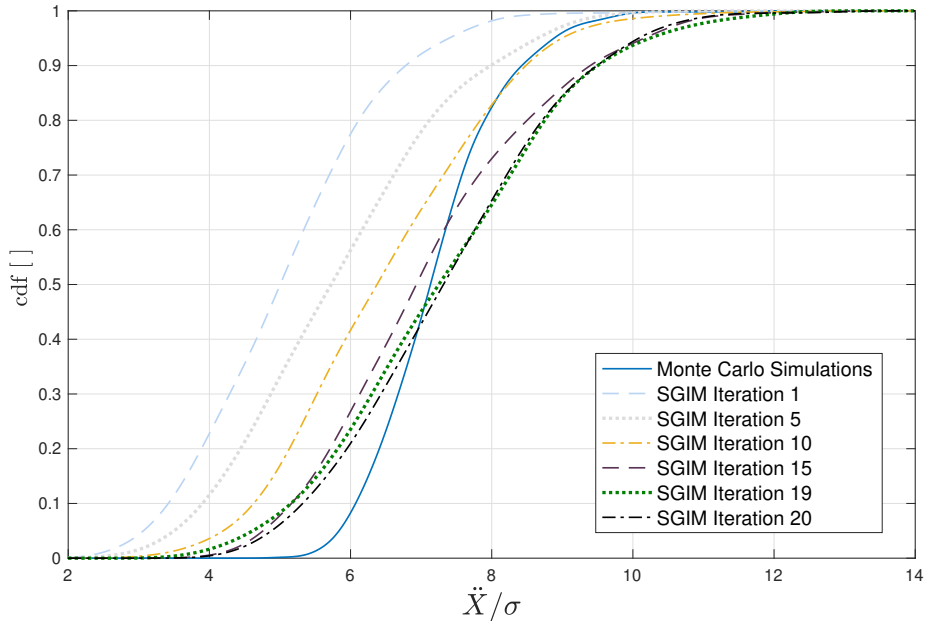

Figure 3.4: The Monte Carlo and SGIM extreme value cdfs in the Duffing oscillator with a non-linearity constant of 0.04.

extreme cdf (3.5% higher). Also, the relative variance difference between the final SGIM iteration extreme cdf compared to the Monte Carlo extreme cdf decreased to a factor of 2.

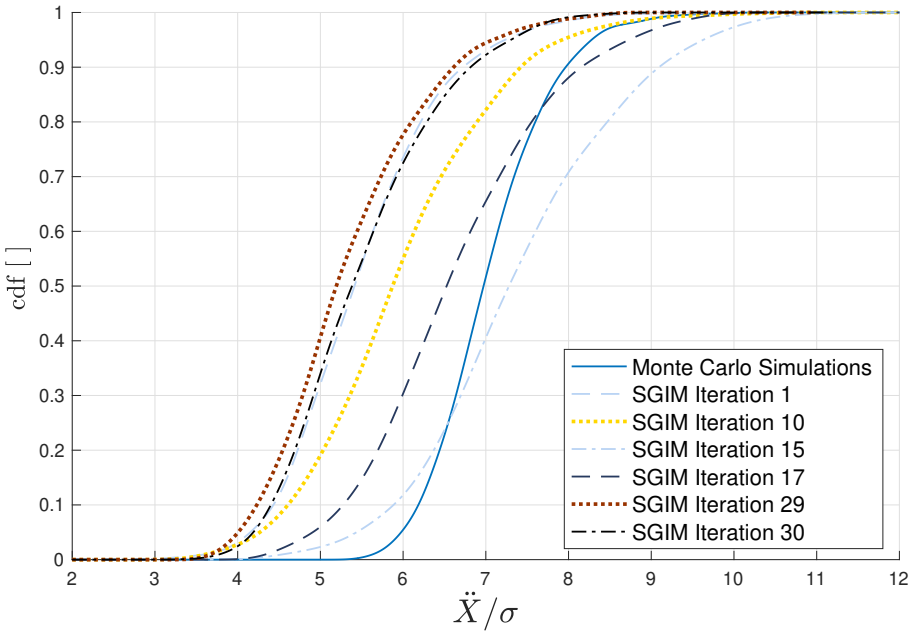

Figure 3.5: The Monte Carlo and SGIM extreme value cdfs in the Duffing oscillator with a non-linearity constant of 0.08.

In Figure 3.5, the SGIM extreme cdfs for $\beta = 0.08$ move toward and eventually surpass by the Monte Carlo extreme cdf by iteration but after iteration 15, the SGIM extreme cdfs regress until eventually re-converging with SGIM iteration 1.

After performing this study, the main takeaway is that the SGIM, in the more linear cases, could generally recover the median of the extremes. However, there was a source of variance that was introduced that resulted in different shaped cdfs compared to the Monte Carlo simulations.

In terms of non-linear limits, it can be seen that as the value of β increases, the ability of the SGIM to recover the extreme cdf remains somewhat constant until $\beta = 0.08$.

At $\beta = 0.08$, an odd phenomenon occurred where it appeared that the SGIM was going to converge to a reasonable level near the Monte Carlo extreme cdf. After the 15th iteration, however, the cdf slipped back until eventually converging on the initial iteration. While this is not necessarily indicative of the SGIM's non-linear limitations, it does provide a starting point to defining the limits. That being said, there are facets within the SGIM iterations that could be modified, such as the DLG time series length or the value of the standard deviation used in the gaussianization, to account for more non-linear problems, as well as the issue concerning how time

evolves when the gaussianization occurs.

With this study in mind, the following applications of the SGIM are presented: hull slamming and the tower base bending moment of an offshore wind turbine.

3.4 Extreme Acceleration during Hull Slams

In this section, the SGIM was applied on a hull slamming model to estimate the extreme cdf for acceleration magnitude as in Edwards et al. (2019b). To study if the SGIM preserved other characteristics, the peak width of the most extreme value from each simulation was also recorded. The peak width is defined as the effective duration of a slamming event and was determined using an algorithm defined in Razola et al. (2016). It can be noted that the magnitude of acceleration and the associated peak width are drivers in human injury aboard ships when faced with a slam as seen in Griffin (1996).

The extreme acceleration cdfs that the SGIM produced was compared with that of 500, 10,800 s Monte Carlo simulations. In the iterations, the DLG produced 500, 2000 s realizations of the extreme pseudo-gaussian process during each iteration. Longer DLG time series were used here to ensure that the transfer functions were more developed each iteration. The model used to simulate heave acceleration with sporadic slams is shown in Equation 3.3 and a visual representation is shown in Figure 3.6.

$$m\ddot{x} + c\dot{x} + k(t)x = F\zeta(t) \tag{3.3}$$

where

$$k(t) = \begin{cases} k + k_s e^{-(1/\tau)t} & \text{if } RV > RV_{thresh} \text{ and } RP < 0 \\ k & \text{otherwise} \end{cases}$$

Here, m represents the mass of the system, c represents linear damping, F is a linear forcing coefficient applied on the time dependent wave elevation $\zeta(t)$, k is the hydrostatic stiffness, k_s is the additional instantaneous stiffness added when a slam occurs, τ is the stiffness decay term associated with a slam, and RV is the relative velocity and RP is the relative position between the mass and the ocean surface. The method by which a slam occurs is consistent with Ochi (1964), but the criteria (notably the threshold relative velocity required for a slam, RV_{thresh},) were

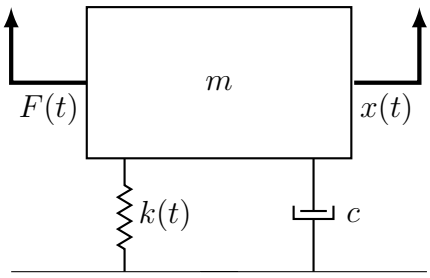

Figure 3.6: A reduced order model of a high speed planing craft, with slamming being modeled by an exponential spring, $k(t)$.

not specifically matched.

The slams were represented by a decaying exponential to emulate the immediate additional stiffness the water surface provides, followed by the water traversing up the hull until the stiffness of the water returns to purely hydrostatic. The system parameters, shown in Table 3.2, were chosen to provide a frequency of slams and magnitude of acceleration during slams comparable to accessible data in a sea state described by an ITTC spectrum with $H_s = 6$m and $T_m = 12$ s.

Parameter	**Value**
$k\,[N/m]$	588.06
$m\,[kg]$	600.00
$RV_{thresh}\,[m/s]$	5.00
$c\,[\frac{Ns}{m}]$	415.80
$F\,[N/m]$	1500.00
$\tau\,[s]$	133.33
$k_s\,[N/m]$	4750.60

Table 3.2: Parameters used for the hull slamming application.

It should be noted that this model is highly non-linear and also non-Gaussian. Therefore, it is expected that the level and speed of convergence may be comparable to one of the Duffing oscillators in Section 3.3 if it can be assumed that the level of non-linearity/non-Gaussianity is the only factor in the success of the SGIM. Figure 3.7 shows a sample pdf of the acceleration to demonstrate the non-Gaussianity of the system. The kurtosis and skewness of the acceleration are certainly indicative of the non-Gaussianity of the system, but the non-Gaussian nature of the model can also be noticed in the minor peak on the positive tail of the pdf.

Figure 3.8 shows the extreme cdfs for the Monte Carlo simulations and the SGIM iterations.

After five iterations, the extreme acceleration cdf of the SGIM appears to have

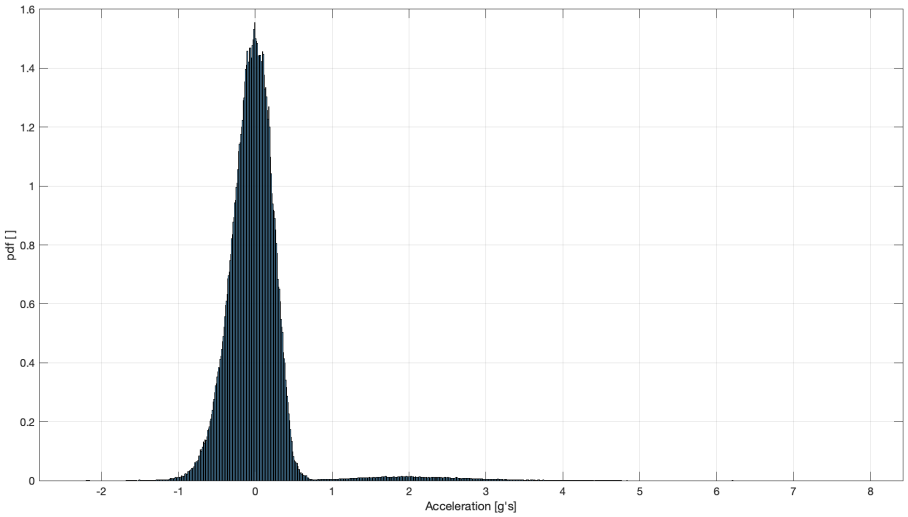

Figure 3.7: Sample pdf of the model's acceleration. Note the minor peak in the positive tail, indicative of the non-Gaussianity.

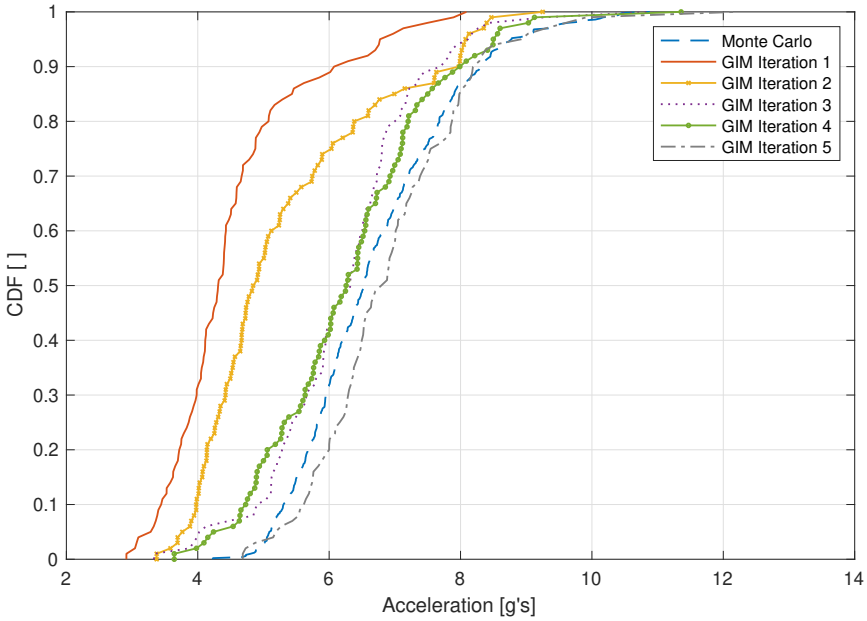

Figure 3.8: The extreme value cdfs for the Monte Carlo simulations and five (S)GIM iterations.

converged with that of the Monte Carlo simulations. It should be noted, however, that the creation of the extreme SGIM cdfs was taken blindly. That is to say, the location of the extreme value was not initially noted. In the DLG, phases are selected such that an extreme occurs at $t = 0$. It follows that the extreme value in the SGIM realizations should also lie around $t = 0$ due to the expected convergence of the sets $Z_{i,G}$ and Z_{NG} This was not the case, however. The extremes in the fifth and final

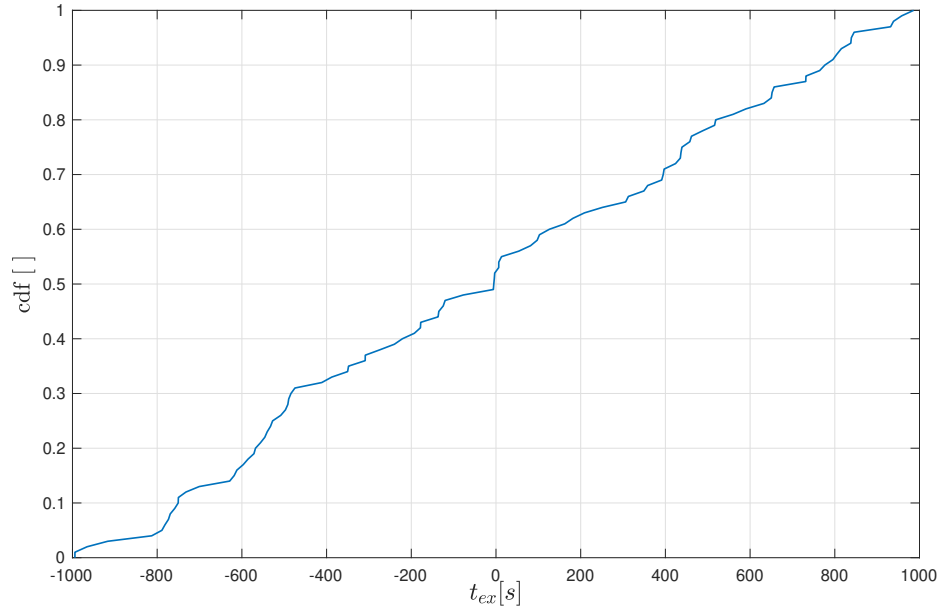

Figure 3.9: The cdf of the locations of the extreme values in 500 simulations of the fifth SGIM iteration. Note that the expected time of the extreme value is at $t_{ex} = 1000s$ with very little deviation.

iteration of the SGIM were actually nearly uniformly distributed across the 2000 s time series, as shown in Figure 3.9.

When inspecting Figure 3.9, it appears that, like any ordinary set of simulations, it is equally probable that the largest value appears anywhere in the sequence. From here, it is logical to say that the DLG time series were too long and led to a sort of forced, artificial convergence. However, the fact that each DLG time series is less than 1/5 the length of each Monte Carlo simulation says otherwise. That still leaves the question: what caused the convergence of the SGIM extreme cdf and the Monte Carlo extreme cdf? This is among the questions that must be answered for the SGIM to be considered legitimate.

Another facet of this application was the study of the duration of the largest acceleration peak and if the SGIM preserves the behavior. The duration of acceleration, or peak width, was determined using the algorithm used in Razola et al. (2016).

The peak width of the largest acceleration peak in each Monte Carlo and SGIM simulation was recorded. The peak width and associated acceleration magnitude were plotted against each other to compare the SGIM with Monte Carlo simulations. Also

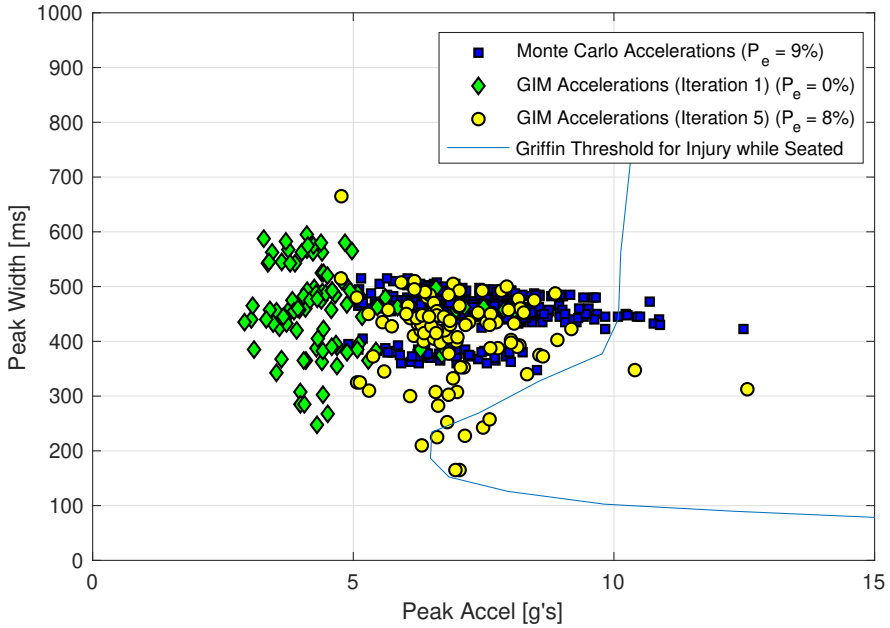

Figure 3.10: Extreme acceleration magnitude and peak width pairs for the Monte Carlo simulations and SGIM iterations 1 and 5.

included is a line from Griffin (1996) which, if crossed by a peak width-magnitude pair, indicates that a standing human would likely be injured. The probability of injury during the largest acceleration, or number of cases for which the peak width-magnitude pair crossed the Griffin line out of the total number of cases, was also recorded. Figure 3.10 shows the peak width-magnitude pairs for each Monte Carlo simulation and of selected SGIM iterations.

The fifth SGIM iteration, which showed convergence with the Monte Carlo simulations in purely magnitude, had a similar probability of human injury to the Monte Carlo simulations. However, the SGIM did not share dual grouping phenomenon of the Monte Carlo simulations. It is unclear if the two clusters of peak width and peak magnitude pairs present in the Monte Carlo simulations is an artifact of the model used or the result of some sort of relationship with the input spectrum. Still, the SGIM provided results that more or less encapsulated the domain and range of the Monte Carlo simulations peak width and peak magnitude pairs.

While the SGIM extreme acceleration cdf converged with that of the Monte Carlo simulations, there are still unexpected consequences that must be understood: the uniformly distributed acceleration extremes across the span of the DLG time series and the change in peak width distribution compared to the Monte Carlo simulations.

There is also the overarching problem with the change in time scales when performing a gaussianization on a time series.

3.5 Extreme Tower Base Bending Moments of Offshore Wind Turbines

In this section, the SGIM was used to determine wave sets that, in conjunction with wind that was random and unconditioned on the waves, led to extreme tower base bending moments in an offshore wind turbine as in Edwards et al. (2019a). To do so, the multi degree of freedom wind turbine simulator OpenFAST (Jonkman and Sprague (2017)) was used with the DTU 10 MW Reference Wind Turbine (Bak et al. (2013)). Even with second order effects from the waves, the tower base bending moment produced by OpenFAST was nearly Gaussian. That being said, as seen in Section 3.3, the near Gaussianity may not result in perfect convergence between SGIM and the "truth". Again, the SGIM was stacked up against Monte Carlo simulations. In the Monte Carlo simulations, a JONSWAP wave spectrum with $H_s = 6$m and $T_m = 12$s was used in conjunction with a Kaimal wind spectrum (Kaimal et al. (1972)) with a mean wind speed of 12 m/s and a turbulence intensity of 0.25. Due to the more complex solver used in OpenFAST, only twenty 40-minute simulations were run for comparison. For the SGIM, four 15-minute simulations were run with solely realizations of waves from the aforementioned JONSWAP spectrum. After five iterations of the SGIM, an ensemble of 200 s wave sets that led to 40-minute extreme wave bending moments was produced. For comparison with the Monte Carlo simulations, the extreme wave sets were input into OpenFAST along with unconditioned realizations of the Kaimal spectrum. The comparison between the Monte Carlo extremes and the extremes produced by the SGIM are shown in Figure 3.11. Also shown are the TEV of interest and the cdf of the instantaneous bending moment.

It should initially be noted that the SGIM extreme bending moment cdf with solely waves overshot the Monte Carlo extreme cdf in both median and variance. However, the addition of unconditioned wind actually lowered both the median value and the variance to a point more in line with the Monte Carlo extreme cdf. Theoretically, in a linear system, the addition of wind would add a mean bending moment and increase the extreme values by at least that mean value. It could be possible that the mean wind speed here increased the tension on the mooring lines thereby increasing

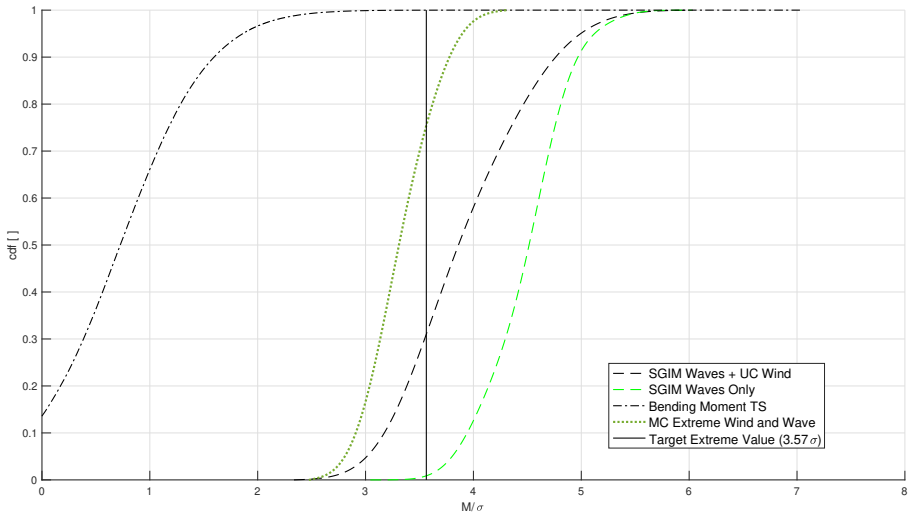

Figure 3.11: The extreme Monte Carlo bending moment cdf compared with the SGIM extreme cdf with solely waves as well as the extreme cdf of SGIM waves with unconditioned wind.

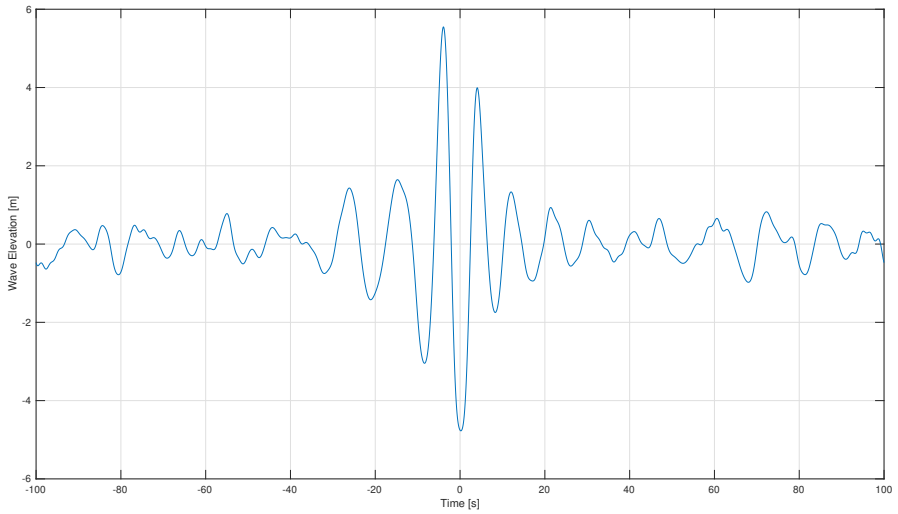

Figure 3.12: The ensemble average of the waves that lead to extreme bending moments after five SGIM iterations.

the stiffness in the system. By increasing the stiffness in the system, the natural frequency increases. By looking at Figure 3.12, it can be reasoned that the waves may have zoned in on the bending moment natural frequency, therefore providing responses much larger than expected from the Monte Carlo simulations.

By increasing the stiffness, the mean wind speed may have detuned the system, resulting in lower extreme values. Still, while the addition of wind brought the SGIM extreme cdf closer to the Monte Carlo extreme cdf, there is still a consider-

able difference between the two. One possible solution may be to perform the SGIM with multiple inputs, being wind and wave. In the multiple input SGIM, there is a challenge in generating two transfer functions from wind and wave to the bending moment for input into the DLG. A technique like Independent Component Analysis (ICA) may be useful in this situation if a machine learning code could be trained to identify what frequency content and other characteristics of the bending moment response come from wind and what comes from wave. There is also an analytical technique in which the frequency content of the wind and wave spectra are alternatively discretized so that when the Gaussianized bending moment response is brought into the frequency domain, the frequencies associated with wind and wave could be picked out.

3.6 Conclusions

In this chapter, the development and progress of a new method called the Stochastic Gaussianization Iteration Method was presented. A systematic approach to defining the non-linear capabilities of the SGIM was attempted with a Duffing oscillator. Various values of the non-linear parameter were used and the extreme cdfs produced by the SGIM were compared with Monte Carlo simulations. While the SGIM was mostly successful in estimating the extreme median, the estimated variance was at least twice as large as compared to the Monte Carlo simulations. Further studies into the parameters within the SGIM such as DLG record length and the standard deviation used in the gaussianization may shed a light on this increased variance.

The SGIM was then applied to find the extreme cdf of acceleration in a hull slamming model. In this application, the SGIM extreme cdf converged with the Monte Carlo extreme cdf after five iterations. Upon closer inspection, however, the location of the extrema were far different than expected. Learning more about how time is affected when a process is "Gaussianized" may be of use when investigating this phenomenon. Also, the effect of the SGIM on other characteristics during extreme events was studied by looking at the duration of each extreme acceleration. Within the criteria of human injury, the SGIM reproduced the results from the Monte Carlo simulations, but provided acceleration peak durations that were more sporadic than the Monte Carlo simulations.

The more Gaussian application of offshore wind turbine base bending moment

was the next application of the SGIM. That being said, the SGIM did not perform as well in it did in the hull slamming application. After studying the waves that led to extreme bending moments produced by the SGIM, it is possible that resonance might have been tripped. The fact that the addition of wind actually lowered the extreme responses further supports this theory, as the wind would have detuned the system. While the SGIM did not necessarily "work", this application provided insight into situations where the SGIM may struggle.

One takeaway from the SGIM is that for a zero-mean and non-skewed process, the original process and the Gaussian transformed version have the same amount of upcrossings in a given return period. It is this insight that inspired the decision to discontinue development on the SGIM and to take a different approach. In the following chapters, this key property of the SGIM method is taken and developed into the Matched Upcrossing Equivalent Linear System (MUELS) method.

Chapter 4

The Matched Upcrossing Equivalent Linear System Method

4.1 Introduction

Understanding the intricacies of multi-degree of freedom non-linear systems requires extensive knowledge or assumptions to be made. It is important from a design perspective to understand the dynamics of other degrees of freedom during an extreme event in a particular degree of freedom so that any structural responses that are affected by said degrees of freedom e.g., bending moment or slamming, can be designed for. It is unrealistic to expect to have a full statistical model for joint interaction between all of the degrees of freedom but it is also risky to apply "load combination factors" (Lloyd's Register, 2020). One method that lands somewhere in between is a time series analysis using the DLG in which an ensemble of input wave realizations that lead to an extreme in one degree of freedom are applied to other degrees of freedom to generate conditional distribution histograms. This method was applied in Seyffert (2018) to investigate the failure probability of stiffened panels undergoing both bending and slamming pressures. In Seyffert (2018), surrogate processes that were linear and correlated with bending moment and slamming were run through the DLG to generate extreme time series realizations which could then be used to understand the simultaneous response in other degrees of freedom. While the method presented is a powerful application of the DLG, it still requires advanced knowledge of the system in having to select the surrogate processes. In this chapter, an alternative method to selecting a surrogate is introduced in the MUELS method.

4.2 Methodology

To identify extreme behavior while also retaining the ability to investigate other responses in the same conditions, the proposed method uses a combination of a to-be

found Equivalent Linear System (ELS) and the Design Loads Generator (DLG). The DLG can produce an ensemble of inputs that lead to extremes for the linear systems, which can in turn be used as input for the non-linear original process. Whether or not these inputs will result in extreme behavior in the non-linear system is related to the method of determining the equivalent linear systems. Often times, at least in linear systems, the level of rarity in the response will be directly related to the number of times the response oscillates past the mean of the process. The question then becomes, for ergodic non-linear systems, is it possible to use extreme behavior information from these linear systems' upcrossing rates to estimate non-linear system maxima? In this method, the mean-upcrossing rate (MUR) is measured from training data for a given input spectrum. After estimating the MUR, linear systems subjected to the same input spectrum with the same MUR can be identified. By using a linear oscillator with two parameters, damping ratio and natural frequency, a contour relating these parameters can be generated such that the linear system has the same upcrossing rate as the training data of the non-linear process. Equation 4.1 shows the differential equation that represents the ELS.

$$\ddot{x} + 2\omega_n \zeta \dot{x} + \omega_n^2 x = \hat{F}(t) \tag{4.1}$$

Here, ω_n is the natural frequency, ζ is the damping ratio, and $\hat{F}(t)$ is the forcing normalized by the unspecified mass of the system. In Ochi (1990b), it was shown that for linear systems like the one in Equation 4.1, the MUR can be described using the moments of the system. Equation 4.2 shows the equation for the mean-upcrossing rate for linear systems forced by a linear zero-mean input spectrum.

$$\omega_z = \sqrt{m_2/m_0} \tag{4.2}$$

where ω_z is the mean-upcrossing frequency, m_2 is the second moment, and m_0 is the zero-th moment. It should be noted that if the system is non-stationary, the MUR shares uncertain correlation with extreme values. The MUELS method does not apply to non-stationary systems in the format described here. Chapter 6 will include discussion of an application of the MUELS method in which non-stationarity is not a limiting factor.

To generate the contours, a set of systems with varying damping ratios and

natural frequencies are swept. For each of the systems, the zero-th and second moments are calculated and the mean-upcrossing frequencies are determined using the following equation.

$$m_k = \int_0^\infty \omega^k |H(\omega; \omega_n, \zeta)|^2 S_{in}(\omega)\, d\omega \tag{4.3}$$

where m_k is the k-th moment, ω is radial frequency, $H(\omega; \omega_n, \zeta)$ is the transfer function of the linear system represented by ω_n and ζ, and $S_{in}(\omega)$ is the input spectrum. The MUR is estimated as a function of the natural frequency and damping ratio and the *MATLAB* function *contour()* builds a contour. The resulting contour is a function of natural frequency and damping ratio at the specified mean-upcrossing frequency of interest. It should be noted that the contour is estimated using an interpolation method. Sufficient accuracy was achieved using around 30 different damping ratios and natural frequencies generate a discrete representation of the zero-upcrossing frequency as a function of the damping ratio and natural frequency. The *contour()* function takes this discrete representation and generates a set of damping ratios and natural frequencies (that may not have been in the original parameter sets) at the MUR of interest. The number of systems along the contour depends on the relationship between the MUR found from the training data and the characteristic frequency in the input spectrum. If the difference between the MUR and input characteristic frequency is significant enough, there may not be any ELS that can represent the non-linear system. That being said, more parameters could be added into the ELS such that systems with the same MUR as the NL system of interest can be discovered. Figure 4.1 shows an example of what one of these contours looks like.

All of the linear systems along the contour have approximately the same MUR as the non-linear process. This is the basis for the Matched Upcrossing Equivalent Linear System (MUELS) method. By matching the MUR, the number of mean-crossing maxima can be expected to be the same, in the mean. Therefore, while there may be some variation in the time series, it is hypothesized here that there is a conditional relationship between the extreme values of the non-linear process and the equivalent linear systems. To classify the rarity, the Target Extreme Value (TEV) (Ochi, 1990b) based off of the linear systems is defined as follows:

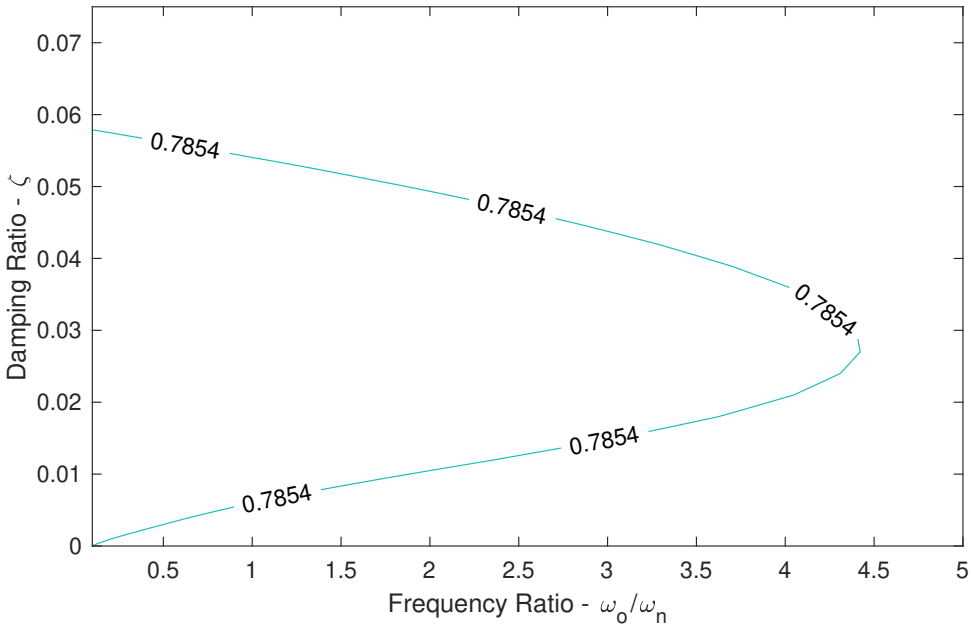

Figure 4.1: An example of a contour for a given mean-upcrossing frequency (0.7854 rad/s).

$$TEV = \sqrt{2ln(n)} \tag{4.4}$$

where n is the number of cycles in a given exposure period.

While the TEV does not have strict meaning to a non-linear process, it is a starting point and more flexible than attempting to estimate a more correct metric for each different non-linear system. By using the TEV as a metric along with a series of linear systems subjected to a specified input spectrum, the DLG can be used to produce extreme realizations of the linear systems at the level specified by the TEV as well as the inputs that lead to those extreme realizations. It should also be noted that the use of the TEV in this case does not assume narrow-bandedness. The gathering of the number of cycles is done empirically, which means all of the moments of the response spectrum are included.

The DLG samples phases from a distribution that is directly influenced by the extreme value distribution of a Gaussian process (Kim, 2012). Since the ELS are linear and are forced by a Gaussian process, they too will be Gaussian. The selected phases for a given realization can be inverted through the transfer function to generate phases for the input realization. The input can then be used as conditional input for the non-linear process of interest.

The DLG generated input realization is firstly a valid realization of the original input spectrum but secondly contains phase and frequency content that excites a system with the same MUR as the non-linear process. This action, while not guaranteeing an extreme non-linear event on the order of the exposure period of interest, can aid in understanding the general behavior of the non-linear system in a rare scenario. In this vein, the complexity within non-linear transfer functions can result in a shift in time for the conditional extreme. In the DLG realizations, the extreme value occurs at a specific time t_0, where t_0 can be set to 0 without loss of generality. When applying these inputs to the non-linear transfer function, the interaction between the DLG phase sets and the non-linear transfer function can result in a shift of the conditional extreme's location away from t_0. As such, when running through the MUELS method, the limits of searching for the largest zero-upcrossing value in a single realization is expanded by one cycle centered at t_0 to account for phase differences between the ELS and non-linear system. That is to say, the search is done for each realization as follows:

$$\hat{x}_i = \max_t x_t(t_0 - T_0 : t_0 + T_0) \tag{4.5}$$

where $i \in [1, N]$ is the realization number, N is the total number of realizations, $\hat{x}$ is the maximum value, and T_0 is the mean period of the response. At this point, the time series can then be "corrected" by shifting the conditional extremes to t_0 if desired. To summarize the MUELS process, Figure 4.2 shows a flowchart outlining the steps in the MUELS method.

The MUELS method is based on the assumption that the conditional extreme maxima of the nonlinear system (i.e., conditional on occurring in the neighborhood of the ELS) is an approximation to the true nonlinear extreme. Along with this aspect, the MUELS method makes no assumption on tail behavior, like what was needed for the SGIM Gaussianization process, and also requires less explicit discrete function manipulation.

In the following chapters, the MUELS method is applied to three distinct systems: a sub-harmonically forced Duffing oscillator, a super-harmonically forced Duffing oscillator, and an impact oscillator. Each of the three systems have marine applications and will test the limits and capabilities of the MUELS method.

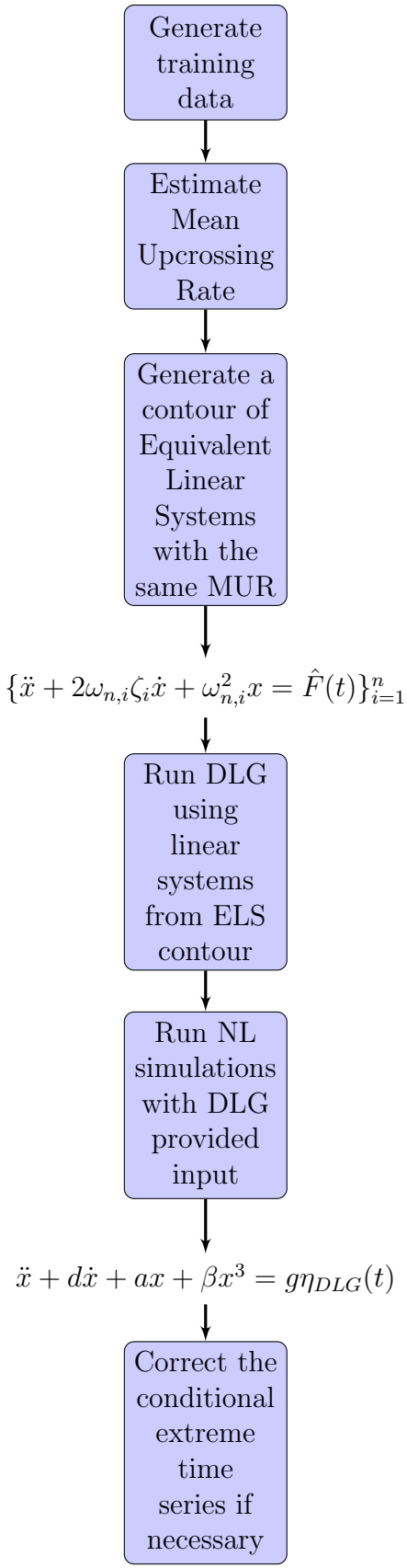

Figure 4.2: The Matched Upcrossing Equivalent Linear System (MUELS) method flowchart

Chapter 5

MUELS Application with a Sub-harmonically Forced Oscillator

5.1 Introduction

While the surrogate process approach proved to be an effective method, experience is needed to select a process that is correlated with the response of interest. Still, it leads one to believe that the DLG can be used in a systematic fashion to estimate extremes of non-linear systems. Here, a methodology is proposed that allows a linear surrogate process to be found from the non-linear process alone. This chapter applies a method based off of this belief: The Matched Upcrossing Equivalent Linear System (MUELS) method.

This chapter is organized as follows: First, the method is applied to a stiffening Duffing Oscillator. A single exposure period run is presented and compared to Monte Carlo simulations to demonstrate the process and outputs of the MUELS method at three different cubic stiffness levels. Then, estimations of the most probable maximum at each of the three different cubic stiffness levels at a wide array of exposure periods are generated using the MUELS method and are compared with MCS and GEVD extrapolations. The recreation of extreme time series using the MUELS method is also shown and compared with extreme Monte Carlo realizations.

5.2 Methodology

In this section, the methodology developed in Edwards et al. (2021) is discussed.

5.2.1 GEVD Extrapolation

By using methods discussed in the Introduction, it is possible to extrapolate the parameters of a GEVD for a given exposure period to those of a different exposure period. The extrapolated GEVD will provide a comparison for the MUELS method at exposure periods without MCS. To do so, the parameters of interest should be

introduced. Equation 5.1 shows the general form of a GEVD cdf (Coles, 2001).

$$F(s;\xi) = \begin{cases} exp(-exp(s)) & \text{for } \xi = 0 \\ exp(-(1+\xi s)^{-1/\xi}) & \text{for } \xi \neq 0 \text{ and } \xi s > -1 \\ 0 & \text{for } \xi > 0 \text{ and } \xi s \leq -1 \\ 1 & \text{for } \xi < 0 \text{ and } \xi s \leq -1 \end{cases} \tag{5.1}$$

Here, ξ represents the shape parameter and $s = (x-\mu)/\sigma$, which non-dimensionalizes the variable of interest, x, with the location parameter, μ, and the scale parameter, σ. The shape parameter dictates which type of extreme distribution a given process follows and does not change with exposure period. That being said, estimations of the shape parameter can vary from exposure period due to the fact that it has not converged. In this dissertation, however, the shape parameter from the training data is used and taken as a constant.

To extrapolate the GEVD parameters from exposure periods of n cycles to m cycles, the following relationships can be derived from the assumption that the shape parameter remains constant:

$$\sigma_m = \quad \sigma_n(m/n)^{\xi} \tag{5.2}$$

$$\mu_m = \quad \mu_n + (\sigma_n/\xi)[(m/n)^{\xi} - 1] \tag{5.3}$$

where subscripts m and n refer to the parameter's value with respect to m and n cycles, respectively.

Of course, Equations 5.2-5.3 assume ergodicity and it is entirely possible to erroneously extrapolate parameters for a non-ergodic system if rare behavior does not show up in the training data. In this chapter, the MUELS method will not be tested with a non-ergodic system, which is suggested by the fact that all pdfs of the oscillator response are uni-modal i.e., not containing multiple attractors. The extrapolated GEVD parameters will be assumed sufficient and confirmed with Monte Carlo Simulations of length equal to the exposure period of interest. Later in the chapter, the EVD extrapolations are used outside of the computational practicality of Monte Carlo simulations as comparison points with the MUELS method.

5.3 Sub-harmonically Forced Oscillator

In this section, the sub-harmonically forced Duffing Oscillator is introduced and pertinent characteristics including qualitative measures of non-linearity are shown, as in Edwards et al. (2021). It should be noted that the "sub-harmonically forced" signifies a forcing by a spectrum with a peak forcing frequency less than the linear natural frequency of the non-linear system. The basis for comparison and the set up for the Monte Carlo simulations are discussed as well.

5.3.1 The Duffing Oscillator

The Duffing Oscillator is a well-studied non-linear model (Miwadinou et al., 2016, Naess, 1994, Sterk, 2016) with marine applications such as roll. However, the extreme behavior of the Duffing Oscillator forced by a typical sea spectrum is less studied. The model for a Duffing Oscillator can be described as shown in Equation 3.1. In this chapter, an input spectrum and a forcing coefficient will be used. The forcing coefficient, g, scales the excitation such that the excitation rms matches the rms for a unit amplitude harmonic sine forcing. Equation 5.4 relates g to the forcing factor F_s and the significant wave height H_s. It can be shown through the rescaling of Equation 3.1 that changing the forcing factor, g, is equivalent to changing the cubic non-linearity coefficient, β.

$$g = \frac{2\sqrt{2}F_s}{H_s} \tag{5.4}$$

The updated Duffing Equation becomes:

$$\ddot{x} + d\dot{x} + ax + \beta x^3 = g\eta(t) \tag{5.5}$$

where $\eta(t)$ is a realization of the input spectrum.

In this chapter, an ITTC spectrum will be used with a significant wave height of $3.0\,m$ and a modal period of $14\,s$. The ITTC spectrum is defined as follows

$$S(\omega) = \frac{5\pi^4 H_s^2}{T_m^4 w^5}\, exp(\frac{-20\pi^4}{T_m^4 w^4}) \tag{5.6}$$

where H_s is significant wave height and T_m is the modal period.

To affect the non-linearity, the forcing constant F_s will be varied. The rest of the

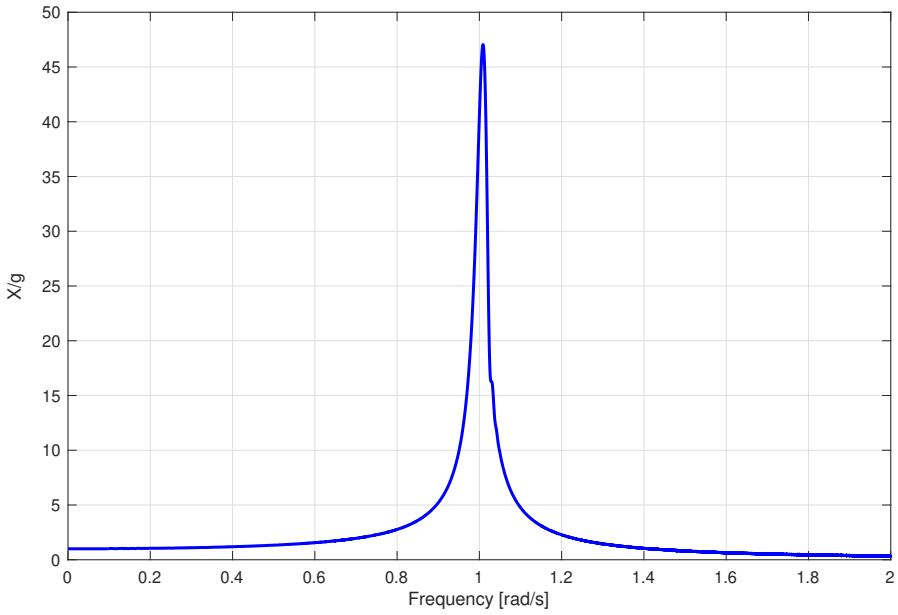

Figure 5.1: Qualitative magnification curves for $F_s = 0.001$. Dashed lines represent an unstable response.

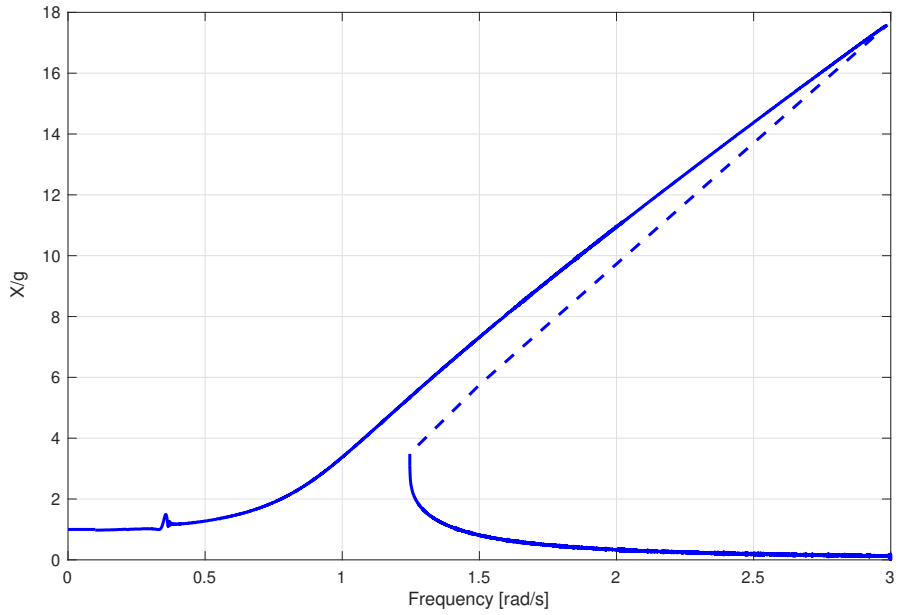

Figure 5.2: Qualitative magnification curves for $F_s = 1$. Dashed lines represent an unstable response.

coefficients will remain constant, with $d = 0.02$, $a = 1$, and $\beta = 0.04$. Figure 5.1-5.3 show relative magnification curves for the different F_s values that are used in this chapter. Note the difference in frequency scales between the figures.

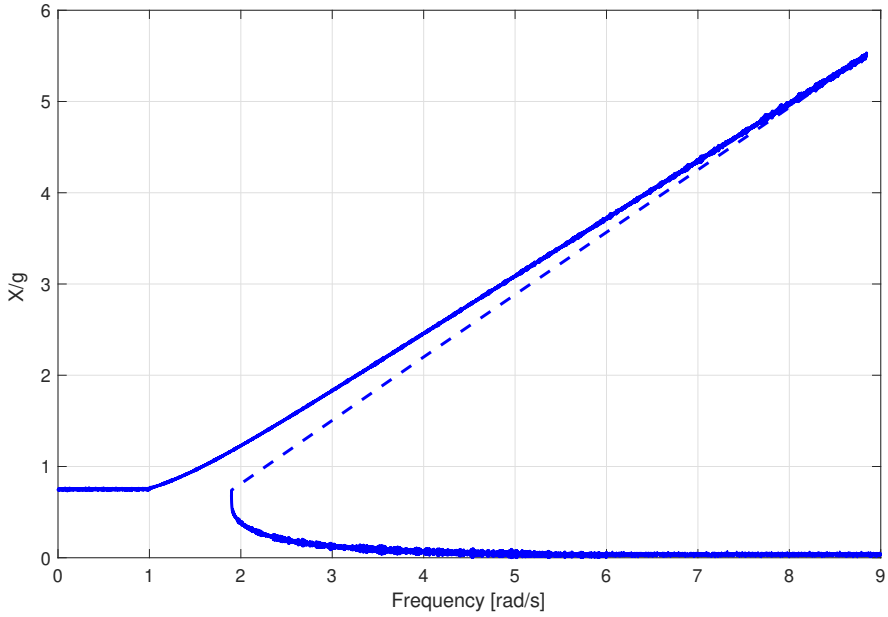

Figure 5.3: Qualitative magnification curves for $F_s = 10$. Dashed lines represent an unstable response.

Since the input spectrum has a predominantly lower frequency ($\omega_m = 0.45\,rad/s$), varying F_s introduces non-linearities more efficiently than varying the cubic stiffness parameter, β. In magnification curves with respect to various β parameters, the response near $\omega = 0.45\,rad/s$ is generally pretty constant and does not have multiple attractors. The three F_s values are selected such that three types of behavior are seen: mostly linear, slightly non-linear, and severely non-linear. These three types of behavior can more easily be noticed by inspecting the probability density functions (pdfs) of the response corresponding to each F_s value. Since the forcing is Gaussian, a linear process would result in a Gaussian output. Figures 5.4 - 5.6 show the estimated distributions of the three considered Duffing Oscillators non-dimensionalized by the respective rms compared to Standard Normal distributions. Table 5.1 compares the important parameters that distinguish the different Duffing Oscillators from a Gaussian Process. Most notably, the kurtosis of a Standard Normal is always 3.00 and the change in the kurtosis as F_s increases indicates the increase in non-linearity of the system.

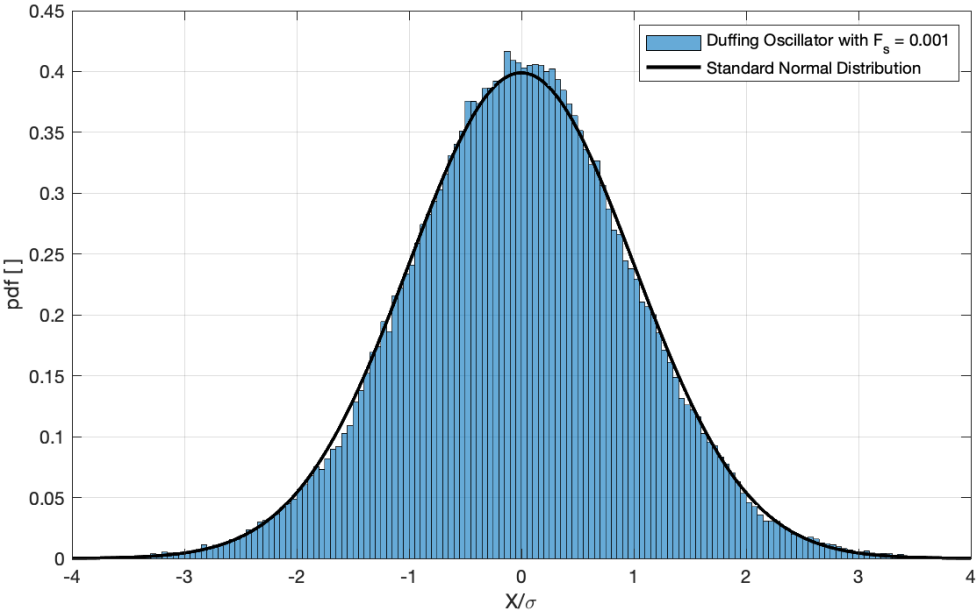

Figure 5.4: The pdf of the non-dimensionalized Duffing Oscillator with $F_s = 0.001$ versus a Standard Normal distribution.

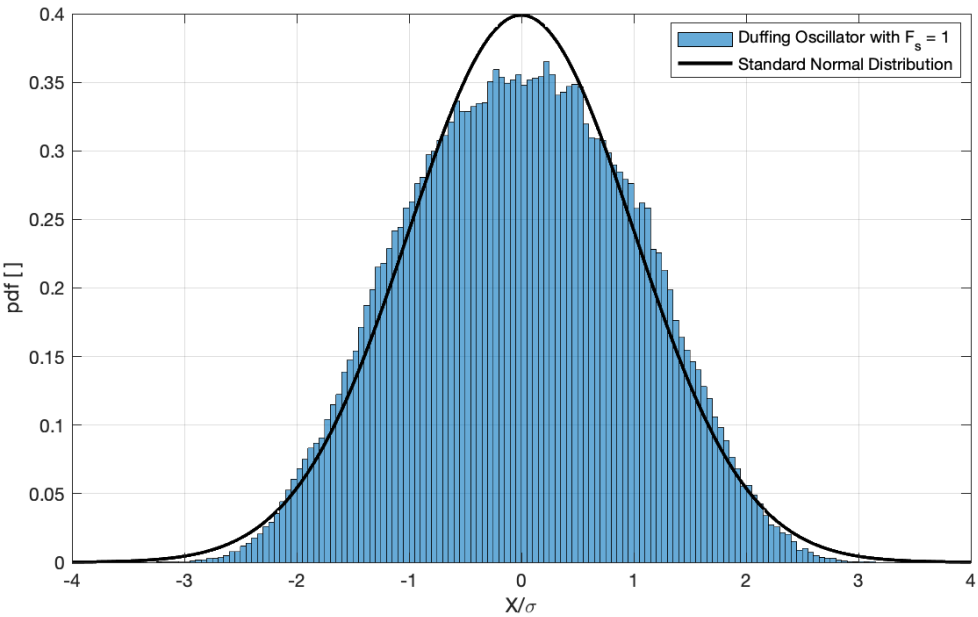

Figure 5.5: The pdf of the Duffing Oscillator with $F_s = 1$ versus a Normal distribution with mean and standard deviation equal to that of the Duffing Oscillator.

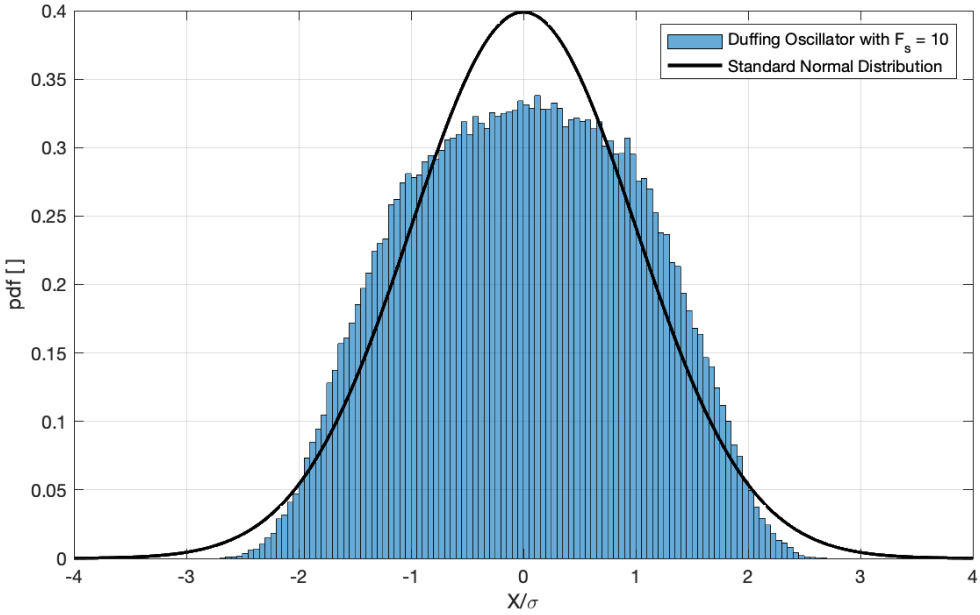

Figure 5.6: The pdf of the Duffing Oscillator with $F_s = 10$ versus a Normal distribution with mean and standard deviation equal to that of the Duffing Oscillator.

Table 5.1: Comparison of non-dimensionalized Duffing Oscillator parameters with the Standard Normal parameters including the mean (μ), standard deviation (σ), skewness (κ_3), and the kurtosis (κ_4).

Parameter	Standard Normal	Duffing $F_s = 0.001$	Duffing $F_s = 1$	Duffing $F_s = 10$
μ	0.00	0.00	0.00	0.00
σ	1.00	1.00	1.00	1.00
κ_3	0.00	-0.01	-0.06	-0.01
κ_4	3.00	3.02	2.50	2.18

It is clear that the low forcing value of $F_s = 0.001$ is very close to linear, as evidenced by the near perfect fit of the Normal distribution. As the forcing increases, the positive cubic non-linearity acts as a stiffening spring and causes a widening effect of the pdf.

One important factor that is of note in the MUELS process is the relationship between the frequency distribution in the response and the input. The engine that drives the MUELS method is the DLG. As mentioned before, the DLG, on a surface level, produces ensembles of extreme realizations of a linear process. A limitation of linear processes is that the relationship between input frequency and output frequency is also linear. That is to say, frequency content in the output must also be contained in the input. In non-linear systems, this is not necessarily the case. Since

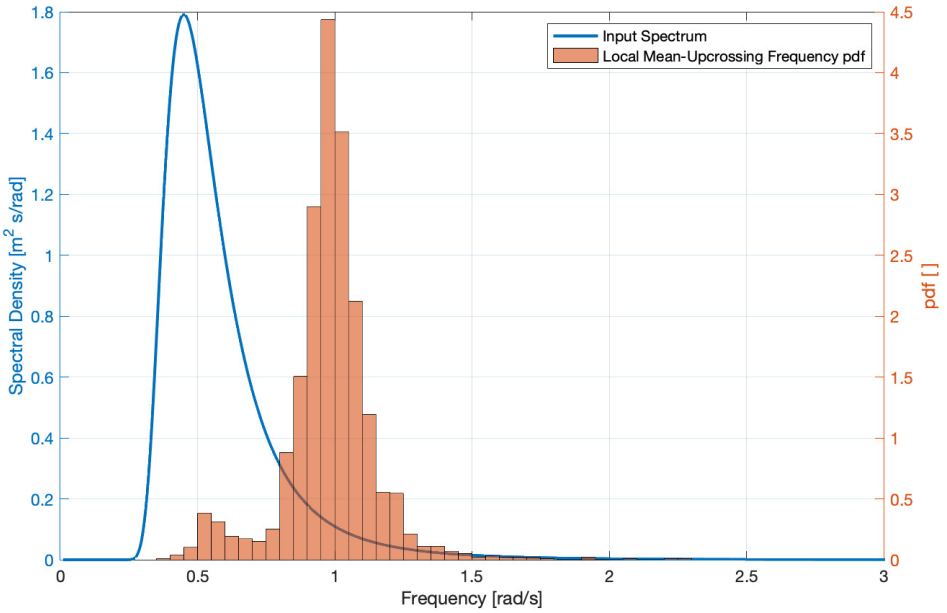

Figure 5.7: A comparison of the local mean-upcrossing frequencies of the Duffing Oscillator with $F_s = 0.001$ and the input spectrum. The average mean-upcrossing frequency is $\omega_z = 0.949\, rad/s$.

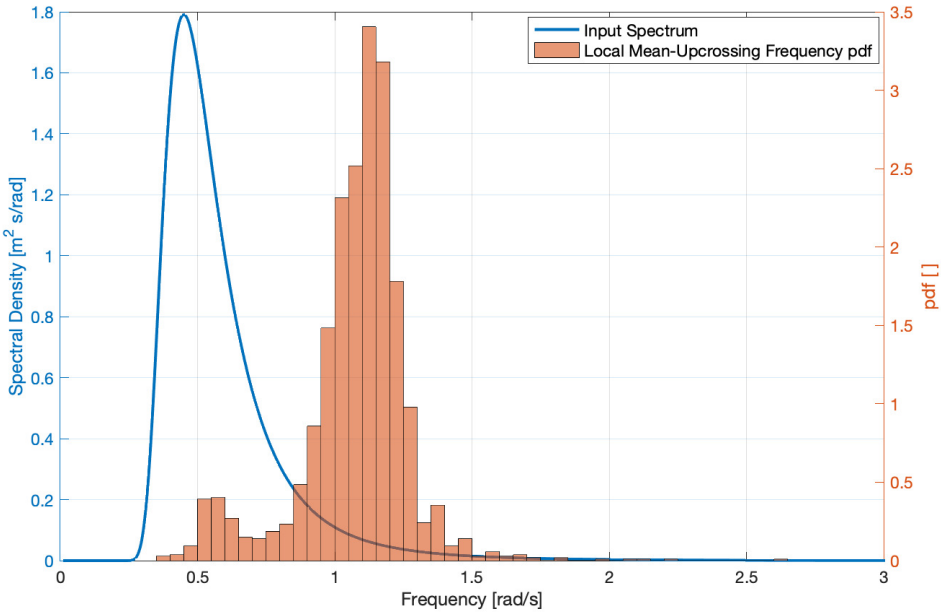

Figure 5.8: A comparison of the local mean-upcrossing frequencies of the Duffing Oscillator with $F_s = 1$ and the input spectrum. The average mean-upcrossing frequency is $\omega_z = 1.024\, rad/s$.

the transfer function of the Duffing Oscillator is not easily obtainable, to demonstrate this, Figure 5.7 - 5.9 show the input spectrum versus the local mean-upcrossing frequencies from sets of Monte Carlo simulations.

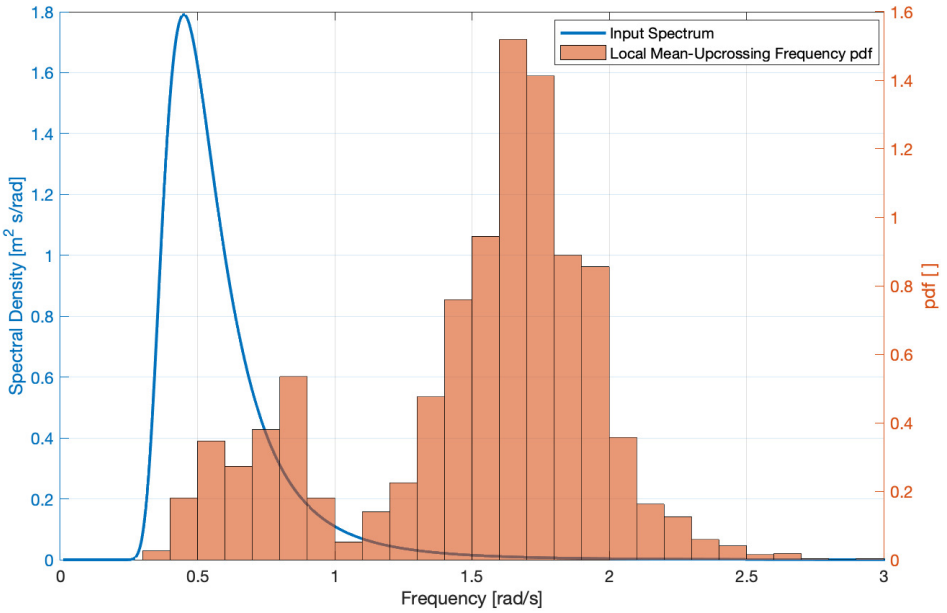

Figure 5.9: A comparison of the local mean-upcrossing frequencies of the Duffing Oscillator with $F_s = 10$ and the input spectrum. The average mean-upcrossing frequency is $\omega_z = 1.275\, rad/s$.

The takeaway from Figures 5.7 - 5.9 is the distribution of frequencies near the linear natural frequency ($\omega_n = 1.00\, rad/s$). As the forcing factor increases, the effective transfer function changes as well. In the $F_s = 0.001$ case, there are spikes near the peak of the input spectrum and near the linear natural frequency which is as expected in a lightly damped linear system. The $F_s = 1$ case is less in line with the expected linear solution, with a large peak shifted from the linear nation frequency. However, the response frequencies do lie within reasonable levels of input energy. In the $F_s = 10$ case, more response is much more elicited in the area where there is very little to no input energy. It is likely that the cubic non-linearity is being manifested in some way here due to the spike in the local zero-upcrossing frequencies near three times the peak input frequency. Herein lies the challenge the MUELS method faces: predicting which distribution of frequencies and phases generate extremes in the linear and non-linear space.

5.3.2 Monte Carlo Simulations

To generate training data for the MUELS method and to have data to compare against, a series of Monte Carlo simulations (MCS) were performed. One of the main benefits of the MUELS method is that it cuts down on computational expense and is meant to work with a limited amount of initial training data. In this application,

the MUELS method will take training data of a given exposure period and estimate extremes at a larger exposure period. As such, two sets of Monte Carlo simulations were run for each F_s value. The timestep used in the MCS was $dt = 0.05$, For the training data, 10,000 runs of 2^{18} points (3.64 hr) were generated with a runtime of about 1 hr on eight processors. For the Monte Carlo simulations at the desired exposure period, 10,000 runs of 2^{22} points (58.25 hr) were generated with a runtime of about 19.5 hr on eight processors.

5.4 Results

In the following section, the results of the MUELS method shown in Edwards et al. (2021) are compared with Monte Carlo simulations. For a simple yet robust comparison between the MUELS method and MCS, the most probable maximum from each series of results is used.

5.4.1 MUELS Results for a Single TEV

In Figures 5.10-5.12 the MUELS ELS with the largest most probable maximum are compared with the 58 hr Monte Carlo runs as well as an extrapolated GEVD formed from the 3.6 hr Monte Carlo runs for each F_s value. The pdf indicated by the dotted line illustrates the ELS marked by the asterisk on the left-hand side of the graph. Note that the response, X, is non-dimensionalized by the root mean square of the underlying process, σ. It should also be noted that the frequency ratio indicated in the contour plots are linear natural frequencies, ω_n, non-dimensionalized by the peak forcing frequency.

While the fit of the "best" MUELS pdf to the MCS pdfs may worsen as F_s increases, the MPM of the "best" MUELS pdf is a decent estimator of the true MPM. Figures 5.13-5.15 track the MPM of the different MUELS systems as a function of the damping ratio versus the Monte Carlo MPM.

Table 5.2 lists the corresponding TEV and "best" parameters for each forcing factor, F_s. It is interesting to note that the ELS natural frequency for $F_s = 0.001$ and $F_s = 1$ both align with the frequency peaks in Figures 5.7-5.8. For $F_s = 10$, however, the relative lack of change in response as damping ratio and natural frequency changed provided a less meaningful result.

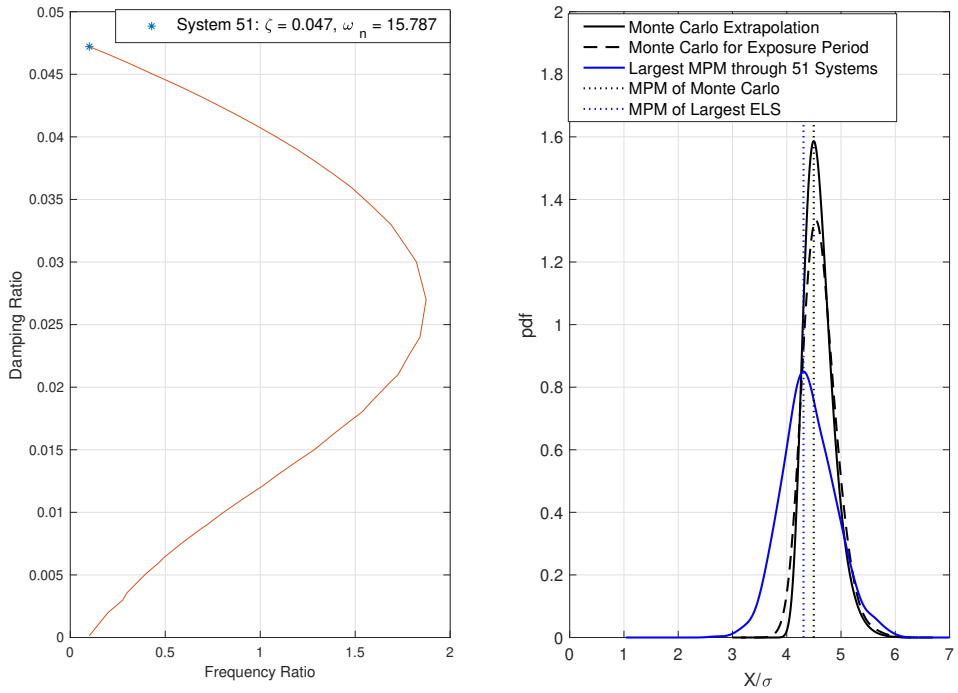

Figure 5.10: The ELS contour and MUELS pdf compared with Monte Carlo methods for $F_s = 0.001$.

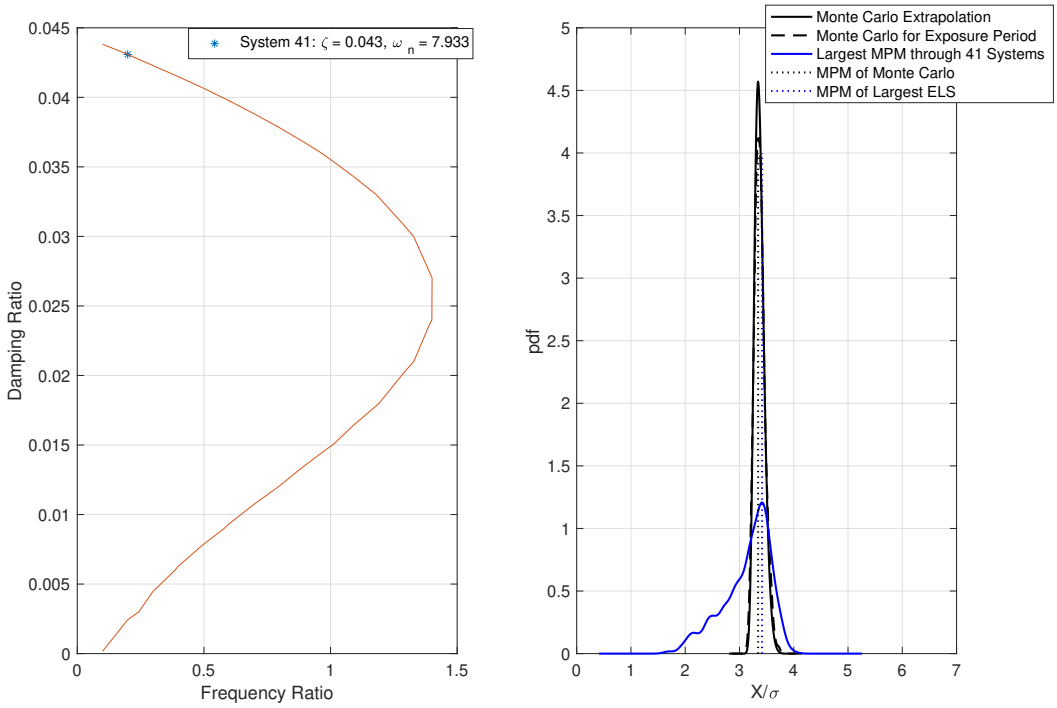

Figure 5.11: The ELS contour and MUELS pdf compared with Monte Carlo methods for $F_s = 1$.

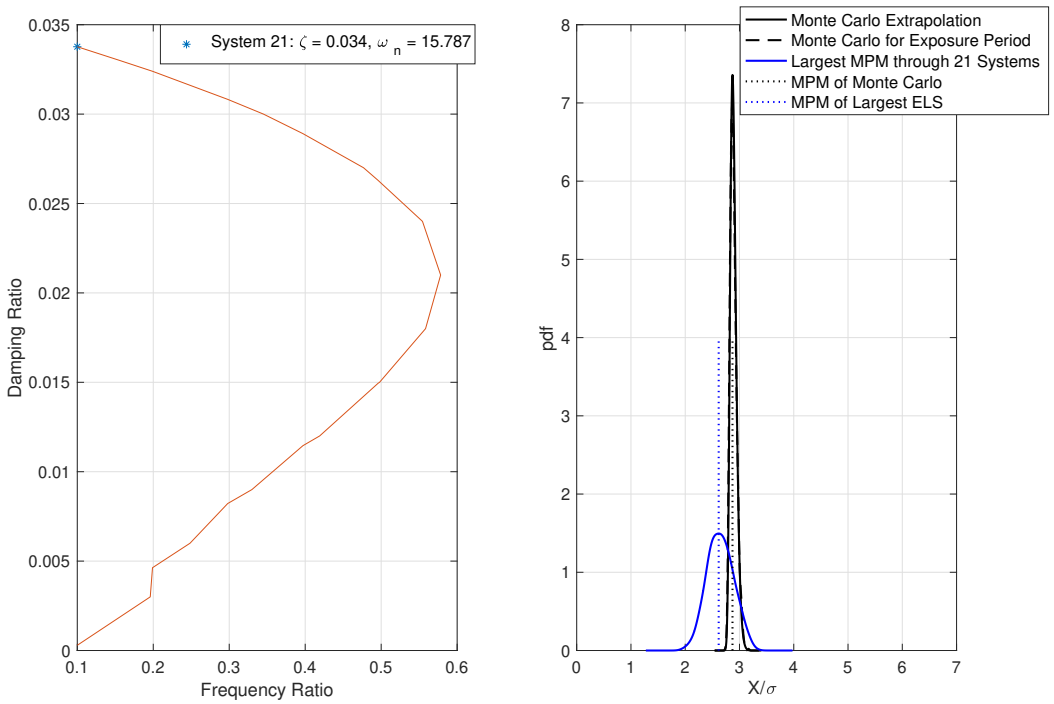

Figure 5.12: The ELS contour and MUELS pdf compared with Monte Carlo methods for $F_s = 10$.

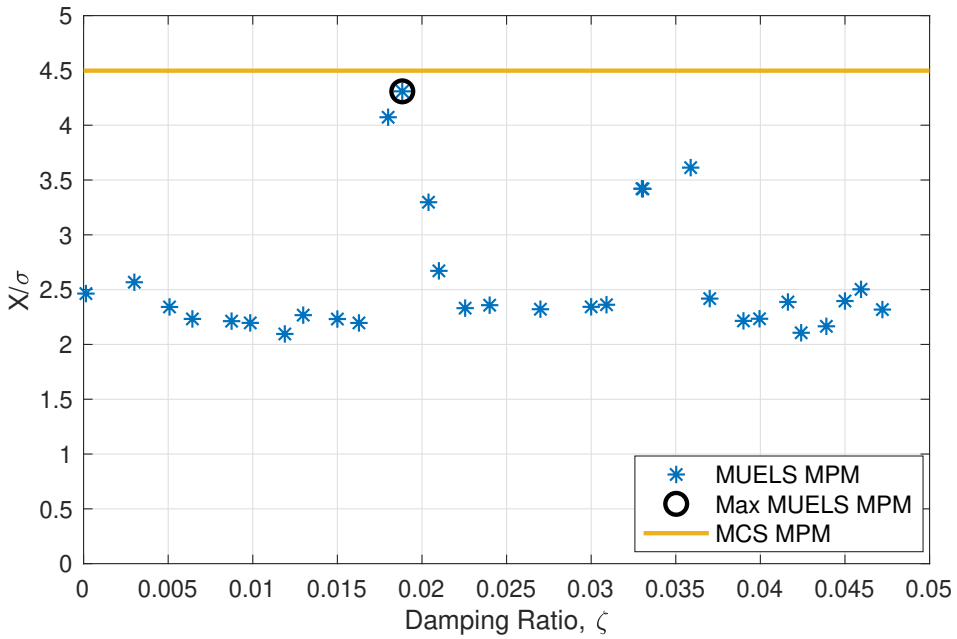

Figure 5.13: The most probable maxima of the MUELS pdfs as a function of the damping ratio, ζ, versus the most probable maximum normalized by the rms of the Monte Carlo Simulations for $F_s = 0.001$

5.4.2 MUELS Performance for Various TEVS

Running Monte Carlo simulations can be a computationally expensive method to estimating extremes for large exposure periods. The computational expense of the

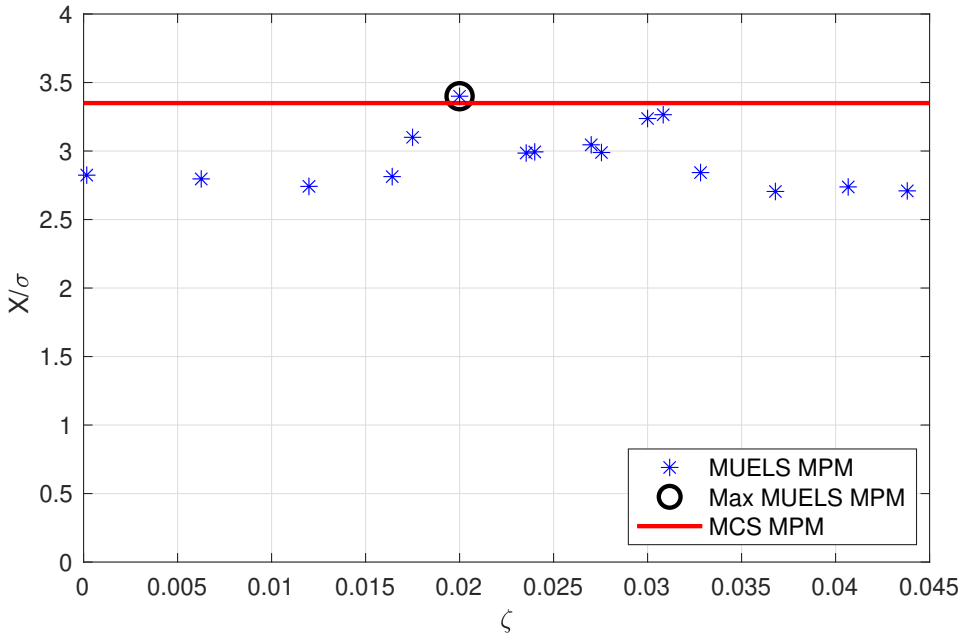

Figure 5.14: The most probable maxima of the MUELS pdfs as a function of the damping ratio, ζ, versus the most probable maximum normalized by the rms of the Monte Carlo Simulations for $F_s = 1$

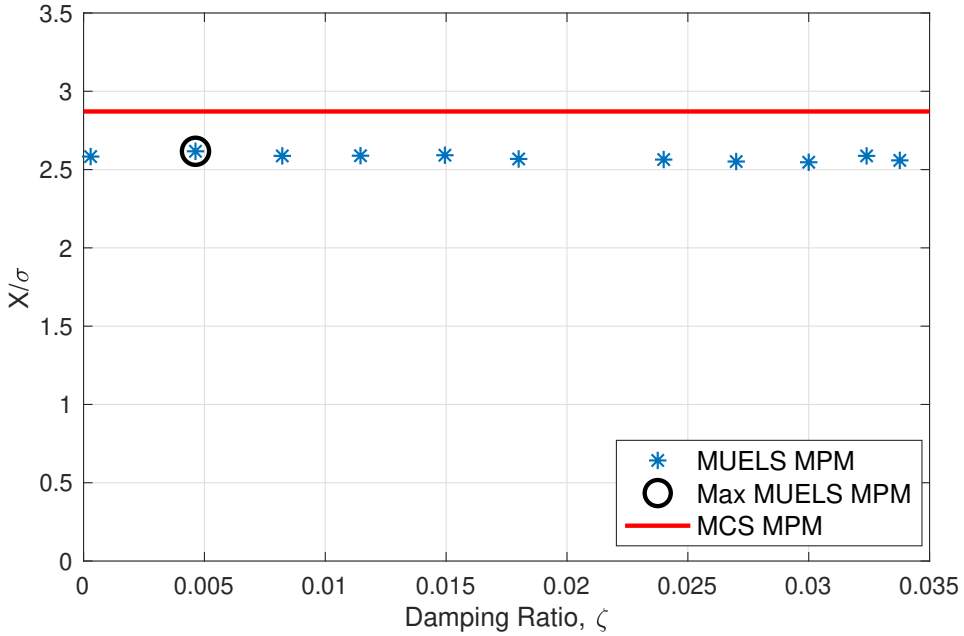

Figure 5.15: The most probable maxima of the MUELS pdfs as a function of the damping ratio, ζ, versus the most probable maximum normalized by the rms of the Monte Carlo Simulations for $F_s = 10$

MUELS method, however, is unaffected by the size of the TEV and therefore length of the exposure period. The following figures show the performance of the MUELS

Table 5.2: The natural frequency and damping ratio of the ELS that provided the largest most probable maximum for each F_s.

F_s	TEV	ω_n [rad/s]	ζ [ ]
10^{-3}	4.554	1.028	0.018
10^{0}	4.573	1.231	0.020
10^{1}	4.621	7.933	0.005

method compared to Monte Carlo simulations of various exposure periods. Additionally, MUELS MPM estimates for $TEV = 6$ and $TEV = 7$ are shown without comparison directly to Monte Carlo simulations, but to GEVD extrapolations based off of the Monte Carlo data from the $TEV = 5.45$ simulations. Monte Carlo simulations were not run for $TEV = 6$ and $TEV = 7$ due to computational limitations. For reference, a TEV of 7 represents around $4.3 * 10^{10}$ zero-upcrossings, or about 10^8 hours. The practicality of an event horizon of that scale may not be of particular interest in the marine industry, but the ability to access it without much issue is an option with the MUELS method.

Figures 5.16-5.18 display the performance of the MUELS method for each forcing factor versus Monte Carlo simulations and GEVD extrapolations. Due to the stochastic nature of the DLG results, ten MPMs were gathered for each set of parameters at the respective TEV and forcing factor, F_s.

It should initially be noted that the DLG is based off of an extrapolation of the Gaussian EVD. That being said, it has been noted that the extreme values provided by the DLG are a lower bound to the true EVD of interest. The general "overshoot" of the MCS MPM at lower TEVs is most likely linked to the Gaussian extrapolation of the DLG.

At larger TEVs, the results from the MUELS method are a lower bound to the MCS MPMs. Here, where the extrapolation made from the DLG is more accurate, the MUELS method follows the basic trend of the DLG. That is not to say that the MUELS method is simply applying Gaussian assumptions or tools to estimate the extremes, but it rather finds a linear system that has a similar return period on the exposure time of interest that can be used as a surrogate to extract input information that leads to extremes in both the linear and non-linear system.

To more rigorously investigate the performance of the MUELS method at the various TEV and forcing factor levels, the Table 5.3 displays the relative percent

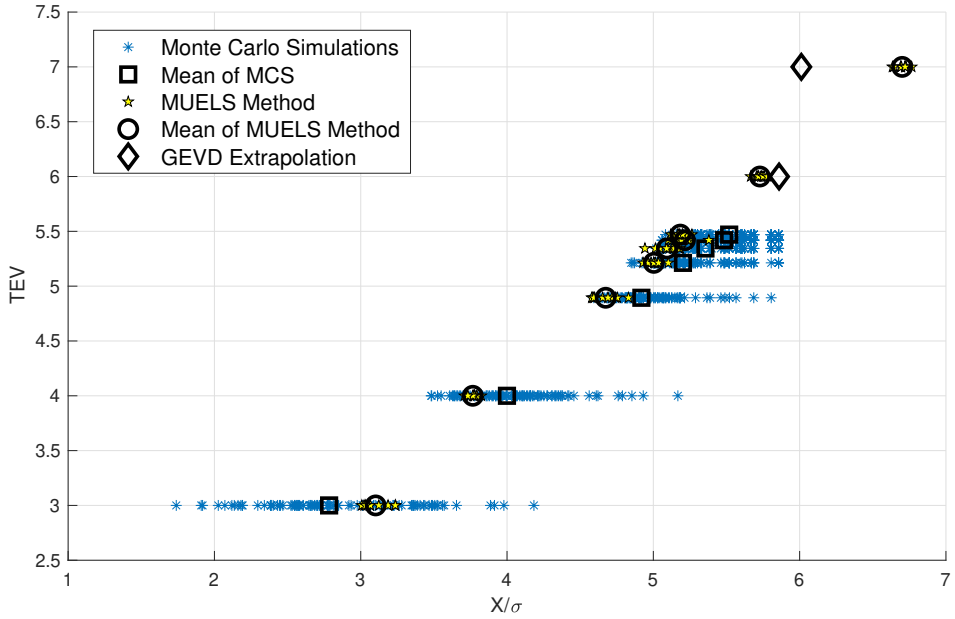

Figure 5.16: Most Probable Maxima collected from exposure periods of different lengths for $F_s = 0.001$ and GEVD extrapolations compared to a collection of the MUELS results. Also shown are the mean values for the MCS and MUELS method.

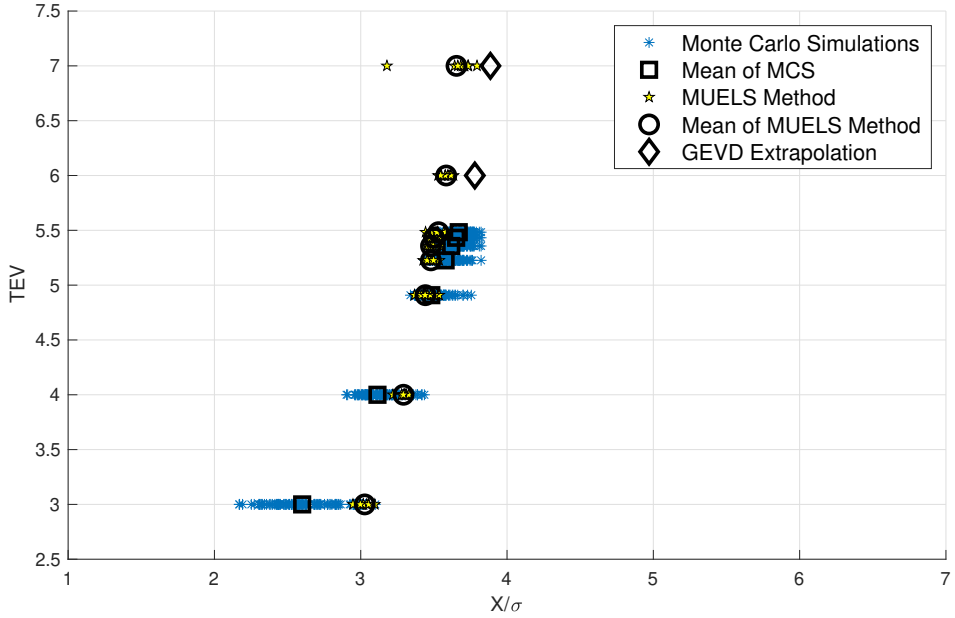

Figure 5.17: Most Probable Maxima collected from exposure periods of different lengths for $F_s = 1$ and GEVD extrapolations compared to a collection of the MUELS results. Also shown are the mean values for the MCS and MUELS method.

error for the MUELS results against the MCS. The error is defined in Equation 5.7.

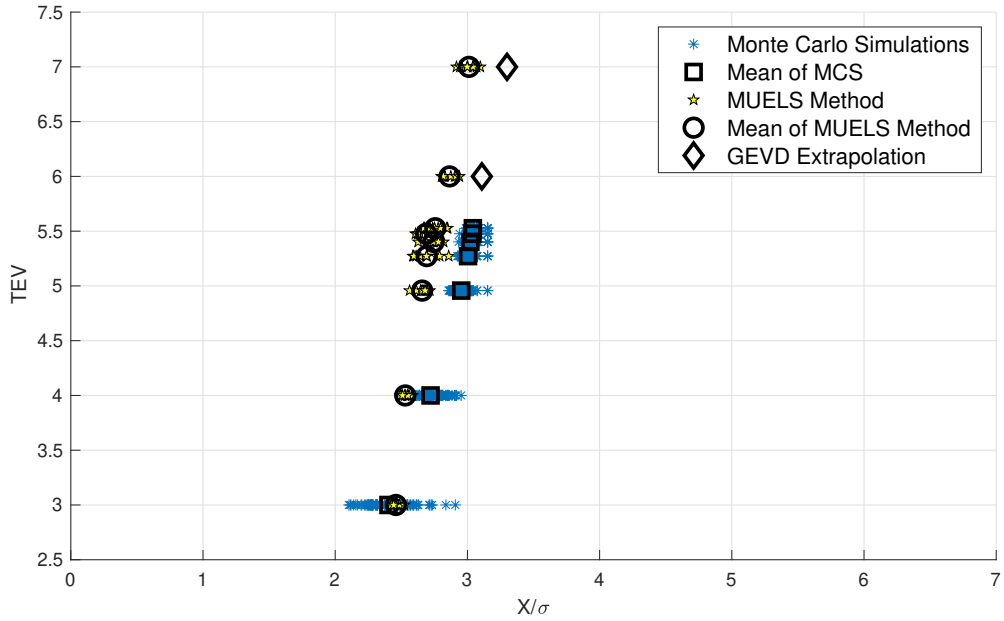

Figure 5.18: Most Probable Maxima collected from exposure periods of different lengths for $F_s = 10$ and GEVD extrapolations compared to a collection of the MUELS results. Also shown are the mean values for the MCS and MUELS method.

$$\epsilon = \frac{\bar{x}_{MUELS} - \bar{x}_{BL}}{\bar{x}_{BL}} \tag{5.7}$$

Here, $\bar{x}_{MUELS}$ is the mean of the MUELS MPMs and $\bar{x}_{BL}$ is the mean of the MCS MPM for TEVs below 6.0 and the most probable maximum of the GEVD extrapolation for TEVs above 6.0. It should be noted that since the zero-upcrossing period becomes amplitude dependent as the forcing factor increases, the corresponding number of peaks per simulation changes. The TEVs listed in the table are those from the $F_s = 1$ set of simulations. While the true TEVs for $F_s = 0.001$ and $F_s = 10$ are not shown in the table, the relative exposure times are unaffected for use of comparison. It should also be noted that the comparisons at the TEVs of 6 and 7 are made between the MUELS method and GEVD extrapolation results.

Table 5.3: The mean error between the MUELS method results and the Monte Carlo simulations at different forcing factors and TEVs.

	TEV								
F_s	**3.00**	**4.00**	**4.92**	**5.22**	**5.36**	**5.43**	**5.49**	**6.00**	**7.00**
10^{-3}	0.114	-0.058	-0.049	-0.038	-0.049	-0.049	-0.061	-0.022	0.115
10^{0}	0.165	0.057	-0.012	-0.028	-0.038	-0.042	-0.038	-0.052	-0.060
10^{1}	0.023	-0.070	-0.100	-0.104	-0.092	-0.11	-0.094	-0.079	-0.087

5.5 Discussion

In general, as discussed in Edwards et al. (2021), the MUELS method provided a lower bound to the Monte Carlo and General Extreme Value Distribution extrapolations. The MUELS method did seem to overshoot the lower TEV results, but this may be the result of essentially changing the experiment at that exposure period. When gathering maxima from the MUELS simulations, the largest point within two cycles of time $t = 0$ is considered the maximum for that particular simulation. The maxima window allows for any leading or lagging in the response of the non-linear differential equation when subjected to the DLG input. For an exposure period on the order of $TEV = 3$, there are around 90 cycles. Given that there are essentially five peaks to choose from in the MUELS simulation, the MUELS results spread to the upper tail of the $TEV = 3$ distribution.

It should also be noted how important and sensitive parameter selection is. If the theory that each non-linear system has a linear system that it shares extreme value inputs with is true, then it can be said that the selection of the linear system's parameters must be precise. Viewing Figure 5.13, the spike at a damping ratio of $\zeta = 0.018$ could have easily been missed with a larger discretization. That being said, there could be a point on the contour between the tested parameters that results in a better system. When looking at Figure 5.15, there is not a distinct peak. However, there could easily be a point in between the tested parameters that could have led to a peak. That being said, in the $F_s = 10$ case, the contour began to "disappear" and only provided 21 parameter sets to work with. Since the zero-upcrossing period increased with increasing F_s, there were less and less sets of ω_n and ζ that resulted in a linear system with the same zero-upcrossing period as the non-linear system. Due to the disappearing effect, one wonders if the best linear system for this particular case is a conventional two-parameter system. The MUELS method can easily be expanded to multiple parameters to generate multi-dimensional contours from which to test linear systems. While the approximation for the $F_s = 10$ case is good, improvements can certainly be made.

Another major component of the MUELS method is the ability to generate realizations of the extreme events at the exposure period of interest. To investigate the performance of the MUELS method, Figures 5.19-5.21 show the ensemble average of

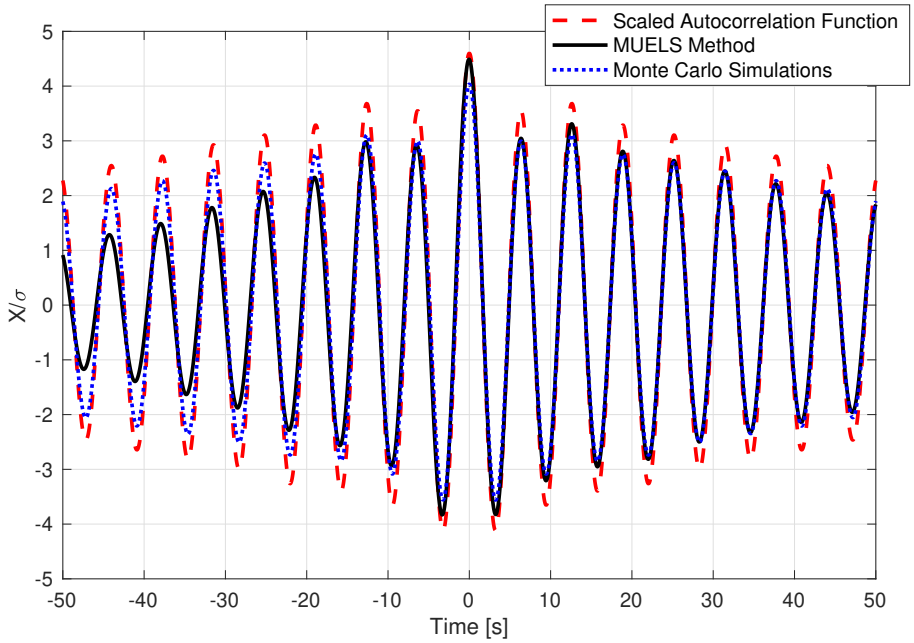

Figure 5.19: The ensemble average of the MUELS results versus the Auto-correlation function and ensemble average of Monte Carlo simulations near extrema for $F_s = 0.001$.

the MUELS results compared with slices of Monte Carlo simulations near extreme values and the scaled Auto-correlation function for TEVs around 4.60.[1] Lindgren (1972) showed the scaled Auto-correlation function (ACF) for a given Gaussian system approximates the shape of the ensemble average of the extreme realizations. The auto-correlation function is scaled by TEV/σ and is shown here to demonstrate the deviation from linearity and Gaussianity.

The goal of the MUELS method is to close the gap on the following expression:

$$E[Y(\tau - \phi/\omega_z)|Z(t) \in \hat{Z}(t)] \approx E[\hat{X}(t)] \tag{5.8}$$

where $Y(t)$ represents the Duffing Oscillator process when introduced to input from the DLG, τ is the location of the extrema in process $Y(t)$, ϕ is the phase shift of $t = \tau$ from $t = 0$, with respect to the zero-upcrossing frequency ω_z, $Z(t)$ is the selected equivalent linear system, $\hat{Z}(t)$ is the set of extreme linear realizations from the DLG run at the TEV of interest, and $\hat{X}(t)$ is the set of non-linear Duffing Oscillator extremes corresponding the exposure period of concern. If Equation 5.8 is an equality, there is no difference between the time series produced by MUELS

[1]Due to the amplitude dependent zero-upcrossing period, the number of cycles in the given exposure period varied with F_s.

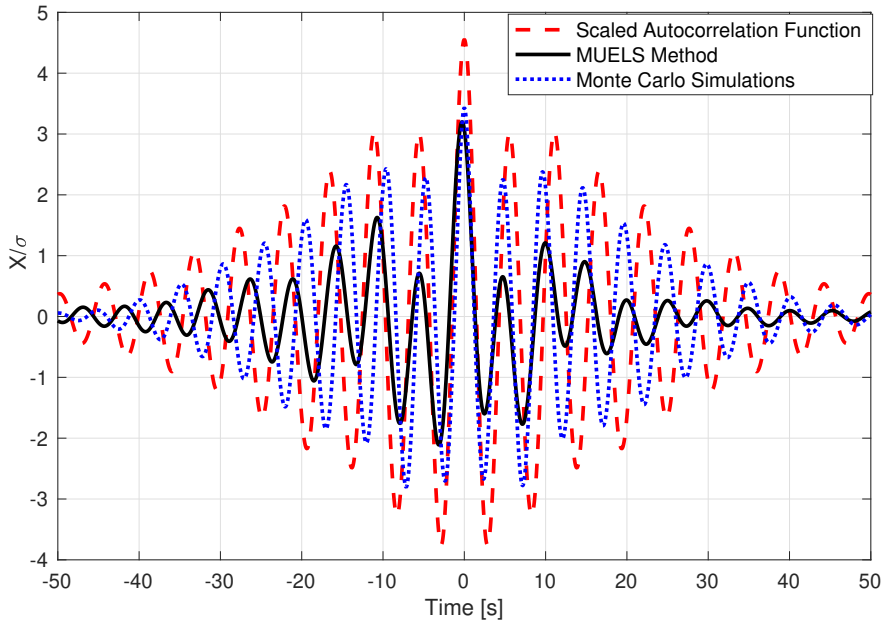

Figure 5.20: The ensemble average of the MUELS results versus the Auto-correlation function and ensemble average of Monte Carlo simulations near extrema for $F_s = 1$.

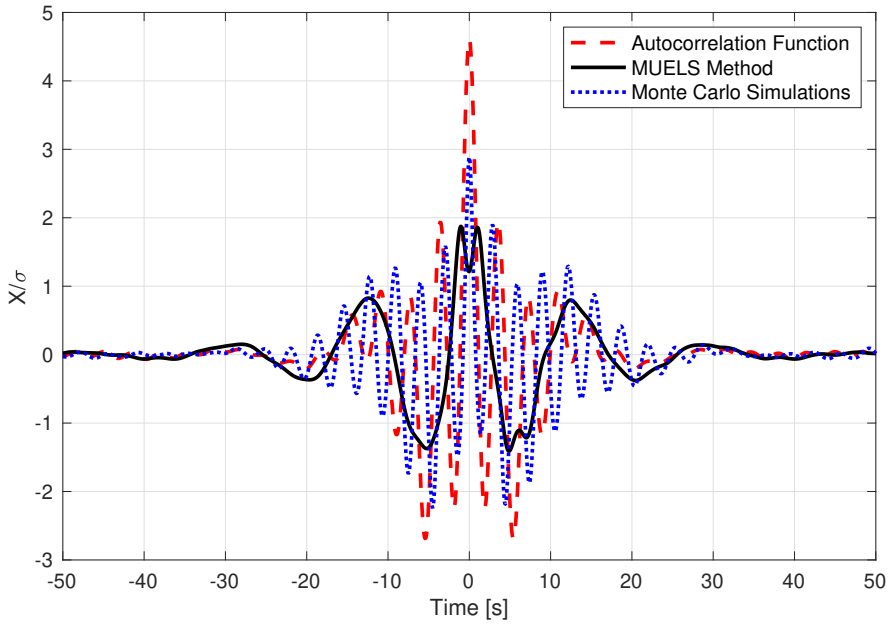

Figure 5.21: The ensemble average of the MUELS results versus the Auto-correlation function and ensemble average of Monte Carlo simulations near extrema for $F_s = 10$.

and the extreme time series from Monte Carlo simulations. As more non-linearities are introduced, the likelihood of reaching the equality decreases, due to increased complexity of non-linear transfer functions and the interaction with the phases that

the DLG produces. The explored forcing factors had various levels of success with reaching equality in Equation 5.8. It follows that the MUELS method could be applied to other oscillators that are defined by differential equations with success dependent on the severity of non-linearity.

In Figure 5.19, the MUELS method generally follows the shape of the Monte Carlo simulations and Auto-correlation function. Since the forcing factor is relatively small and the exposure period is moderate, the Duffing Oscillator with the given parameters is nearly Gaussian. As such, the DLG performs well and the MUELS method almost acts as an identity matrix in the transform from input to extreme realizations. The MUELS method does show some asymmetric behavior, however, which may point to some level of dependence on initial conditions. It should be noted that the initial conditions for all MUELS runs are from a stationary, mean position or $[0; 0]$ and the MUELS records were run from $t = [-200, 200]s$, with the expected extrema near $t = 0s$.

The asymmetry is more distinct in the $F_s = 1$ case in Figure 5.20. While the MUELS method reproduced extrema on the order of the MCS, it appears that the exact reproduction was lost due to phase differences in the input. Figure 5.20 is also demonstrates the non-linearity added by increasing the forcing factor. If the Duffing Oscillator was still a linear operator, the resulting output should have been Gaussian since the input was Gaussian. Since the MCS for $F_s = 1$ vary from the ACF, the ensemble average of the Duffing Oscillator near extrema contradict Lindgren's results and are clearly non-linear and non-Gaussian. However, the MUELS method, while using the Gaussian principles in the DLG, was able to nearly reproduce the extreme behavior seen in the MCS.

In the $F_s = 10$ case, there is a distinct difference between the three time series. The ACF does little aside from displaying the increased degree of non-linearity. The difference in the MCS and MUELS results, however, are more notable. The ensemble average of the MUELS method not only under-predicts the MCS, but also is composed of much lower frequency content. In this case, the extrema produced by the MUELS method were spread around $t = 0$ in a nearly symmetric fashion. Figure 5.22 shows the extrema phase shift distribution for the $F_s = 10$ MUELS realizations.

The distribution of phases in Figure 5.22 appears to be predominantly leading or lagging around $\pm 60°$. The reasoning behind this distribution is an active area of

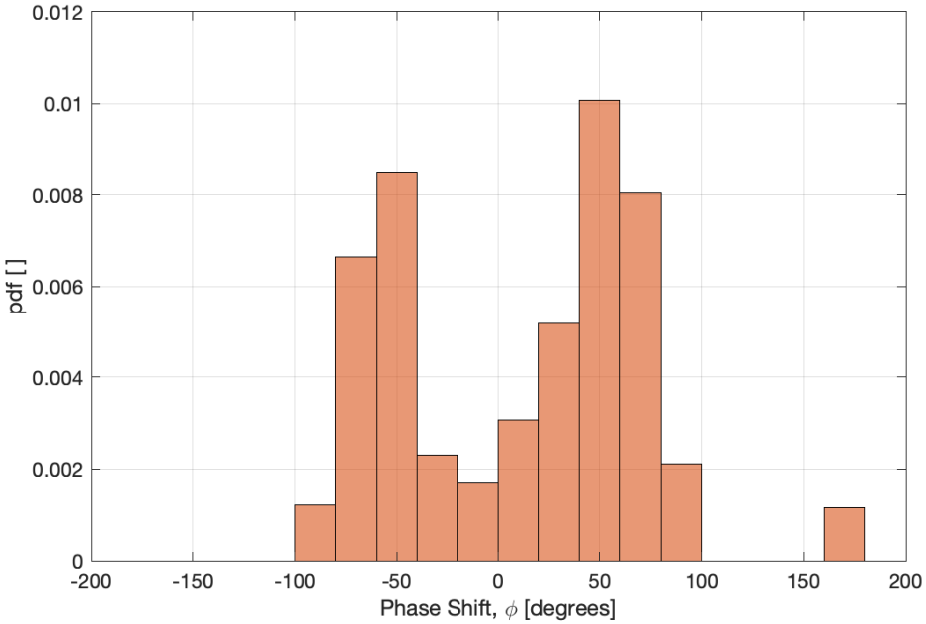

Figure 5.22: The phase distribution for $F_s = 10$ MUELS extrema with respect to $t = 0\,s$ and $\omega_z = 1.301\,rad/s$.

research. To help correct for the phase difference in producing the MUELS realizations, a time shift was made. By moving the global location of each extrema, $t = \tau$, to line up with the global time $t = 0$, the asymmetry effect was removed and the gap in Equation 5.8 was reduced. Figure 5.23 shows the MCS extreme ensemble average, and the centered ensemble average of the MUELS method for $F_s = 10$.

In Figure 5.23, it appears that the higher frequency content is similar to that of the MCS but the phase difference resulted in the appearance of a lower frequency and lower peak value in Figure 5.21. It is likely that this phase difference is more random throughout the different realizations of the MUELS method and result in the shape of the ensemble average in Figure 5.21.

The existence of the low frequency content is also of interest. It appears that there is some level of low frequency content in the ACF and MCS, as evidenced around $t = \pm 25\,s$ where the higher frequency oscillations move with some low frequency mean. To look further into the frequency content, Figure 5.24 shows an FFT of the MUELS method data and the MCS for $F_s = 10$.

In Figure 5.24, it can be seen that the MUELS and MCS frequency decompositions share common frequency groups but differ on which group is the dominant one. The issue with frequency discretization in the contour shows here since the best lin-

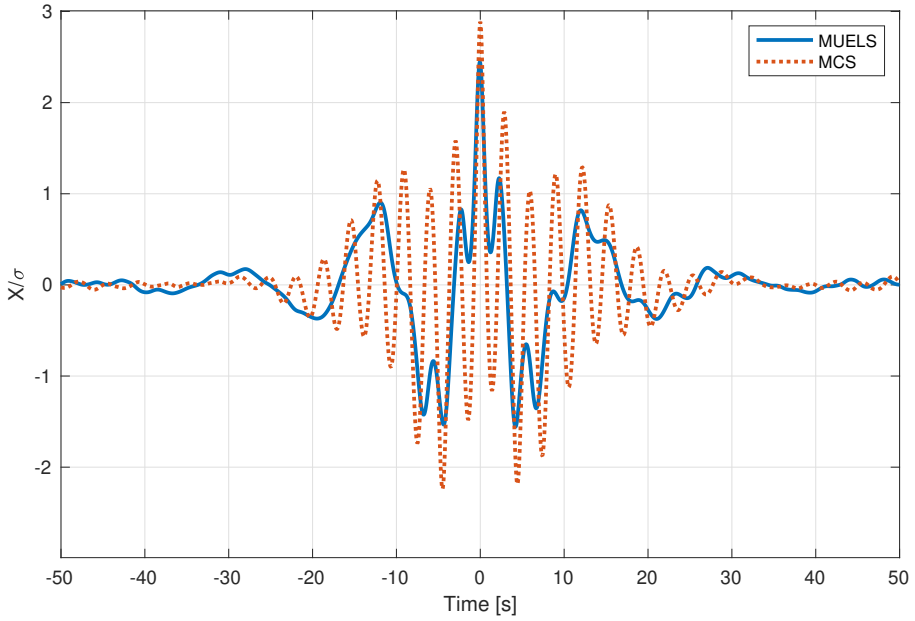

Figure 5.23: The centered ensemble average of the MUELS results versus the Auto-correlation function and ensemble average of Monte Carlo simulations near extrema for $F_s = 10$.

ear system for $F_s = 10$ had a natural frequency of around $8.0\,rad/s$. Since the wave spectrum is close to narrow banded, the meaningful forcing frequencies range from about $0.2-2.0\,rad/s$. With essentially a unit response at the meaningful frequencies, the resulting forcing is set up to produce a response at the peak forcing frequency of $0.45\,rad/s$, which matches that of the MUELS method. Again, the need for a more finely discretized contour and/or a higher dimensional contour from which to select parameters is suggested.

Table 5.4 tabulates the key features of the MUELS method results and MCS results. It should be noted the $F_s = 10$ stats are from the time shifted ensemble average and the zero-upcrossing frequency was calculated using all of the MUELS realizations rather than the ensemble average.

Table 5.4: The mean error between the MUELS method results and the Monte Carlo simulations at different forcing factors and TEVs.

F_s	TEV	$\omega_n\,[rad/s]$	ζ	$\omega_p\,[rad/s]$	$\omega_{z,MCS}\,[rad/s]$	$\omega_{z,MUELS}\,[rad/s]$	$\frac{max(MUELS)}{max(MCS)}$
10^{-3}	4.55	1.03	0.02	0.45	1.01	1.01	1.11
10^{0}	4.57	1.23	0.02	0.45	1.60	1.54	0.93
10^{1}	4.62	7.93	0.01	0.45	2.62	2.10	0.86

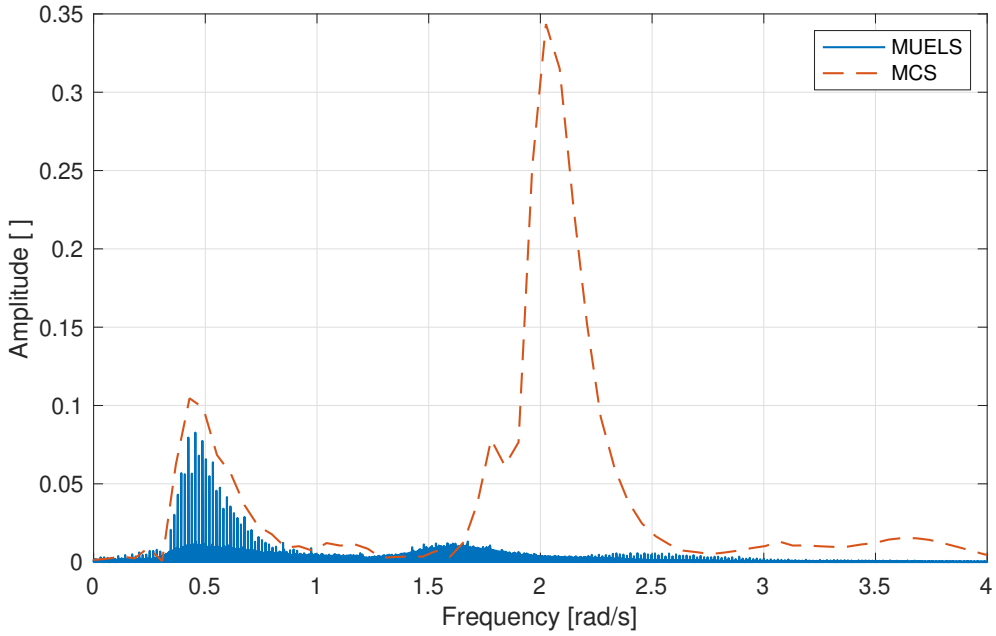

Figure 5.24: A Fast Fourier Transform of the ensemble average of the MUELS results and Monte Carlo simulations for $F_s = 10$.

5.6 Conclusion

In this chapter, the MUELS method was demonstrated using the Duffing Oscillator at various levels of non-linearity, as in Edwards et al. (2021). The single TEV test showed that the MUELS method produced pdfs that had various levels of overlap with the MCS extreme pdfs and could predict the most probable maximum within 10% in the most non-linear case ($F_s = 10$). In the multiple TEV test, the MUELS method produced results that were generally a lower bound within 11% of the Monte Carlo and GEVD extrapolated results, performing better in the more linear cases ($F_s = 0.001, F_s = 1$) than the more non-linear case ($F_s = 10$). It should be noted that this margin is sufficient for some applications. When looking at the time series comparisons, the MUELS method was able to nearly reproduce the ensemble average maximum and zero-upcrossing frequency when compared to Monte Carlo simulations. Most of the realizations for the $F_s = 0.001$ and $F_s = 1$ case could be considered candidates for extreme realizations of the Duffing Oscillator at the given parameters. While the $F_s = 10$ case required a time shift correction and the ensemble average was still visibly different from the Monte Carlo time series, a number of the individual time series could be considered extreme realizations of the Duffing

Oscillator at the given TEV.

That being said, a method to identify MUELS realizations that belong to the set of extreme realizations of the non-linear system is currently being studied. By using an Acceptance-Rejection (A-R) method, unlimited realization from MUELS could be produced and run through a A-R method to obtain the desired number of realizations that can be considered extreme realizations of the non-linear system.

Another matter to consider is uncertainty of the results. There exists an intrinsic "uncertainty" within the randomness of the DLG phase selection but there is also statistical uncertainty as well. While Figures 5.13-5.15 include results from multiple samples, more could be done to reduce uncertainty. The GEVD parameters used for comparison will include confidence bounds in future work and more samples of the MUELS results will be include to reduce bias and other uncertainty.

Overall, in this chapter, it was shown that the MUELS method was able to estimate extreme characteristics of a sub-harmonically forced Duffing Oscillator with varying levels of non-linearity with a sufficient level of accuracy. Further improvements and limitations of the MUELS method are studied further in this dissertation to understand the potential of this novel technique.

The next chapter details applying the MUELS method to a super-harmonically forced system. In certain conditions, a super-harmonically forced Duffing oscillator could display stochastic bifurcations which involve "jumping" between two oscillatory domains of attraction. The non-linear dynamics displayed in a system with a stochastic bifurcation not only provide another non-linear limitation test for the MUELS method but also show that the MUELS method is an effective tool for rare behavior identification.

Chapter 6

Super-harmonically Forced Duffing Oscillator

6.1 Introduction

In this chapter, a Duffing oscillator under higher peak frequency forcing is investigated with the MUELS method. Not only does the super-harmonically forced Duffing oscillator display interesting dynamics, but it also provides another test to explore the non-linear limits of the MUELS method. Furthermore, the stochastic bifurcation property of the Duffing oscillators used in this chapter provides a basis for the system identification ability of the MUELS method. The methodology of the super-harmonically forced Duffing oscillator study, including a novel stationarity test, is presented. Then, probability density function and time series behavior near extremes comparisons are made between the MUELS method and Monte Carlo simulations.

6.2 Methodology

In this section, the problem is set up and the methods used for analysis are introduced and explained. First, the Duffing oscillator is reintroduced and the specific interesting characteristics are discussed. Second, a stationarity test designed to estimate the relative stationarity of three Duffing oscillator configurations is developed. Third, the selected system parameters are detailed and the set up of the Monte Carlo simulations is discussed.

6.2.1 Problem Statement

To demonstrate the capability of the MUELS method to identify extreme characteristics in non-stationary systems, Duffing oscillators with fixed system parameters excited by a sea spectrum and variable forcing factor were used. The Duffing oscillator can be representative of roll motion in ships due to the cubic stiffness term representing the non-linear restoring force. Identifying extreme characteristics of

roll motions is of utmost importance due to potential capsize or damage to crew, machinery, or cargo. With the right set of parameters and forcing factor, the Duffing oscillator can exhibit stochastic bifurcations (Namachchivaya, 1990). Thus, the Duffing oscillator is a practical and relevant model to investigate. The equation of motion for the Duffing oscillator is as follows:

$$\ddot{x} + d\dot{x} + \alpha x + \beta x^3 = F_s \eta(t) \tag{6.1}$$

where x is displacement, a dot represents a derivative with respect to time, d is linear damping, α is linear stiffness, β is cubic stiffness, F_s is the forcing factor, and $\eta(t)$ is a stochastic time series drawn from an ocean-wave spectrum. In this chapter, an ITTC spectrum (ITTC, 2002) was used with a significant wave height of 3.0 and a modal period of 2.1 s. The forcing factor, F_s is the key parameter in determining the level of non-stationarity

The stochastic bifurcations present with the certain parameters generate statistics that change with time, resulting in non-stationary processes. In this chapter, these bifurcations are used as a measure of stationarity as well as a characteristic that may or may not be known about the system.

6.2.2 Stationarity Tests

In this application, the weak-sense definition of stationarity the primary focus. A weak-sense stationary process essentially has a mean that is constant in time i.e., no trends, as well as a variance that does not change with time. The non-stationary systems investigated in this chapter had a bifurcation into two distinct domains of attraction with differing rms values. As such, the stationarity tests performed were done by calculating a moving root mean square (rms) of each time series. By calculating the moving rms, any excursions into the other domain of attraction were detected by counting the number of threshold upcrossings of the moving rms. The moving rms is a system function in *MATLAB* that calculates the rms of overlapping, variable length windows centered about a given point (Matlab, 2016). Since all of the processes in this chapter are zero-mean, the rms is a measure of the moving standard deviation and therefore variance. The key parameter in the moving rms metric is the window size, or the number of points that are included in each calculation of the rms. For this chapter, a window size of 10,000 points was selected such that

extremes from a given basin did not influence the moving rms enough to provide any misidentified excursions into the large attractor while ensuring that individual exceedances could be separated from each other. Of course, there are uncertainties or expected fluctuations with estimating moving mean and variance. To account for these uncertainties, probability distributions of the moving rms were estimated using a kernel density estimator (kde) and the x-value at the largest magnitude peak of said distribution was considered a principal value. Using the x-value of the largest magnitude peak as the principal value is essentially taking the most probable rms of the most represented attractor as the basis for potential stationarity. Given the fact that the moving rms is essentially a filter and it "smooths" out exceedances with window size selection, the rarity of threshold exceedances is increased even more. Therefore, a measure of Gaussian rareness was applied to set the threshold and account for any natural variations. The rareness of an event in a Gaussian process is typically normalized by the standard deviation of the process, like mentioned in Section 6.1. In this chapter, the threshold was set at 10 standard deviations of the moving rms above the mean rms for the entire time series. The moving rms pdfs were not necessarily Gaussian but by using a larger number of standard deviations, the probability of non-exceedance does increase and is sufficient for this application. To determine the standard deviation of the moving rms, the variance of a truncated pdf of the moving rms was calculated. The truncation point of the moving rms pdf was determined by cutting the pdf off at a point that the principal attractor was no longer represented. An example pdf of the moving rms along with the truncation point are shown in Figure 6.1.

It can be said with reasonable confidence that excursions above this threshold likely are a result of the rms, and therefore variance, changing with time rather than statistical uncertainty. It should be noted at this point that exceedances are defined in this chapter to be the amount of upcrossings of the moving rms above the threshold. An example graph of one of these tests can be seen in Figure 6.2.

Note that in this case, a moving rms window of 10,000 points was used and that there are four exceedances above the threshold.

6.2.3 System Parameters

System parameter selection was done such that there were interesting dynamics and three systems of varying non-stationarity. Table 6.1 lists the fixed system parameters

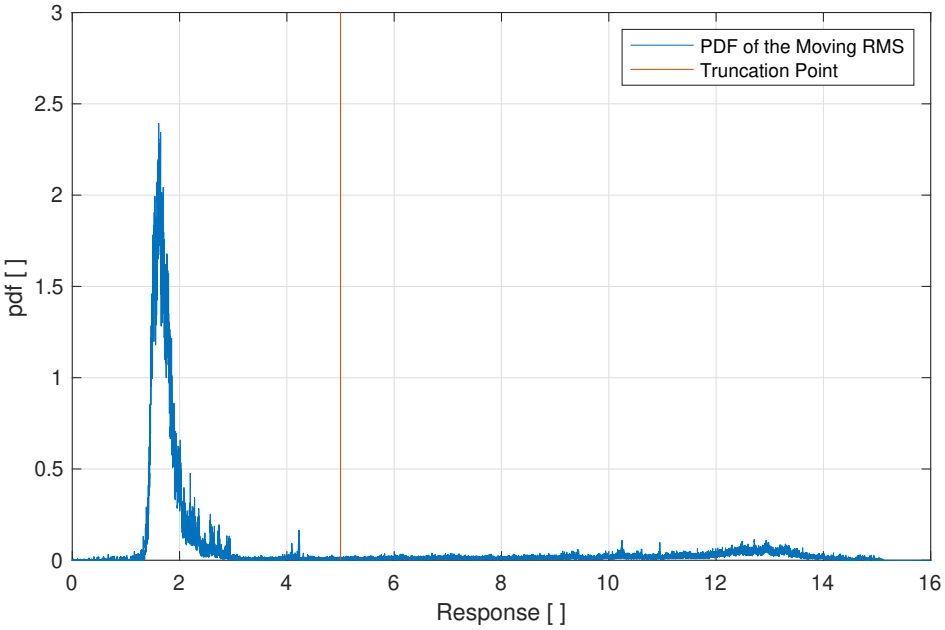

Figure 6.1: An example pdf showing where the truncation point was placed for estimated statistics for the dominant attractor.

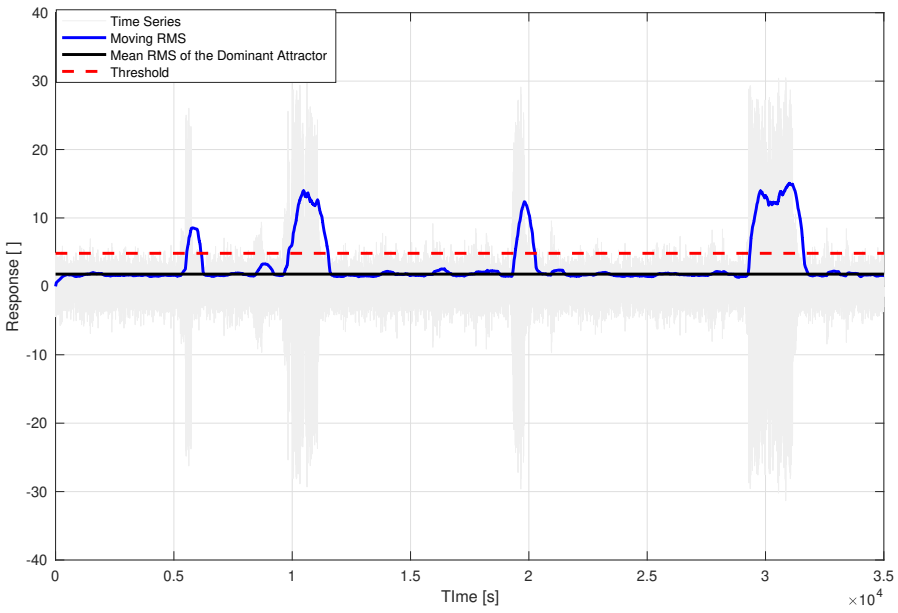

Figure 6.2: The moving rms of an example Duffing oscillator shown versus the threshold and the average rms of the dominant attractor.

including the modal period, T_m and the significant wave height, H_s, of the ITTC spectrum.

The forcing factors were selected such that there was a system that was station-

Table 6.1: Values for the system parameters.

Parameter	Value
d	0.02
α	1.00
β	0.04
T_m	2.10
H_s	3.00

ary i.e., zero excursions in the stationarity test, a system with some non-stationarity i.e., one or two excursions per time series, and a system with major non-stationarity i.e., several excursions per time series. It follows that the systems with the non-stationarity feature "jump" to a larger domain of attraction. These interesting dynamics are a result of the system parameter selection, namely F_s and T_m. The tests discussed in Section 6.2.2 were used to modulate the degrees of non-stationarity. Each test was run for 10 time series of length 2^{22} points and a $dt = 0.05\,s$ and the number of excursions for each time series and forcing factor were recorded and averaged. The forcing factors, threshold information, and average number of excursions are shown in Table 6.2 and Figures 6.3-6.5 show characteristic graphs of the stationarity tests.

Table 6.2: Forcing factors selected for analysis, the standard deviation of the dominant attractor, σ_{DA}, the threshold for counting excursions and the average number of threshold exceedances for an exposure period of 58.3 hr. Note that fewer excursions indicate more stationary processes. Stationary processes have a very high probability of having zero excursions.

F_s	σ_{DA}	Threshold	N_{exc}
10.0	0.85	1.06	0.0
14.7	1.36	2.58	0.8
17.0	1.78	6.41	18.2

In Figures 6.3-6.5, the excursions above the given threshold increase as the forcing factor increases. It should be noted that the number of excursions for the $F_s = 14.7$ case ranged from zero to two excursions in a given time series. In the $F_s = 14.7$ and $F_s = 17.0$ cases, it is clear that the variance change with time and the processes are not stationary.

To provide a more intuitive measure of the non-stationarity, magnification curves for each system are shown in Figures 6.6-6.8 and extreme pdfs for 58-hour exposure periods are in Figure 6.9.

Note that at the peak forcing frequency of $3.0\,rad/s$, which corresponds to the modal period of $2.1\,s$, there are two stable responses for each forcing factor. These

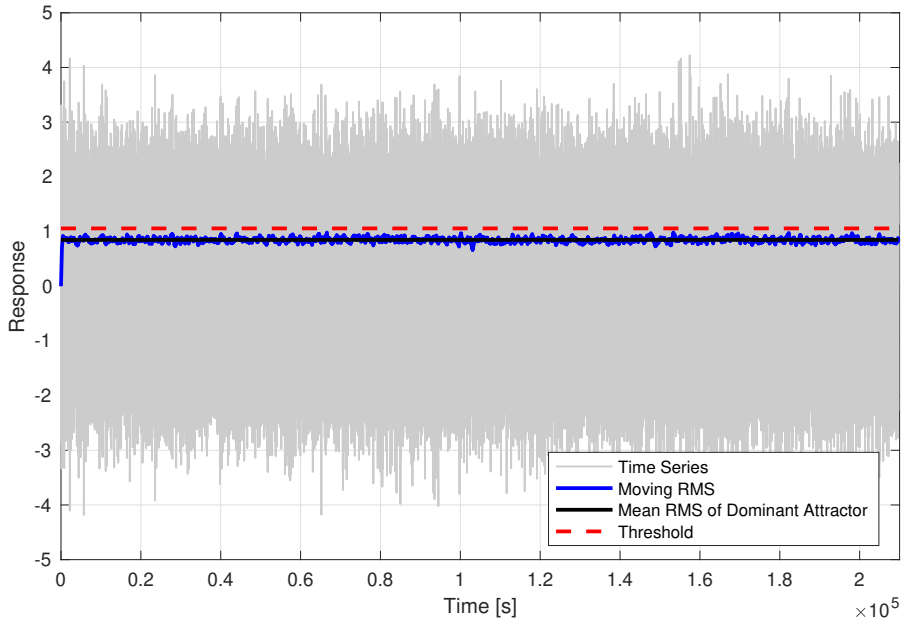

Figure 6.3: An example stationarity test for $F_s = 10.0$. Note that there are no excursions in this example.

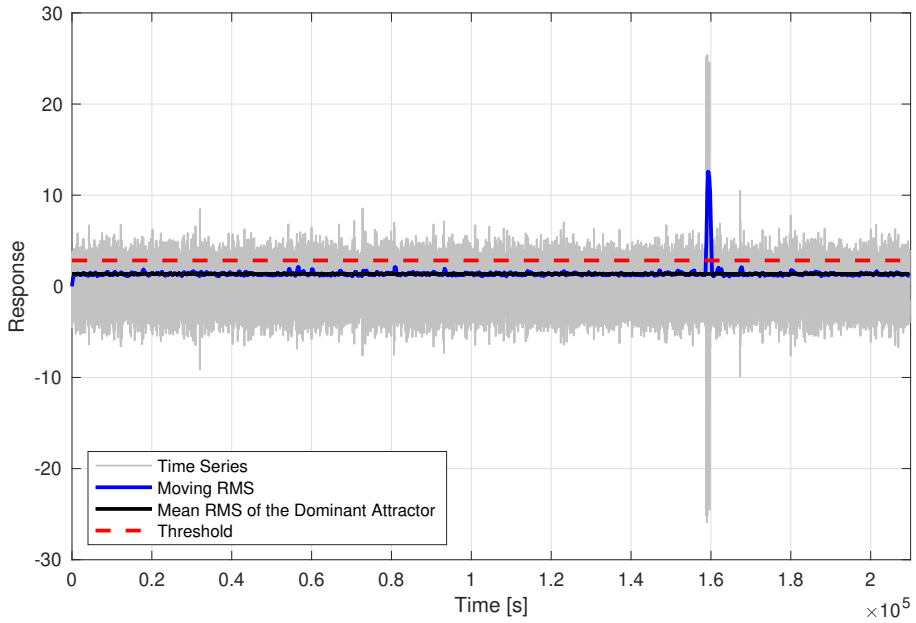

Figure 6.4: An example stationarity test for $F_s = 14.7$. Note that there is a single excursion in this example.

stable responses act as domains of attraction for the oscillator. The magnitude of the larger stable response decreases with an increasing forcing factor which explains the increase in frequency of excursions into the larger domain. The upper branch

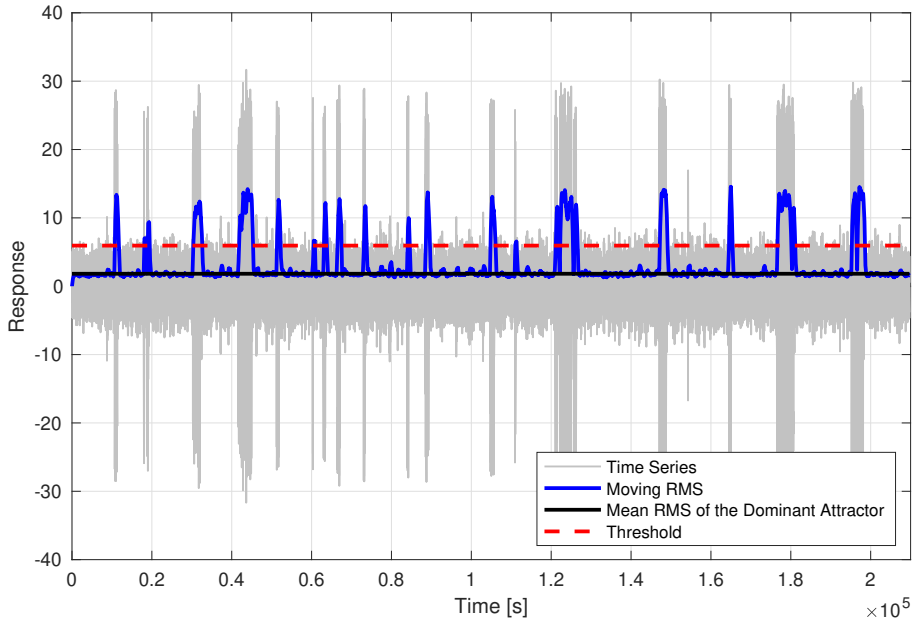

Figure 6.5: An example stationarity test for $F_s = 17.0$. Note that are 19 discrete excursions in this example.

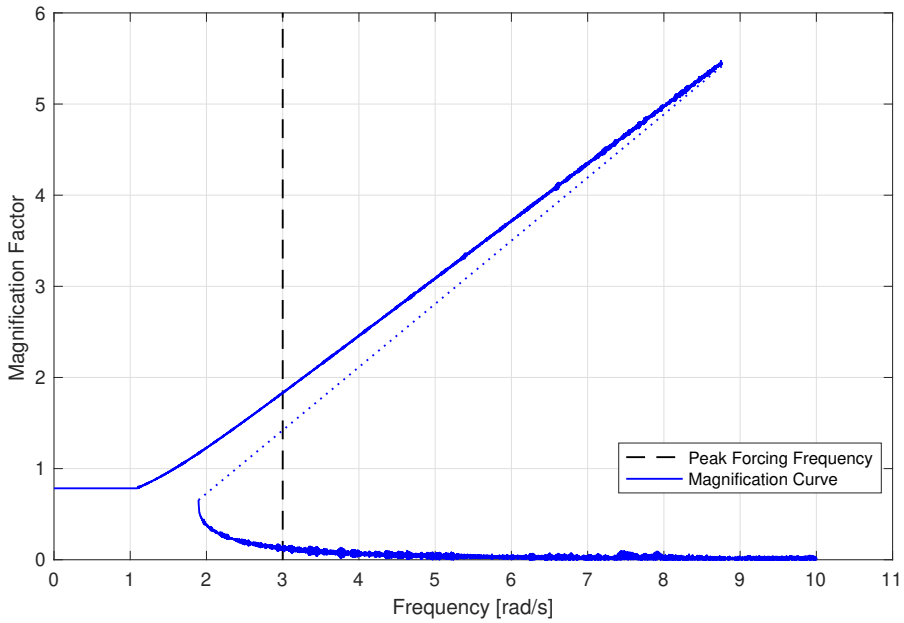

Figure 6.6: Magnification curve for $F_s = 10.0$ along with the peak forcing frequency. Note that the dotted line is an unstable branch.

is generally not sustained for extended periods of time, but larger forcing factors can result in a longer duration of upper branch oscillations. Simply put, weak sense stationarity dictates that both the mean and variance remain constant in time. While

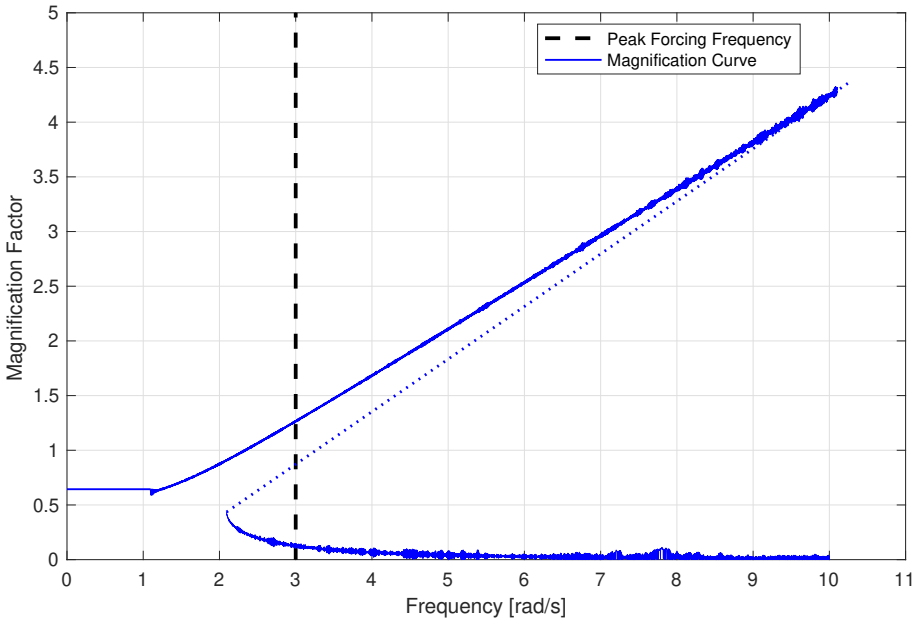

Figure 6.7: Magnification curve for $F_s = 14.7$ along with the peak forcing frequency. Note that the dotted line is an unstable branch.

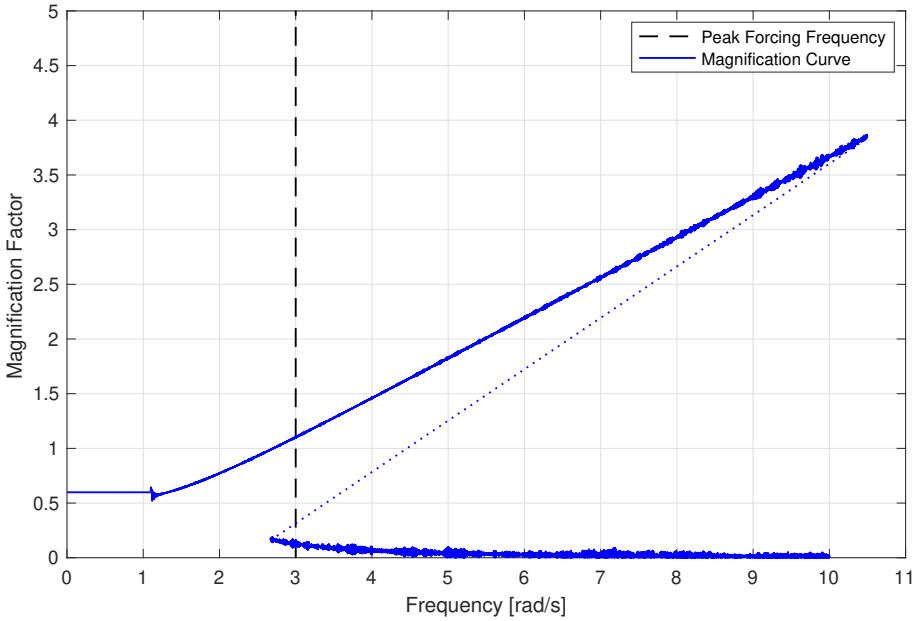

Figure 6.8: Magnification curve for $F_s = 17.0$ along with the peak forcing frequency. Note that the dotted line is an unstable branch.

the mean of each time series remains constant, it is clear that the variance would change due to the excursions into the larger domain.

The three extreme pdfs for the different forcing factors give an idea of how often

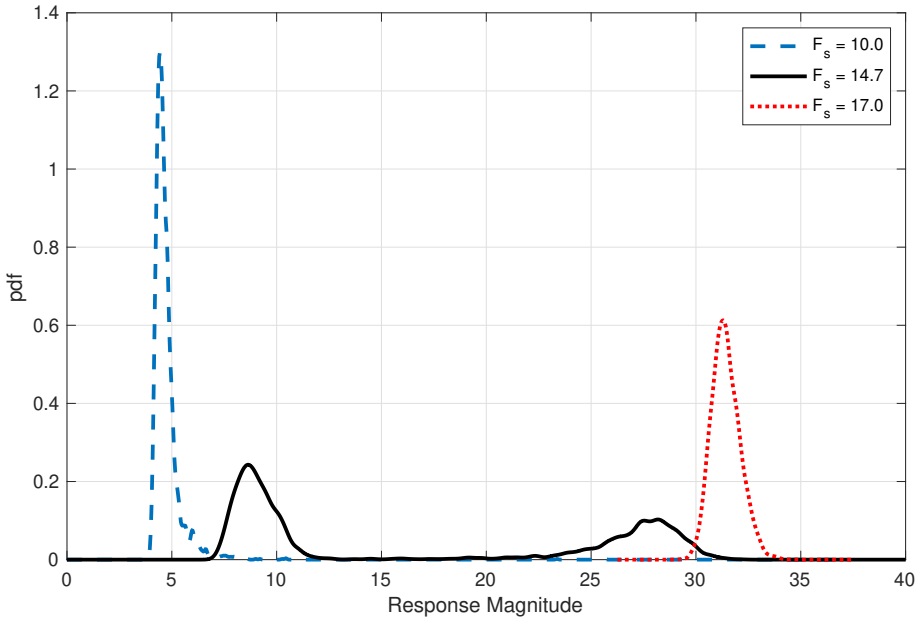

Figure 6.9: Kernel density estimated probability density functions for the largest value in a 58-hour long time series for each forcing factor.

exceedances occur. Note that these are drawn from the maximum value in each of 4,000 Monte Carlo simulations of length $N = 2^{22}$ points. In the $F_s = 10.0$ case, the extreme pdf is almost entirely limited to lower domain of attraction while the $F_s = 14.7$ case is split between the two domains of attraction. The $F_s = 10.0$ case did have 5 total excursions in the entire set of 4,000 Monte Carlo simulations of length $N = 2^{22}$. Each time series in the $F_s = 17.0$ case had an exceedance, and the extreme pdf reflects that.

6.2.4 Matched Upcrossing Equivalent Linear System (MUELS) Method

To generate extreme realizations of a non-linear system such as the Duffing oscillator, the MUELS method, developed in Edwards et al. (2021), was used. It should be noted that the MUELS method uses the Target Extreme Value (TEV), as discussed in Section 6.1, as a metric for the return period. The TEV measures rareness of Gaussian processes and does not necessary share a correlation with rareness of non-Gaussian or non-stationary processes.

It should also be noted that in this chapter, the DLG is set up to produce 1,000 realizations of 100 seconds for each MUELS run. Furthermore, 2,048 frequency components were used to ensure fine enough discretization for the various linear natural frequencies and resulting transfer functions. The current method to select

parameters is to choose the set that results in the extreme pdf whose peak has the largest x-value. This method is used due to the lower bound property inherent to the DLG (Kim, 2012).

6.2.5 Monte Carlo Simulations

For sake of comparison, Monte Carlo simulations (MCS) were also performed. For each system, 4,000 runs of 2^{22} points with a dt of 0.05 s, or 58.3 hours, were generated. The time frame of 58.3 hours corresponds to a TEV of about 4.80 in each forcing factor case, with slight variations following the change in upcrossing period. The MUELS method was trained with time series of length 2^{18}, or 3.6 hours, and the DLG return period was selected to match the length of the Monte Carlo simulations. It should be noted that for the $F_s = 14.7$ case, the excursion into the more extreme domain, around 14,000 seconds in Figure 6.4 does not always appear in the 58-hour time series. In fact, in the 4,000 simulations, an excursion into the larger domain occurred in 57% of the simulations. This irregularity was intentional to be representative of systems for which there is a limited amount of data and that may have unknown dynamics.

The comparison of the MCS and the MUELS method was done using a practical approach. The computational expense for the MCS and MUELS method were compared. It should be noted that the desired exposure period of 58.3 hours plays a role in the computational expense and the comparison would differ with a different exposure period. The extreme pdf of a non-linear process for a given exposure is useful in design but not always easy to generate. So, the extreme pdfs generated from MCS results were compared to extreme pdfs generated from MUELS method results using selected ELS parameters. While the actual magnitude of the extreme values is useful to have, the time series are also vital so that the response of other degrees of freedom during an extreme event can be observed. As such, the time series structure of the MCS and MUELS method results near extremes was also compared. Lastly, the effect of TEV selection for the MUELS method was also investigated to see if there is a relationship between the TEV selected for the MUELS method and the true extreme characteristics for the return period of interest.

6.3 Results and Discussion

In this section, the results of the different studies are presented and discussed.

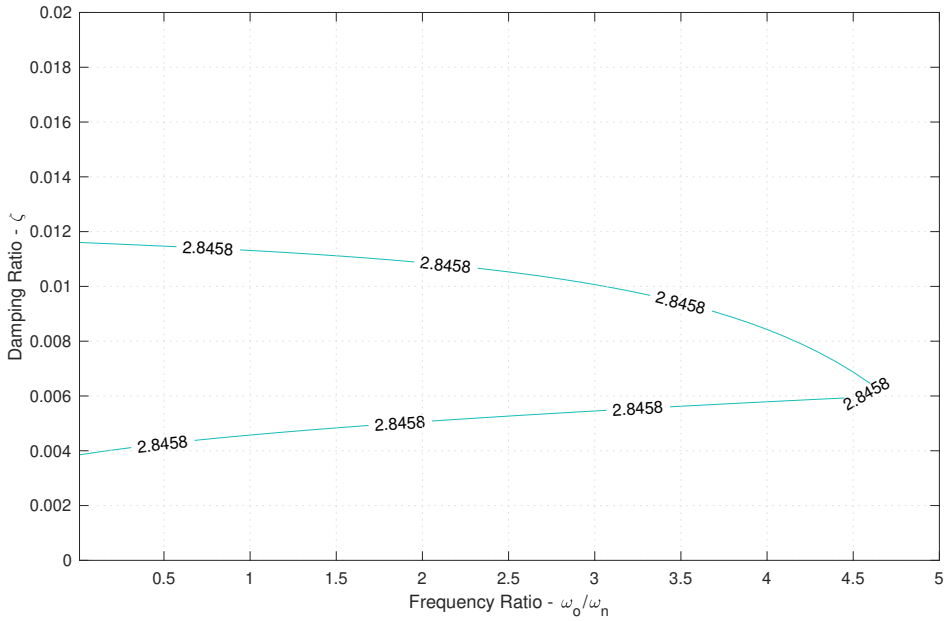

Figure 6.10: The equivalent linear system contour for $F_s = 10.0$ along with the zero-upcrossing frequency of $2.8458\,rad/s$. Note that ω_o is the peak frequency of the input spectrum and ω_n is the linear natural frequency.

6.3.1 MUELS Method Performance at a Fixed TEV

For each forcing factor value, around 20 sets of parameters were input as equivalent linear systems into the DLG. It should also be noted that while the return period for each forcing factor was the same, the zero-upcrossing period, and therefore the TEV, changed. Figures 6.10-6.12 show the contours for each forcing factor.

As seen in Figures 6.10-6.12, increasing forcing factor shifts the contour to the left. As the Duffing oscillators become more and more non-linear and non-stationary through increased forcing factor, there are fewer equivalent linear systems available to represent the Duffing oscillators. As such, the probability that there exists a linear system that shares inputs that lead to extremes with the non-linear system of interest decreases. It should be noted that the parameters from these contours are sampled such that about 20 sets of parameters were selected for input into the DLG for the purpose of simplicity and speed. Furthermore, the bulk of these sets of parameters fall near the bend in the contours, at frequency ratio values above 1.0, due to the *contour()* function in MATLAB. The majority of resulting natural frequencies fall below 1.0 rad/s which may have an effect on the performance of the MUELS method due to the distance between the ELS natural frequencies and the

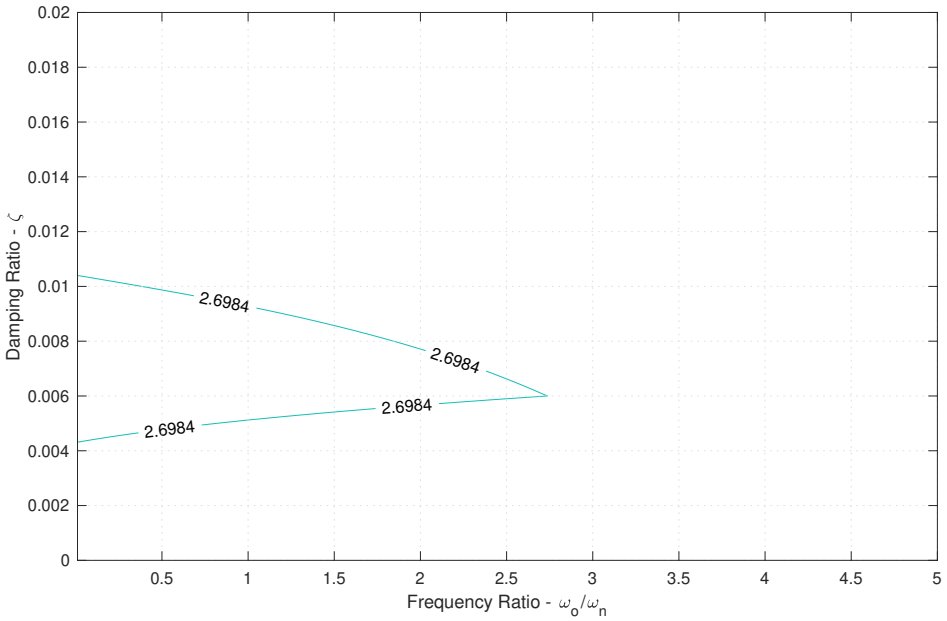

Figure 6.11: The equivalent linear system contour for $F_s = 14.7$ along with the zero-upcrossing frequency of $2.6984\,rad/s$. Note that ω_o is the peak frequency of the input spectrum and ω_n is the linear natural frequency.

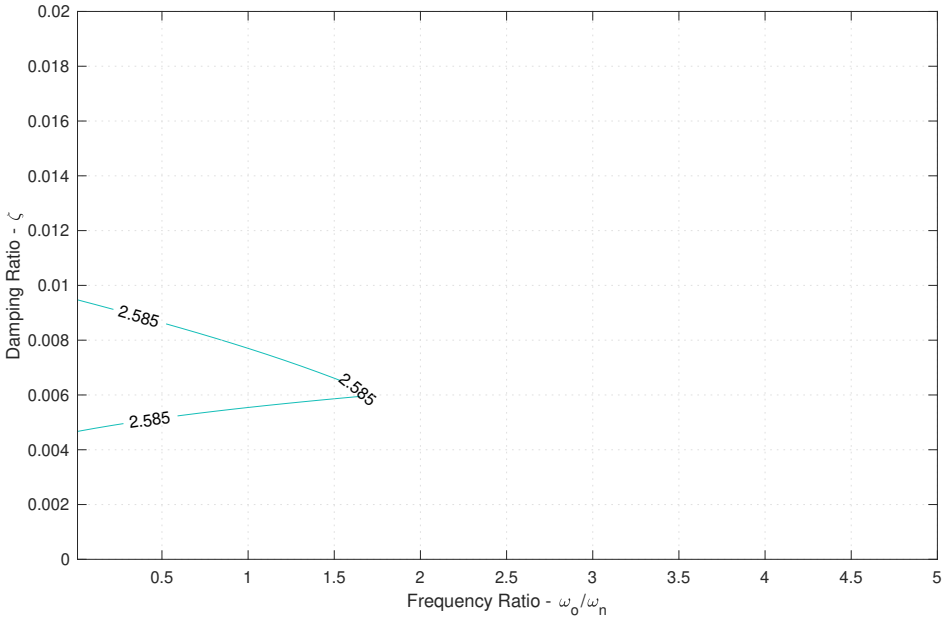

Figure 6.12: The equivalent linear system contour for $F_s = 17.0$ along with the zero-upcrossing frequency of $2.5850\,rad/s$. Note that ω_o is the peak frequency of the input spectrum and ω_n is the linear natural frequency.

peak forcing frequency. While it is possible that increasing this discretization i.e., using more parameter sets from around the contour, would increase accuracy and

performance, only around 20 parameter sets from each contour were used for this application.

Table 6.3 outlines the TEV and selected parameters for each forcing factor. Note that the parameter selection process is detailed in Section 6.2.4.

Table 6.3: The TEV for the given return period as well as the selected linear natural frequencies, ω_n, and damping ratios, ζ, for each forcing factor.

F_s	TEV	$\omega_{n,sel}$	ζ_{sel}
10.0	4.793	0.059	0.006
14.7	4.774	0.196	0.009
17.0	4.761	0.148	0.006

It should be noted that the linear natural frequencies and resulting transfer functions selected have little overlap with the energy from the input spectrum. Further investigation into the importance of prioritizing systems whose transfer functions overlap more with the input spectrum will be considered in future work. Still, the MUELS method showed promise despite the non-ideal frequency overlap.

One of the major benefits of the MUELS method is the increase in computational efficiency compared to Monte Carlo simulations. In this application, a single MUELS run for each forcing factor, including gathering training data and producing 1,000 realizations, took 14,705 seconds on a quad-core processor. To produce 4,000 Monte Carlo simulations for the same return period of 58 hours took 144,840 seconds on eight cores. While there were more MCS produced, it should be noted that the realizations produced by the MUELS method were 100 seconds in length and producing 3,000 simulations more per parameter set would add about 900 seconds per parameter set, or about 18,000 seconds for an entire MUELS run. The current configuration of MUELS, which takes about 10-15% of the time of Monte Carlo simulations, allows for some increase in detail. One area that could improve the accuracy of the MUELS method would be, as mentioned earlier, a finer discretization of the contour to examine more parameter sets.

Figures 6.13-6.15 show the selected MUELS extreme pdf and the extreme Monte Carlo pdf for each forcing factor. Note that each pdf was generated using a kernel density estimator.

In the $F_s = 10.0$ case, the MUELS method extreme pdf predicted the most probable maximum of the Monte Carlo simulations quite well. The MUELS method pdf does have a larger standard deviation than the MCS pdf but has a large amount

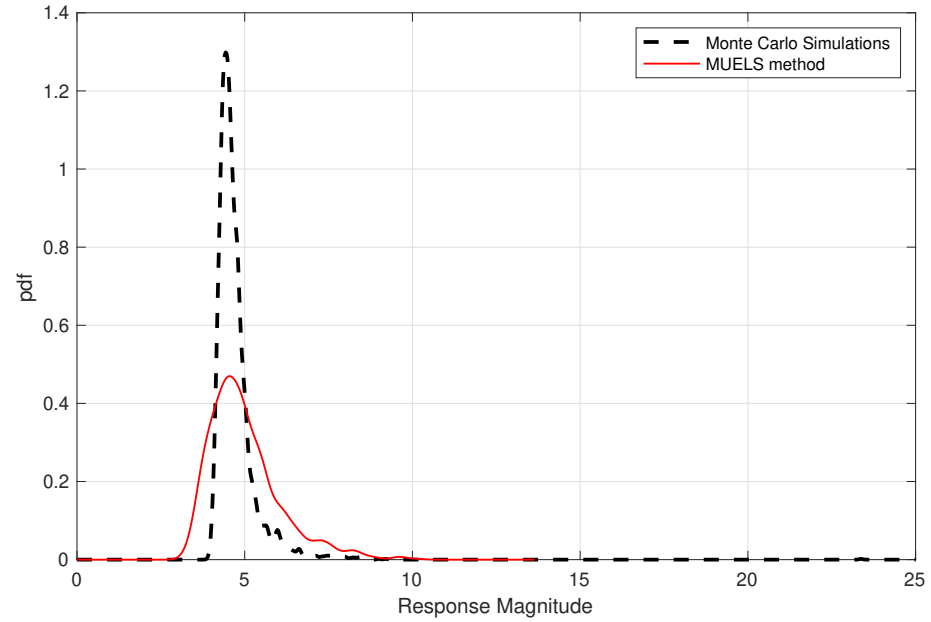

Figure 6.13: The extreme value pdf for the Monte Carlo simulations and the selected extreme value distribution for the MUELS method for $F_s = 10.0$.

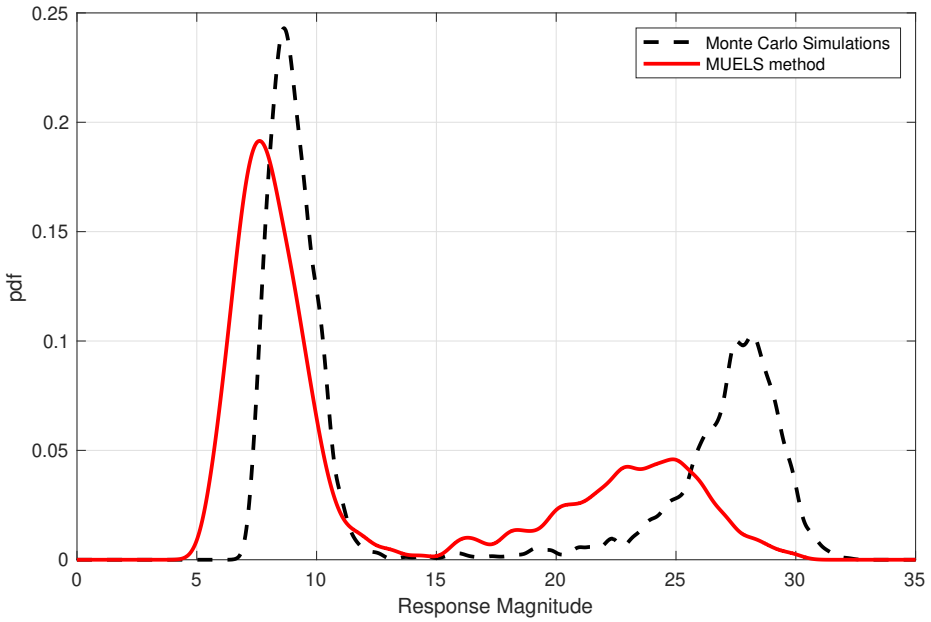

Figure 6.14: The extreme value pdf for the Monte Carlo simulations and the selected extreme value distribution for the MUELS method for $F_s = 14.7$.

of overlap and therefore valid extreme realizations.

The MUELS method was able to recover the two attractors in the $F_s = 14.7$ case successfully. The under-prediction here could be the result of the TEV given the

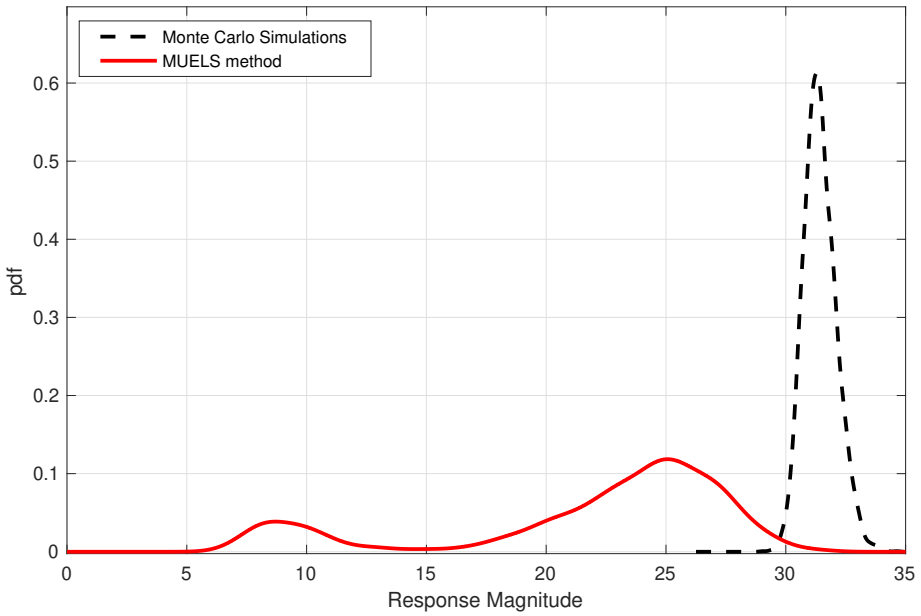

Figure 6.15: The extreme value pdf for the Monte Carlo simulations and the selected extreme value distribution for the MUELS method for $F_s = 17.0$.

levels of non-linearity that have been introduced or since there are now essentially two return periods to examine: that of the small attractor and that of the large attractor. While the MUELS method does under-predict the MCS in the most probable maxima of both attractors, there is still a good amount of overlap that can provide valid extreme realizations.

In the $F_s = 17.0$ case, the MUELS method retained some realizations that did not contain excursions. Furthermore, the amount of overlap between the MUELS method pdf and the Monte Carlo pdf is reduced even more.

The immediately evident and important characteristic of the $F_s = 14.7$ pdf is the bi-modality while the $F_s = 10.0$ and $F_s = 17.0$ cases exhibit uni-modality in the smaller domain of attraction and larger domain of attraction, respectively. The most obvious comparison we can make between the MCS and MUELS method is the x-value location of the peaks and the area of each of the peaks. It should be reiterated that each peak is representative of a different domain of attraction, as indicated in Section 6.2.2. As such, the area, A_i for $i = 1, 2$, and the x-value of the maximum of each peak, X_i for $i = 1, 2$, were used to compare the MUELS method with the Monte Carlo simulations. Table 6.4 shows the specified characteristics of the extreme MCS and MUELS pdfs and the mean absolute percentage error between the two.

Table 6.4: Comparison of pertinent pdf characteristics between the MUELS method, X_{MU}, and Monte Carlo simulations, X_{MCS}). Also shown is the mean absolute percentage error (MAPE), ϵ, between the MUELS method and MCS. Note that for $F_s = 10.0$ and $F_s = 17.0$, there was only one attractor and therefore only one peak to compare.

	$F_s = 10.0$			$F_s = 14.7$			$F_s = 17.0$		
Stat.	X_{MU}	X_{MCS}	ϵ	X_{MU}	X_{MCS}	ϵ	X_{MU}	X_{MCS}	ϵ
$\hat{X}_1$	4.55	4.44	0.03	7.62	8.64	0.12	8.71	N/A	N/A
A_1	1.00	1.00	0.00	0.66	0.57	0.16	0.16	N/A	N/A
$\hat{X}_2$	N/A	N/A	N/A	25.02	28.19	0.11	25.52	31.29	0.18
A_2	N/A	N/A	N/A	0.34	0.43	0.21	0.84	1.00	0.16

It should be noted that there were a limited number of excursions in the $F_s = 10.0$ Monte Carlo simulations which is not reflected in the significant figures shown. That being said, the performance of the MUELS method for $F_s = 10.0$ was good. This was expected, as the $F_s = 10.0$ case is nearly linear, which resulted in a closer match between the ELS and the actual oscillator. While the MUELS pdf had more variance, as seen in Figure 6.13, it provides a solid foundation to produce an infinite number of extreme realizations at any return period of interest.

For $F_s = 14.7$, the MUELS method under-predicts the MCS in both peak x-value and number of simulations with excursions. The under-prediction could be due to the MUELS method reaching the non-linearity limits or it could be due to the TEV selection. For this section, the TEV was determined simply by using the return period of 58.3 hours and the zero-upcrossing period for each forcing factor. It is important to reiterate that the TEV becomes less meaningful as more non-linearity is introduced. The TEV is still a good starting point but cannot be expected to produce accurate results without any changes made to account for non-linearity. Further discussion on the TEV choice follows in the Section 6.3.3.

For $F_s = 17.0$, the MUELS method under-predicted the MCS again. In fact, there were a number of DLG inputs that did not result in an excursion in the 100-second realization. The under-prediction here is most likely the result of both TEV selection and reaching the non-linear limits of the MUELS method. Still, the large attractor x-value of the peak fell within 20% of the MCS most probable maximum and there are a number of realizations that overlap with the Monte Carlo extreme pdf. In practice, the amount of overlap would not be known but schemes are being developed to form an acceptance-rejection method based off of extreme value theory and knowledge of the system to be able to estimate the amount of overlap between

the true extreme value distribution and the extreme pdf from the MUELS method.

6.3.2 Time Series Comparison

One of the major benefits of the MUELS method is the ability to produce any number of time series realizations that lead to an extreme response. It should be reiterated that the difference between just running Monte Carlo simulations and the MUELS method is that the MUELS method uses the DLG to produce multiple sets of input realizations from different equivalent linear systems of relatively short length. After the equivalent linear system parameters are selected, the DLG is capable of producing many realizations for that set of linear parameters that potentially lead to extremes in the non-linear system of interest. That being said, it is important to compare the MUELS method time series with Monte Carlo simulations to ensure that the time series have the similar characteristics near extremes. It should be noted that the phase sampling procedure in the DLG results in input time series that lead to linear extremes at $t = 0$. Inputting the time series into the non-linear system will not necessarily result in an extreme or potential extreme at $t = 0$ and that is reflected in the ensemble average time series. The lag is more noticeable when compared to the Monte Carlo simulation ensemble average near extremes which was set to have the extreme at $t = 0$ so the magnitudes were scaled and normalized to match the relationship between the peak value of the largest attractor for the Monte Carlo simulations and the MUELS method. Figures 6.16-6.18 show these normalized ensemble averages near extremes for the Monte Carlo simulations and the MUELS method for each forcing factor.

In the $F_s = 10.0$ case, the MUELS method and Monte Carlo simulations have very similar mean frequencies near $t = 0$ as well as the magnitudes of the peaks leading up to the extreme value. Since the $F_s = 10.0$ case is the most linear and therefore more immediately compatible with the DLG, it follows that it would produce time series that are closer to Monte Carlo simulations. It also seems to capture the dynamics shown in the Monte Carlo simulations further away from the extreme.

In the $F_s = 14.7$ case, the MUELS method ensemble average seems to have a lower characteristic frequency than the Monte Carlo simulations. This may be a result of the lag mentioned earlier as the zero-upcrossing period should remain constant due to the fact that the input time series are valid realizations of the input spectrum. It is also interesting to note that the minimum value of the MUELS method after

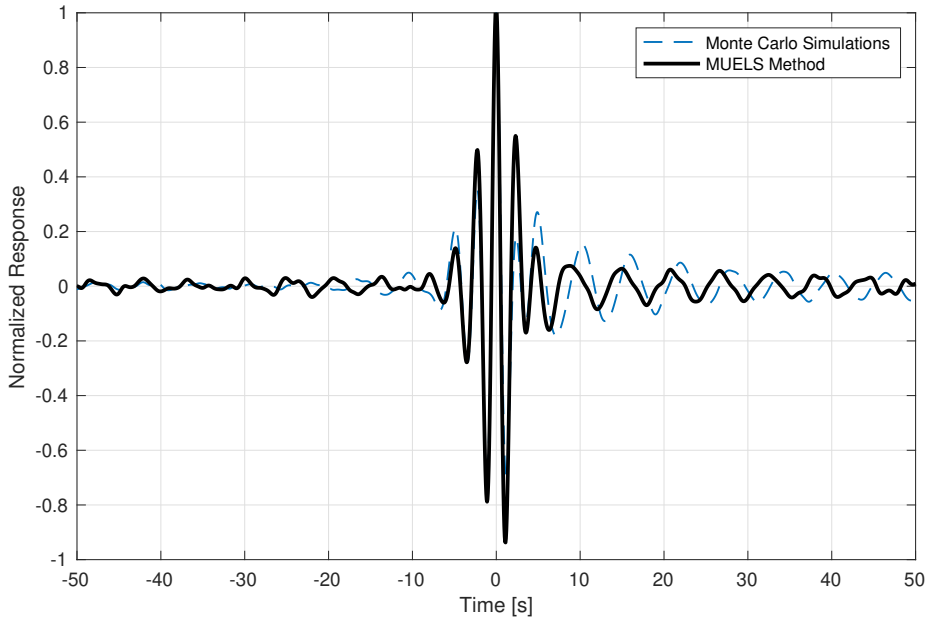

Figure 6.16: Ensemble average of the time series near extremes for Monte Carlo simulations and the MUELS method for $F_s = 10.0$. Note that the MUELS method results are not centered.

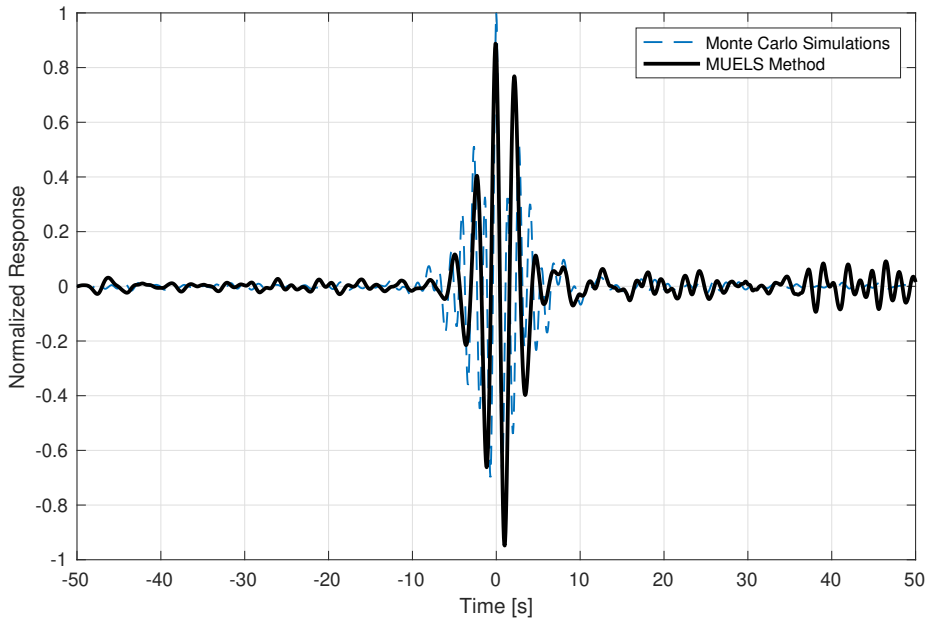

Figure 6.17: Ensemble average of the time series near extremes for Monte Carlo simulations and the MUELS method for $F_s = 14.7$. Note that the MUELS method results are not centered.

the positive peak follows the behavior of the Monte Carlo simulations while having larger magnitude than the positive maximum of the MUELS method.

In the $F_s = 17.0$ case, the MUELS method again has a lower characteristic

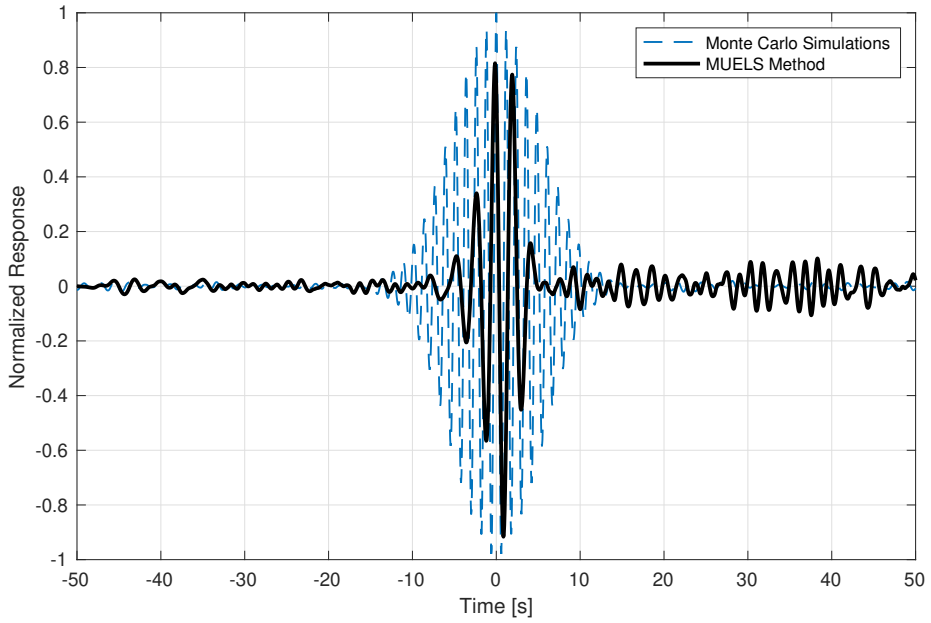

Figure 6.18: Ensemble average of the time series near extremes for Monte Carlo simulations and the MUELS method for $F_s = 17.0$. Note that the MUELS method results are not centered.

frequency than the MUELS method. The buildup to the maximum is not as gradual or symmetric as shown in the Monte Carlo ensemble average but again recentering the MUELS time series would reduce some of these deviations.

A future comparison between the MUELS method and Monte Carlo simulations would center the MUELS ensemble average to have a clearer comparison between the magnitudes of the ensemble average between the MCS and MUELS method. That being said, while the recentering would improve the MUELS method performance relative to the Monte Carlo simulations, there may be another point of improvement in the TEV selection.

6.3.3 Alternate Target Extreme Value Investigation

The MUELS method uses the Target Extreme Value (TEV) as a metric for return period. Since the TEV is not necessarily indicative of the return period, the relationship between the MUELS method at different TEVs to the return period of interest is important to develop. As such, the lower attractor area, or the area of the extreme probability density function for which the Duffing oscillator is in the lower of the two domains of attraction, was used as a key metric. To reinforce the Monte Carlo simulation results with a classic extreme value approach, the excursions into the larger domain of attraction were assumed to be a Poisson process. For a Poisson

process, the probability that a given time period has zero excursions into the larger domain is as follows:

$$P_0 = e^{-rt} \tag{6.2}$$

where r is the rate of excursions per unit time and t is the time period of interest. The rate, r, was solved for using the number of excursions from a TEV of 4.8 to reflect the Monte Carlo simulations that a designer may have access to.

Additionally, two methods for determining the MUELS parameter sets are included. The first method, method "A", is as discussed in Section 6.2.4, where the parameter set that results in the larger attractor peak with the largest x-value is selected. This method is based on the fact that the DLG is a lower-bound solution and selecting the largest x-value follows that fact. The second method, method "B", attempts to match the lower attractor area with the Poisson approximation by selecting the parameter set that results in a lower attractor area as close as possible to the Poisson model results. This method requires the Poisson model to be fit, which in turn requires Monte Carlo simulations. The Poisson parameters were solved using the lower attractor area for the TEV around 4.8 since the most amount of data could be used. It should also be noted that the Monte Carlo results for TEVs other than around 4.8 were resampled or concatenated from the 4,000 simulations of length $N = 2^{22}$. For a TEV of 6.0, over 300 of the original time series were concatenated, resulting in about 12 time series representing a data point. The recycling of the excursions here is not ideal but shows the general trend of how the number of excursions change with exposure period and forcing factor. Figures 6.20 shows the lower attractor area for the Monte Carlo simulations, the Poisson model, and the two MUELS parameter selection methods for each forcing factor.

In the $F_s = 10.0$ case, the fit of the Poisson does not account for any noticeable excursions in the TEVs shown. There were a few excursions in the set of Monte Carlo simulations run which may have been noticed, but any attempt to predict change for longer return periods using a Poisson model may result in under-prediction of excursions. There were only 12 time series constructed through concatenation corresponding to a TEV of 6.0 (about 44,000 hours), so it is hard to say whether or not the shift in lower attractor area from a TEV of 5.5 (about 2,500 hours) is artificial or not. The MUELS method showed slight movement as the TEV increased, but

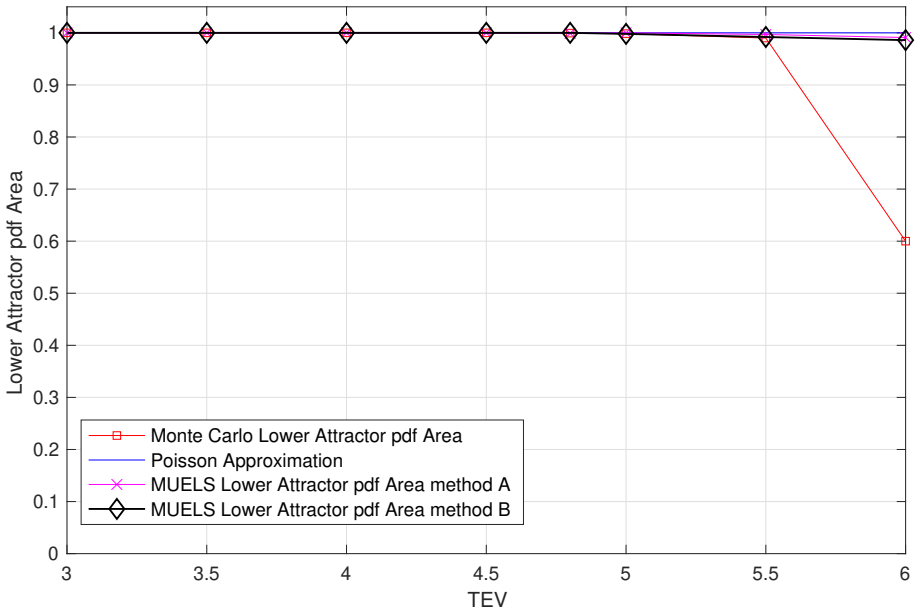

Figure 6.19: Comparison of lower attractor pdf area between the MUELS method, MCS, and a Poisson approximation for various TEVs with $F_s = 10$.

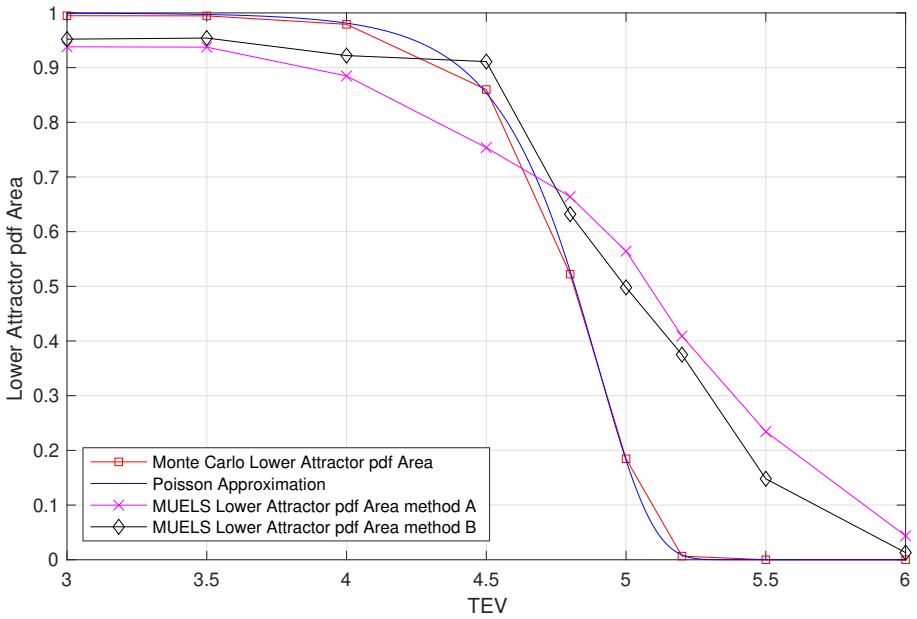

Figure 6.20: Comparison of lower attractor pdf area between the MUELS method, MCS, and a Poisson approximation for various TEVs with $F_s = 14.7$.

not much more than a few percent. That being said, the MUELS method could still provide time series of these excursion events in a much quicker fashion than Monte Carlo simulations while also signaling that the behavior may be changing as exposure

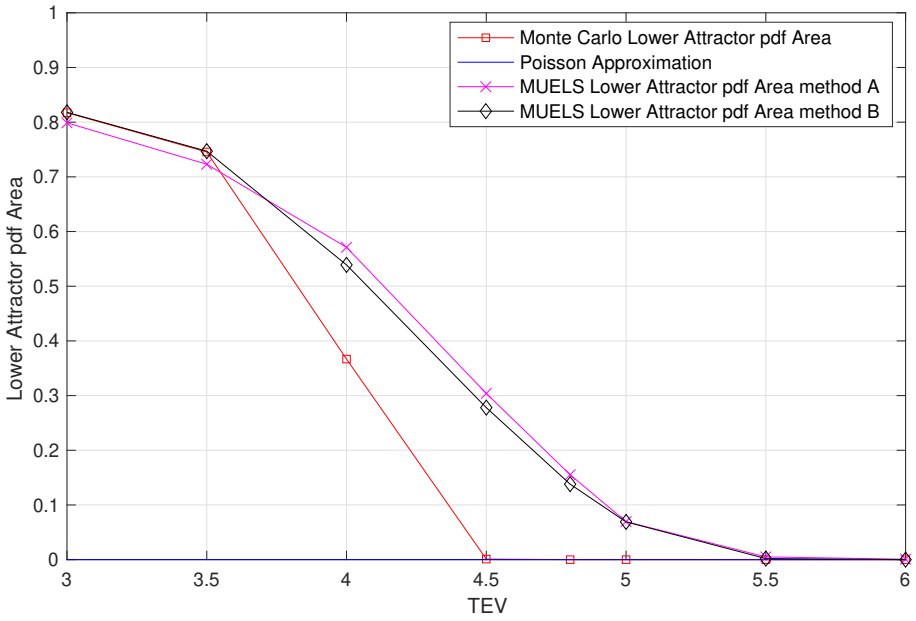

Figure 6.21: Comparison of lower attractor pdf area between the MUELS method, MCS, and a Poisson approximation for various TEVs with $F_s = 17$.

period increases.

In the $F_s = 14.7$ case, it is immediately evident that the MUELS method over predicts excursions for lower TEVs. Since the DLG is based off of the asymptotic nature of extreme value theory, over-prediction at smaller return periods is not unusual. When the TEVs increase, the MUELS method begins to under-predict the excursions by probabilities ranging from 0.2-0.4, depending on the method. It is clear that the relationship between the exposure period of interest and the TEV is not direct nor simple. That being said, the speed and flexibility of the MUELS method allow for many runs to be completed at various TEVs.

The $F_s = 17.0$ case had the opposite issue of the $F_s = 10.0$ case in that the Poisson approximation predicted that all TEVs would have at least one excursion. Here, a different method could have been used to estimate the parameter r such as least squares or simply selecting a lower TEV to make the fit off of. For sake of continuity, however, the same method was used. The MUELS method follows the general trend of the Monte Carlo results with a lag as the TEV increases. The differential between the lower attractor area in Monte Carlo results and the MUELS methods were generally smaller than in the $F_s = 14.7$ case, with a probability differential maximum around 0.3 at a TEV of 4.5. At this point, it is clear that the difference between

method "A" and method "B" is small enough to be inconsequential.

The general over-estimation of the lower attractor by the MUELS method is affected by the use of the TEV as a metric for rarity. As mentioned in Section 6.1 the DLG uses Gaussian extreme value theory for generating extreme events. The extreme events and therefore input time series scale in return period with Gaussian extreme value theory and, while still valid inputs into the non-linear system, cannot be expected to produce non-linear extremes for the return period of interest without thought. That being said, the "best" TEV for a given return period can be estimated by using a pdf distance metric between Monte Carlo simulations and MUELS results. To measure the distance between two pdfs, an adaptation of the match distance was used. The following equation estimates the distance between two discrete pdfs:

$$d_m(F_{MCS}(x), F_{MUELS}(x) = \sum_{i=1}^{N} |F_{MCS}(x_i) - F_{MUELS}(x_i)| \tag{6.3}$$

where d_m is the match distance, $F(x)$ is the discrete cumulative distribution function for the given method, and N is the number of points in the cdf. While the magnitude of the distance is not especially informative, the relative distance among the MUELS results for each TEV will allow for comparison. Figures 6.22-6.24 show the match distance for each forcing factor as a function of TEV.

For each forcing factor, the smallest match distance was at a different TEV from that used in Section 6.3.1. To see how much impact using this alternative TEV would make, Figures 6.25-6.27 show the MUELS pdfs for the minimum match distance along with the MUELS method for a TEV of around 4.8 and the Monte Carlo simulations. Note that given the little difference between method "A" and method "B", just method "A" will be shown.

In general, the improvement of the MUELS method, at least visually, seems relatively minor. The TEV is one variable that affects the MUELS method's performance with regard to finding a linear system that has similar extreme characteristics to the non-linear system and return period of interest. Other pieces like the discretization of the parameter contour and the DLG's extrapolation methods also contribute to the performance of the MUELS method and can be tuned along with the TEV to improve the MUELS method results.

Table 6.5 shows the updated TEV MUELS pdf characteristics and errors as com-

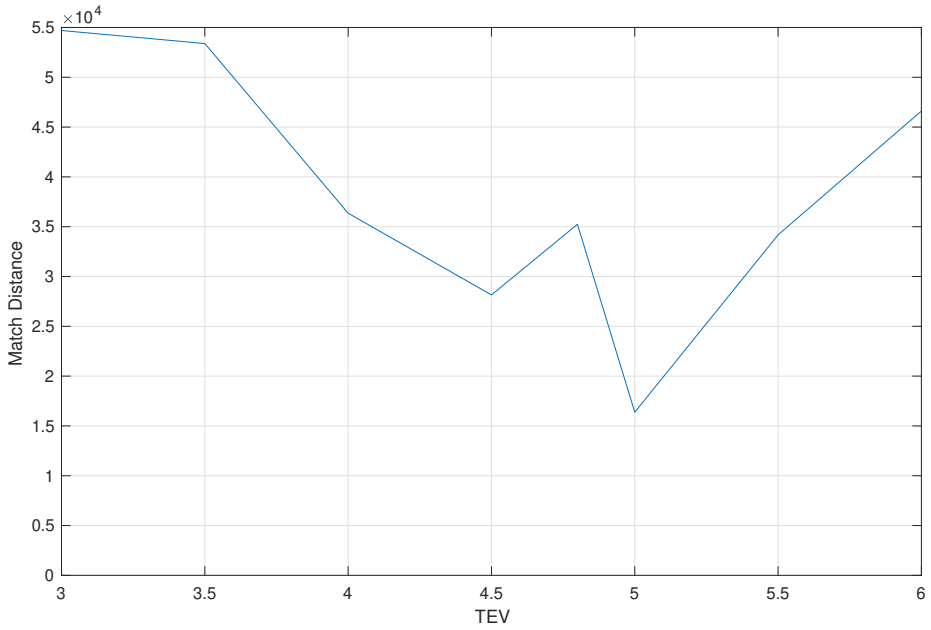

Figure 6.22: Match distance between the MUELS method at various TEVs and Monte Carlo simulations for $F_s = 10.0$.

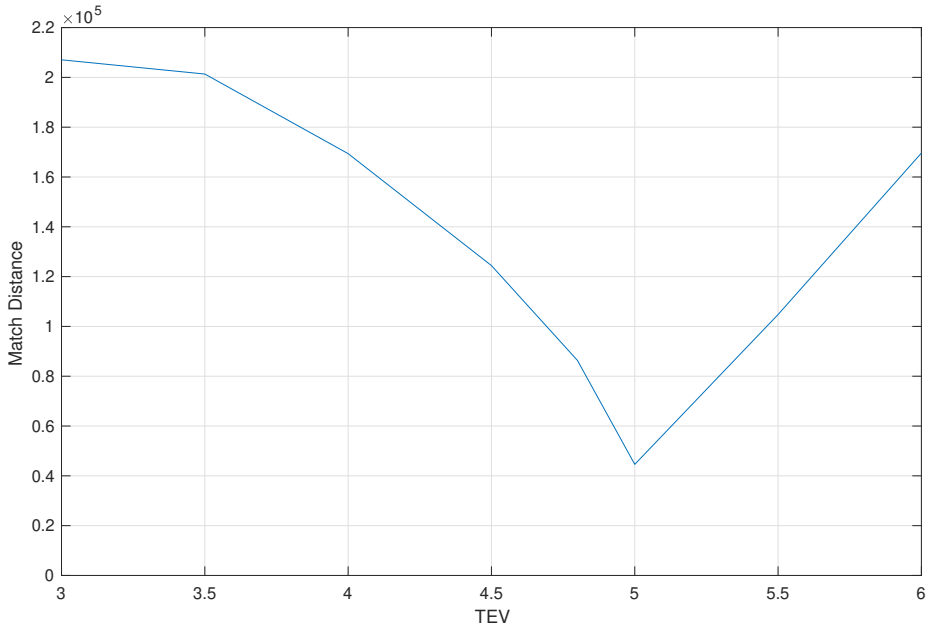

Figure 6.23: Match distance between the MUELS method at various TEVs and Monte Carlo simulations for $F_s = 14.7$.

pared to Monte Carlo simulations for the return period of interest. The significant figures were increased to include any outlier behavior e.g., high attractor events in the $F_s = 10.0$ systems or time series without excursions in the $F_s = 17.0$ case.

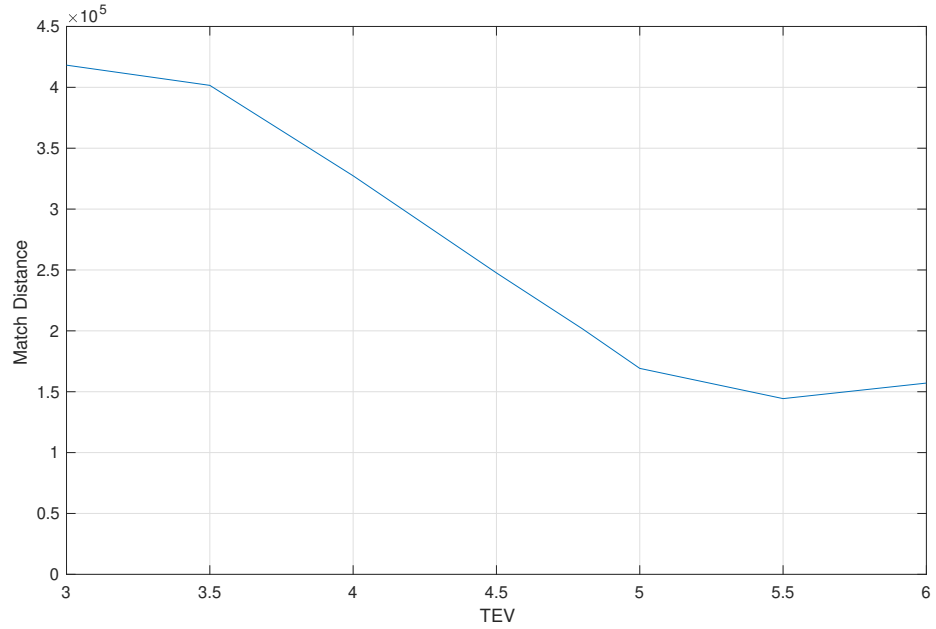

Figure 6.24: Match distance between the MUELS method at various TEVs and Monte Carlo simulations for $F_s = 17.0$.

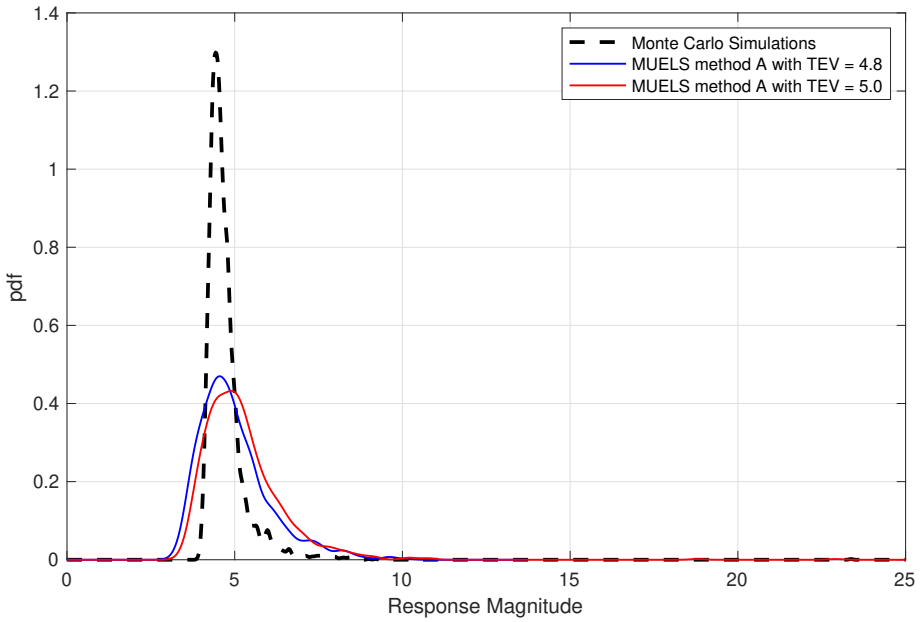

Figure 6.25: Comparison of MUELS method pdfs using a TEV on the order of the return period (TEV = 4.8) and the MUELS method pdf at the TEV which has the minimum match distance to the Monte Carlo simulations for $F_s = 10.0$.

Comparing Table 6.5 and Table 6.4, it seems the match distance favored reducing difference between the attractor areas of the MCS and MUELS method as opposed to specific x-values of the peaks. Still, at least visually, both the $F_s = 14.7$ and

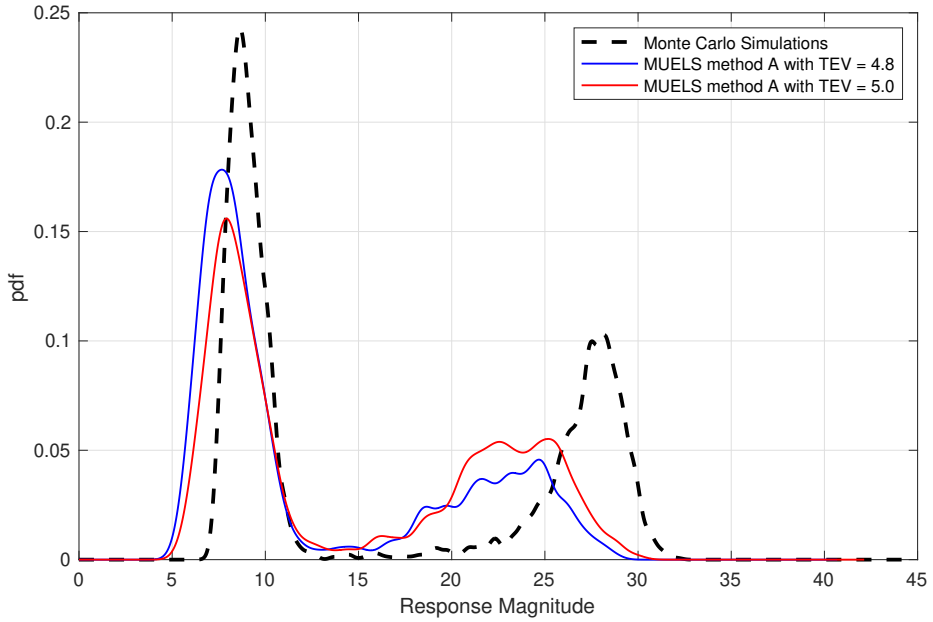

Figure 6.26: Comparison of MUELS method pdfs using a TEV on the order of the return period (TEV = 4.8) and the MUELS method pdf at the TEV which has the minimum match distance to the Monte Carlo simulations for $F_s = 14.7$.

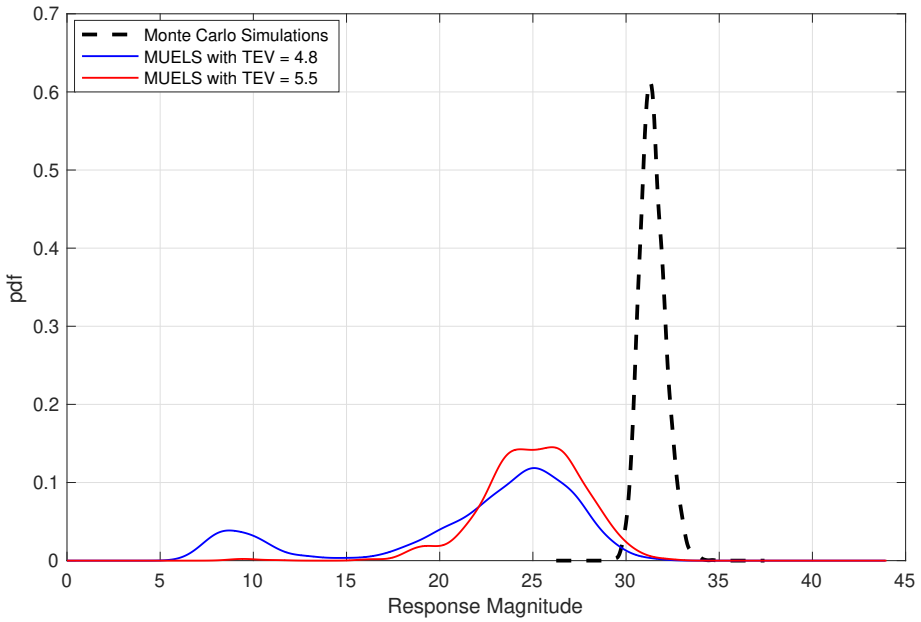

Figure 6.27: Comparison of MUELS method pdfs using a TEV on the order of the return period (TEV = 4.8) and the MUELS method pdf at the TEV which has the minimum match distance to the Monte Carlo simulations for $F_s = 17.0$.

$F_s = 17.0$ case noticeably improve with an increased TEV. That being said, other improvements can be made, most notably in the discretization of the contour by

Table 6.5: Comparison of pertinent pdf characteristics between the MUELS method with updated TEV and Monte Carlo simulations.

	$F_s = 10.0$			$F_s = 14.7$			$F_s = 17.0$		
Stat.	X_{MU}	X_{MCS}	ϵ	X_{MU}	X_{MCS}	ϵ	X_{MU}	X_{MCS}	ϵ
$\hat{X}_1$	4.898	4.436	0.104	7.917	8.64	0.084	9.455	N/A	N/A
A_1	0.998	0.999	0.002	0.550	0.57	0.033	0.005	N/A	N/A
$\hat{X}_2$	22.906	23.370	0.020	25.247	28.19	0.104	24.881	31.289	0.205
A_2	0.002	0.001	2.000	0.450	0.43	0.043	0.995	1.000	0.005

prioritizing linear natural frequencies closer to the peak frequency used.

6.4 Conclusion

In this chapter, the abilities and the limits of the MUELS method were tested. Three systems of varying non-linearity and non-stationarity were used to compare the MUELS method with the conventional method of Monte Carlo simulations. The three particular systems tested the MUELS method's flexibility in rare behavior identification, as in the $F_s = 10.0$ case, and in adjusting for increasing non-linearities. The key characteristic in each of the systems was the number of excursions into a domain of attraction with peak magnitudes two to three times larger than the base domain of attraction's peaks. In general, the MUELS method under-predicted extreme characteristics found using Monte Carlo simulations but remained within about 20%. That being said, the computational expense of the MUELS method was only 10-15% of the Monte Carlo simulations on a less computationally powerful set up. The reduced load could allow for a larger number of potential surrogate linear systems for the MUELS method to test.

One of the major benefits of the MUELS method is the ability to produce time series realizations of conditional extremes. In comparing the ensemble average of the MUELS method and Monte Carlo simulations near extremes, it was found that there was a degradation in accuracy as non-linearity increased. One chief cause of this is likely due to the fact that while the DLG produces extreme linear time series with a maximum at $t = 0$, there is no basis for those inputs to provide a non-linear realization with a maximum at exactly $t = 0$. With that said, a centering of the maximum values before taking the ensemble average would certainly improve both the ensemble average magnitude and average period when compared to Monte Carlo simulations.

After changing the TEV to minimize the match distance between the MUELS

method extreme pdf and Monte Carlo simulations, improvement was made in estimating number of time series with excursions but not so much in terms of peak x-value. Further studies into a different distance metric that prioritizes peak x-values as well as into finer discretized parameter contours would improve the MUELS method performance even more.

Chapter 7

Slamming Application using the MUELS method

7.1 Introduction

In this chapter, the impact oscillator used as an SGIM application in Chapter 3.4 is revisited. An additional approach to the MUELS method, called the surrogate MUELS method, is introduced and compared to the traditional MUELS approach as well as Monte Carlo simulations.

7.2 Methodology

The impact oscillator from Chapter 3.4, repeated in Equation 7.1, imitates expected accelerations from hull slams and features physics-informed components such as the relative velocity threshold and exponential decay of the stiffness. As such, it provides a "real world" application as well as another test of the non-linear limits of the MUELS method.

$$m\ddot{x} + c\dot{x} + k(t)x = F\zeta(t) \tag{7.1}$$

where

$$k(t) = \begin{cases} k + k_s e^{-(1/\tau)t} & \text{if } RV > RV_{thresh} \text{ and } RP < 0 \\ k & \text{otherwise} \end{cases}$$

Here, RV is the relative velocity between the oscillator and the wave surface, RP is the relative position between the oscillator and wave surface, τ is the exponential decay constant, and k_s is the added slamming coefficient. As in Chapter 3.4, a threshold relative velocity, RV_{thresh} is used as a trigger for slams as in Ochi (1990a) and the negative relative position ensures submergence for a slam.

The ITTC sea spectrum and model parameters were kept the same as in the

SGIM application and are repeated in Table 7.1 for convenience.

Parameter	Value
$H_s\ [m]$	6
$T_m\ [s]$	12
$k\ [N/m]$	588.06
$m\ [kg]$	600.00
$RV_{thresh}\ [m/s]$	5.00
$c\ [\frac{Ns}{m}]$	415.80
$F\ [N/m]$	1500.00
$\tau\ [s]$	133.33
$k_s\ [N/m]$	4750.60

Table 7.1: Parameters used for the hull slamming application using the MUELS method.

One of the major benefits of the MUELS method is the inherent search for "surrogate" processes. With that being said, there is still the opportunity to take advantage of knowledge of the system. The MUELS method will be used in two separate ways in this chapter.

First, the MUELS method was used as has been shown throughout this dissertation: the zero-upcrossing period of the process was estimated and then a series of linear systems with the same zero-upcrossing period were entered into the DLG where input realizations were collected and used as input into the non-linear system of interest. In this application, the zero-upcrossing period of the acceleration of the impact oscillator was estimated and the acceleration transfer functions for the linear systems were used. Equation 7.2 shows the form of the linear systems' transfer functions given unit mass.

$$H_{accel}(\omega) = \frac{-\omega^2 \tilde{F}(\omega)}{(\omega^2 + \omega_{n,j}^2) + 2i\zeta_j\omega_{n,j}\omega} = -\omega^2 H_{disp}(\omega) \tag{7.2}$$

Here, $\tilde{F}(\omega)$ is the complex magnitude of the forcing as a function of frequency, ω, i signifies imaginary components, $\omega_{n,j}$ is the j^{th} system linear natural frequency, and ζ_j is the j^{th} system damping ratio. Also note the relationship between the linear transfer functions of acceleration and displacement.

The second way the MUELS method was used was to take advantage of the relationship between slamming events and extreme velocities, as in Seyffert (2018). Here, the zero-upcrossing period of the velocity of the impact oscillator was estimated and linear systems whose velocities shared the same upcrossing rate for the given

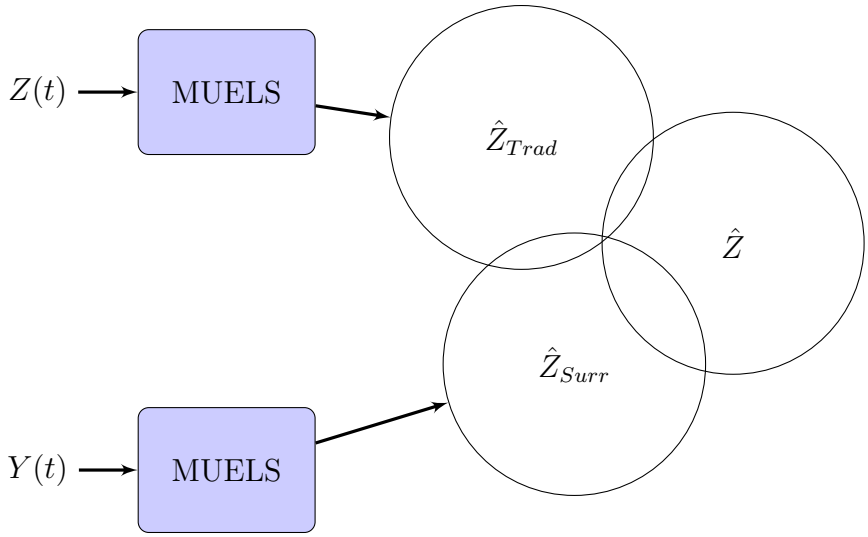

Figure 7.1: The basic structure of the traditional and surrogate MUELS methods. Note that the outputs from each method are both conditional extremes of the non-linear process of interest but provide different results.

input spectrum were entered into the DLG. Equation 7.3 shows the form of these transfer functions.

$$H_{velocity}(\omega) = \frac{i\omega\tilde{F}(\omega)}{(\omega^2 + \omega_{n,j}^2) + 2i\zeta_j\omega_{n,j}\omega} = i\omega H_{disp}(\omega) \tag{7.3}$$

Again, note the relationship between the velocity and displacement transfer functions. In this case, the inputs that lead to extreme velocities of the linear systems are still valid inputs into the non-linear system of interest and can be used to gather conditional extreme accelerations. It should also be noted that given the introduction of knowledge about the slamming process into the system, it is expected that this second method will perform better than the first method mentioned above.

For simplicity and consistency, the first method discussed above will be called traditional MUELS and the second method will be called surrogate MUELS. Figure 7.1 simplifies and generalizes traditional and surrogate MUELS as discussed above.

In Figure 7.1, the major difference between the traditional and surrogate MUELS methods lies in the input process: $Z(t)$ in the traditional case and $Y(t)$ in the surrogate case. Both of these methods result in conditional extremes i.e., $\hat{Z}_{Trad}$ and $\hat{Z}_{Surr}$, for the $Z(t)$ process but are expected to be at least somewhat different, due to the likely difference in zero-upcrossing period between the $Y(t)$ and $Z(t)$ processes. As such, Figure 7.1 reflects the similarity and expected improvement in

the surrogate method in the ensemble of extremes between the traditional method, $\hat{Z}_{Trad}$, the surrogate method, $\hat{Z}_{Surr}$, and the true extremes of the process for the given exposure period, $\hat{Z}$.

In this chapter, the extreme pdfs represented by $\hat{Z}_{Trad}$, $\hat{Z}_{Surr}$, and $\hat{Z}$ are compared qualitatively and through the match distance metric as seen in Chapter 6.3.3. Due to the time domain solution and slamming threshold sensitivity, the time step was set to $dt = 0.0025\,s$ and the return period was set to 3 hours, or $N = 2^{22}$ points. The true extremes of the process, $\hat{Z}$, were estimated using 2,000 Monte Carlo simulations of length $N = 2^{22}$ under the parameters specified in Table 7.1. Each MUELS method was preceded by 1,000 simulations of length $N = 2^{18}$ to obtain an estimate of the zero upcrossing period for the process of interest i.e., acceleration for traditional MUELS and velocity for surrogate MUELS. It should also be noted that the DLG was set to produce 1,000 simulations of length $t = 100\,s$ for each linear system. While this study is meant to be a comparison between the MUELS method and the SGIM for this particular problem, the MUELS method is more focused on searching many linear systems and the change from having the DLG produce $100\,s$ realizations as opposed to the $2,000\,s$ realizations from the SGIM resulted in a more computationally efficient approach but less straightforward comparison. Further discussion on this will take place in the next section.

7.3 Results

One of the key differences between the traditional and surrogate MUELS methods is the difference in upcrossing rate. The difference in upcrossing rate leads to a different set of equivalent linear systems to be scanned for each approach. Figures 7.2-7.3 show the system parameter contours for the acceleration and velocity.

The main takeaway from the parameter contours is the relative constant damping ratio, at least compared to displacement contours e.g., Figure 4.1. The flattening of the contours is a result of the velocity and acceleration transfer function for the linear systems and the resulting moment calculation. The change in form of the moment calculation in the acceleration and velocity, which effectively introduces additional frequency terms, alters the dependence on the damping ratio. While the damping ratio is relatively constant, the candidate frequencies had an extensive range. The wider sampling of linear natural frequencies is important in investigating

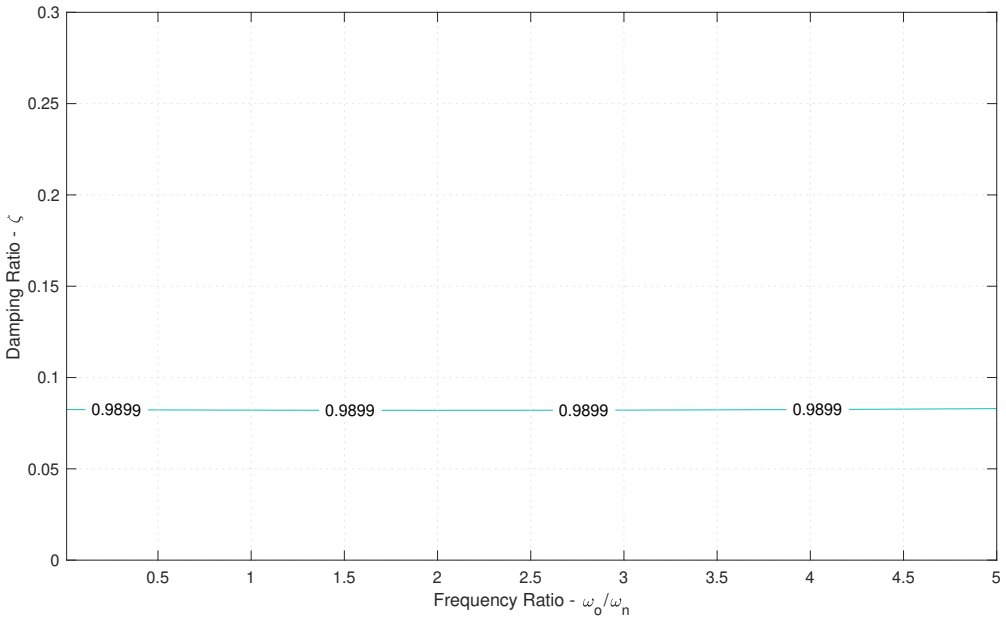

Figure 7.2: Impact oscillator acceleration equivalent linear system parameter contour for a zero-upcrossing frequency of $0.9899\,rad/s$.

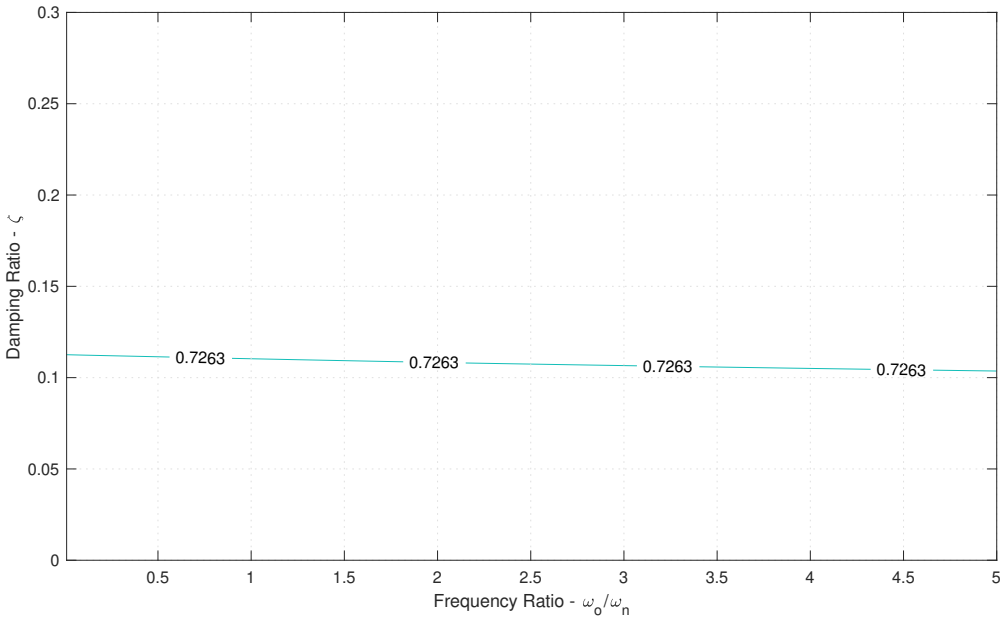

Figure 7.3: Impact oscillator velocity equivalent linear system parameter contour for a zero-upcrossing frequency of $0.7263\,rad/s$.

the sensitivity of parameter selection on MUELS results. From these contours, 26 sets of parameters were sampled uniformly as potential linearization candidates and were entered into the DLG.

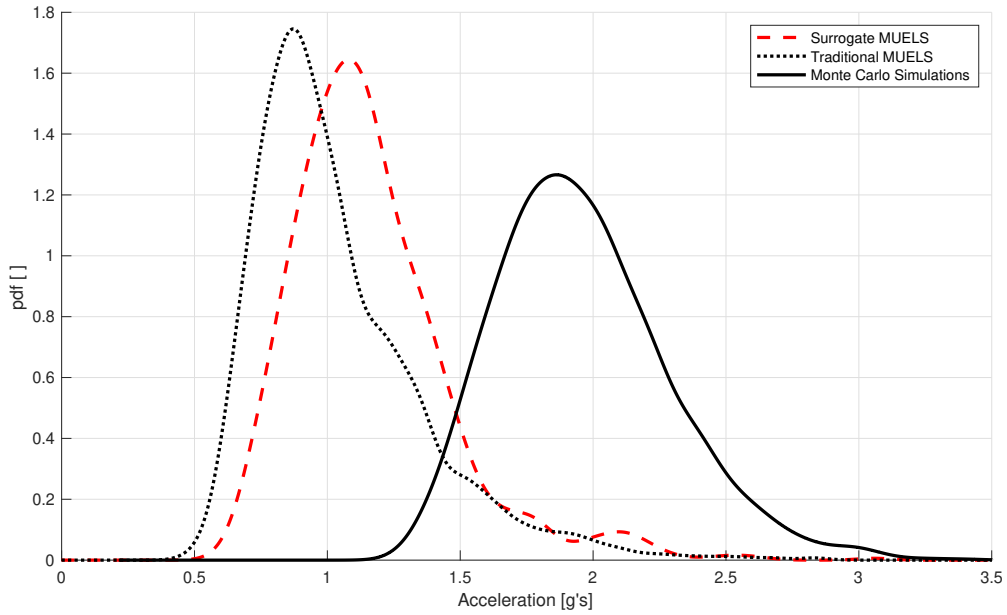

Figure 7.4: Comparison of traditional and surrogate MUELS method pdfs using a TEV on the order of the return period (TEV = 3.85) compared to Monte Carlo simulations.

Figure 7.4 shows the extreme pdfs for both the traditional and surrogate MUELS method along with the extreme pdf from 2,000 Monte Carlo simulations.

From Figure 7.4, it is clear that the introduction of knowledge into the system through a surrogate process improved extreme pdf estimation. While both methods underestimated the Monte Carlo simulation results, the surrogate MUELS method lowered the match distance to the Monte Carlo extreme pdf by 12% compared to the traditional MUELS method. Additionally, the surrogate MUELS method appeared to recover some of the peak realizations from the Monte Carlo simulations, as evidenced by the local maximum around 2.1 $g's$. The recovery here along with existence of lower extrema led to investigation into the acceleration extrema being extracted from the impact oscillator forced by DLG input realizations. As a precursor to a process that has some similarities to an acceptance-rejection method, a slamming verification scheme was developed. Using the event function option in *MATLAB*'s `ode45`, the time stamps from slamming events could be recorded. The DLG continually produced realizations until there were at least 1,000 realizations with a slamming time stamp within one velocity zero upcrossing cycle of $t = 0\,s$. The results of this scheme are shown along with the traditional and surrogate MUELS methods and the Monte Carlo simulations in Figure 7.5.

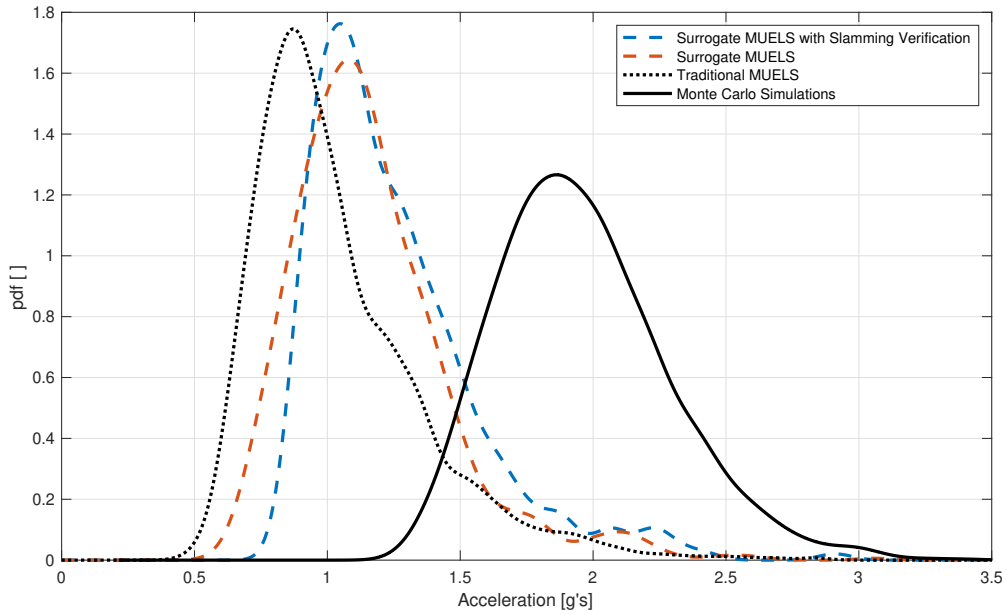

Figure 7.5: Comparison of traditional, surrogate, and surrogate with slamming verification MUELS method pdfs using a TEV on the order of the return period (TEV = 3.85) compared to Monte Carlo simulations.

Figure 7.5 again shows improvement of the MUELS method with respect to the Monte Carlo simulations. The addition of slamming verification provided an additional reduction of 10% in match distance to the Monte Carlo simulation extreme pdf. It also appears that the recovery of most probable extreme behavior is slightly recovered as evidenced by the local maximum around $2.25\,g's$.

More importantly, the slamming verification technique opens the door to post processing the MUELS results. Having established a level of confidence in a GEVD extrapolation, an acceptance-rejection scheme could be developed such that only realizations in line with the GEVD would be accepted. The efficiency of this acceptance-rejection method would vary from system to system, but would be related to the amount of overlapping area between the "best" MUELS method and the GEVD. Since the production of these short, conditionally extreme time series is rapid, this proposed technique would be more computationally efficient than brute force Monte Carlo simulations. In the end, a recreated GEVD pdf with realizations of extreme events, along with the inputs that lead to them, would be available for study.

Chapter 8

Conclusion

8.1 Summary

Extreme behavior prediction techniques used today often make assumptions and have subsequent shortcomings. Additionally, in a design context, the extreme response of a single degree of freedom rarely tells the whole story. Realistically, the effects of other degrees of freedom during an extreme event for a particular degree of freedom should be considered. Given the random nature of the ocean environment, it follows that load factors or singular time series are not sufficient to describe the conditional behavior of these other degrees of freedom. The development of a tool that could be used for a complete total system statistical analysis, the Matched Upcrossing Equivalent Linear System (MUELS) method, was the focus of this dissertation.

The development of the MUELS method began with exploration of the Stochastic Gaussianization Iteration Method (SGIM). The SGIM uses the Design Loads Generator (DLG) and a transformation of a non-linear process into the Gaussian domain to produce a ensemble of input time series realizations that lead to conditional extremes in the non-linear domain. Applicability to various levels of non-linearity was shown in applications to an impact oscillator as well as offshore wind turbine bending moment. Iterative cycling of the updated systems increased the success of the SGIM but ultimately removed some of the physics and enforced extrapolation assumptions on rare events. Still, the SGIM brought to light an interesting question: do there exist linear systems that share input realizations that lead to extremes with a non-linear system of interest?

That very question gave rise to the MUELS method. The MUELS method works in conjunction with the DLG to test a series of linear systems that share an average zero-upcrossing rate with the non-linear system of interest. The DLG provides input

time series realizations that produce extreme values in each of the linear systems which can then be used as input into the non-linear system of interest. Having an ensemble of input time series realizations that lead to an extreme allows for study into the total response of a system under extreme conditions. Additionally, the MUELS method reduces the computational expense significantly compared to Monte Carlo simulations.

The MUELS method addresses shortcomings in current methods through the following features:

- The method produces an ensemble of critical wave time series realizations rather than a single, average input that leads to a predetermined response.
- These wave inputs are valid realizations of a sea spectrum and can produce potential extreme events for a given exposure period as well as the simultaneous response of other degrees of freedom.
- The contour search technique gives a level of understanding about the non-linear system of interest and may be sufficient as a search for a surrogate process.
- The MUELS method can produce an at least the same number of extreme time series realizations for a given return period significantly faster than Monte Carlo simulations.

The development of the MUELS method builds off of the work in Alford (2008), Kim (2012), and Seyffert (2018) by extending the use of the DLG. Steps were taken in Kim (2012) to apply the DLG to non-linear processes and the introduction of surrogate processes was made in Seyffert (2018). With the MUELS method, the user no longer has to specify an explicit surrogate process but can instead search over a contour of linear systems which can be adapted to any linear differential equation for maximum flexibility.

8.2 Contributions of Current Work

Steps have been taken to bolster extreme event design techniques in classification rules, such as the load combination strategies discussed in the DNV-GL high speed

and light craft rules (DNV-GL, 2020), the load combination cases listed in the trimaran rules (Lloyd's Register, 2020), or the equivalent design wave suggested by ABS in the SafeHull-Dynamic Loading Approach (ABS, 2018). While each method considers the response other degrees of freedom during an extreme of a particular degree of freedom, the stochastic nature of the sea is not taken into account. Given the randomness of the environment, it follows that the responses during these extreme events will also be random and have distributions. Therefore, it is important to understand the simultaneous variable effects of the other degrees of freedom during an extreme of a particular degree of freedom.

The development of the MUELS method in this dissertation is a novel approach to this problem. The MUELS method is capable of producing an ensemble of input time series realizations that lead to conditional extreme responses and are also valid realizations of the input spectrum. With these inputs, the distribution of other degrees of freedom during an extreme event can be better understood and a more informed design decision can be made. The MUELS method is especially powerful when considering that no assumptions need to be made or advanced knowledge of the system is needed to interface with the DLG.

The study on the extreme characteristics of a stochastically forced Duffing oscillator in this dissertation in Chapters 5-6 is also a new development. The Duffing oscillator has marine applications with the ability to add a softening spring so it follows that studying the extreme characteristics is of design and academic interest. Discovering the variable stochastic bifurcations as a function of forcing factor as well as exploring the non-linear limits of the MUELS method were both significant contributions as well.

In fact, the application with the non-stationary Duffing oscillator in Chapter 6 showed the ability of the MUELS method to discover potentially unknown dynamics of a system. In the lowest forcing case ($F_s = 10.0$), only six of 1000, 58-hour Monte Carlo simulations had a bifurcation into the more extreme domain. The MUELS method quickly and efficiently produced time series realizations containing bifurcations, which may have gone undiscovered otherwise. From a practical perspective, discovering this behavior in an efficient manner would allow for CFD runs to be used more effectively.

8.3 Future Work

As discussed throughout the dissertation, one of the main benefits of the MUELS method is the quick production of input time series realizations that lead to extreme events. With that comes the ability to simulate responses of other degrees of freedom using those same input time series realizations to understand the conditional distributions at a higher level. The next step for the MUELS method is to examine such a system and compare the results to guidance set out by one of the classification societies mentioned in Section 8.2, as in Seyffert (2018).

Where the MUELS method diverges from Seyffert (2018) is in the fact that a surrogate process does not need to be specified. As degrees of freedom become more complex, however, more flexibility in the linear systems could be beneficial to better encapsulate the dynamics. With that, a multi-dimensional contour to select additional parameters for a more complex linear system would likely improve the MUELS method's performance. It is here that additional knowledge into the dynamics of the system e.g., the order of the linear differential equations, could be imparted though it would not be necessary.

It would also be beneficial to study the sensitivity of the MUELS contour parameters in further detail. Given the lower-bound nature of the DLG, it would be advantageous to explore more systems with linear natural frequencies near a peak frequency in the response spectrum of interest to produce the largest possible responses.

Lastly, an application with the Large Amplitude Motion Program (LAMP) (Lin and Yue, 1991) would further expand the usefulness of the MUELS method as well as LAMP itself. With LAMP, the extreme, non-linear responses of a computer model ship could be estimated using ensembles of input time series from the MUELS method. The level of response provided by the MUELS wave realizations could be compared to GEVD estimations for a particular degree of freedom like the vertical bending moment. Since the length of input time series is adjustable, the time constraints in using a high-fidelity non-linear time series code such as LAMP would be manageable.

Bibliography

ABS. *'SafeHull-Dynamic Loading Approach' for vessels*, 2018.

Alford, L. K. *Estimating Extreme Responses Using a Non-Uniform Phase Distribution*. PhD thesis, University of Michigan, 2008.

Anastopoulos, P. A. and Spyrou, K. J. Evaluation of critical wave groups method in calculating the probability of ship capsize in beam seas. *Ocean Engineering*, 187, 2019.

Bak, C., Zahle, F., Bitsche, R., Kim, T., Yde, A., Henriksen, L., Nararajan, A., and Hansen, M. Description of the DTU 10 MW reference wind turbine. Technical report, DTU Wind Energy, 2013.

Belenky, V., Glotzer, D., Pipiras, V., and Sapsis, T. P. Distribution tail structure and extreme value analysis of constrained piecewise linear oscillators. *Probabilistic Engineering Mechanics*, 57, 2019.

Broccardo, M. and Kiureghian, A. D. Multicomponent nonlinear stochastic dynamics analysis by tail-equivalent linearization. *Journal of Engineering Mechanics*, 142, 2016.

Chai, W., Naess, A., Leira, B. J., and Bulian, G. Efficient monte carlo simulation and grim effective wave model for predicting the extreme response of a vessel rolling in random head seas. *Ocean Engineering*, 123:191–203, 2016.

Coles, S. *An Introduction to Statistical Modeling of Extreme Values*. Springer-Verlag London, 2001.

Deutch, C. V. and Journel, A. G. *Geostatistical Software Library and User Guide*. Oxford University Press, 2nd edition, 1998.

DNV-GL. *Rules for Classification: High speed and light craft*, 2020.

Echard, B., N.Gayton, and Lemaire, M. AK-MCS: An active learning reliability method combining kriging and monte carlo simulation. *Structural Safety*, 2011.

Edwards, S. J., Collette, M., and Troesch, A. W. Wind and wave environments that lead to extreme loads on offshore structures. OCEANS, 2019a.

Edwards, S. J., Collette, M., and Troesch, A. W. Prediction of human injury due to impact. Practical Design of Ships and Offshore Bodies, 2019b.

Edwards, S. J., Troesch, A., and Collette, M. Estimating extreme characteristics of stochastic non-linear systems. *Ocean Engineering*, 225, 2021.

Elishakoff, I. and Crandall, S. H. Sixty years of stochastic linearization technique. *Meccanica*, 52, 2017.

Fujimura, K. and Kiureghian, A. D. Tail equivalent linearization method for nonlinear random vibration. *Probabilistic Engineering Mechanics*, 22, 2007.

Gong, X., Zhang, Z., Maki, K., and Pan, Y. Full resolution of extreme ship response statistics. In *33rd Symposium on Naval Hydrodynamics*, 2020.

Göteman, M., Engström, J., Eriksson, M., Leijon, M., Hann, M., Ransley, E., and Greaves, D. Wave loads on a point-absorbing wave energy device in extreme waves. *Journal of Ocean and Wind Energy*, 2(3), 2015.

Griffin, M. *Whole-Body Vibration and Health*. Academic Press, 1996.

Grigoriu, M. *Applied Non-Gaussian Processes*. Prentice Hall, 1995.

Hann, M., Greaves, D., Raby, A., and Howey, B. Use of constrained focused waves to measure extreme loading of a taut moored floating wave energy converter. *Ocean Engineering*, 148, 2018.

Ismaili, M. A. and Bernard, P. Asymptotic analysis and linearization of the randomly perturbed two-wells duffing oscillator. *Probabilistic Engineering Mechanics*, 12(3), 1997.

ITTC. The specialist committee on waves - final report and recommendations to the 23rd ittc. In *Proceedings of the 23rd International Towing Tank Conference*, volume 2, pages 505–736, 2002.

Jensen, J. J. Stochastic procedures for extreme wave load predictions - wave bending moment in ships. *Marine Structures*, 22:194–208, 2009.

Jensen, J. J., Andersen, I. M. V., and Seng, S. Stochastic procedures for extreme wave induced responses in flexible ships. *International Journal of Naval Architecture and Ocean Engineering*, 6:1148–1159, 2014.

Johnson, M. E. *Multivariate Statistical Simulation*. John Wiley and Sons Inc., 1987.

Jonkman, J. and Sprague, M. *OpenFAST*. NREL, 2017.

Kaimal, J., Wyngaard, J., Izumi, Y., and Coté, O. Spectral characteristics of surface-layer turbulence. *Quarterly Journal of the Royal Meteorological Society*, 98, 1972.

Kim, D.-H. *Design Loads Generator: Estimation of Extreme Environmental Loadings for Ship and Offshore Applications*. PhD thesis, University of Michigan, 2012.

Kiureghian, A. D. The geometry of random vibrations and solutions by FORM and SORM. *Probabilistic Engineering Mechanics*, 15:81–90, 2000.

Leadbetter, M. On crossings of levels and curves by a wide class of stochastic processes. *Annals of Mathematical Statistics*, 37(1):260–267, 1966.

Leadbetter, M. and Rootzen, H. Extremal theory for stochastic processes. *The Annals of Probability*, 16(2), 1988.

Leadbetter, M., Lindgren, G., and Rootzén, H. *Extremes and Related Properties of Random Sequences and Processes*. Springer-Verlag, 1983.

Lin, W. and Yue, D. Numerical solutions for large-amplitude ship motions in the time domain. In *18th Symposium of Naval Hydrodynamics*, 1991.

Lindgren, G. Local maxima of gaussian fields. *Arkiv för Matematik*, 10(1-2), 1972.

Lloyd's Register. Rules for classification of trimarans. Technical report, July 2020.

Matheron, G. The intrinsic random functions and their applications. *Advanced Applications of Probability*, 1973.

Matlab. dsp.movingrms, 2016. URL `https://www.mathworks.com/help/dsp/ref/dsp.movingrms-system-object.html`.

Michelen, C. and Coe, R. Comparison of methods for estimating short-term extreme responses of wave energy converters. In *Proceedings of OCEANS2015 - MTS/IEEE Washington*. IEEE, 2015.

Miwadinou, C., Hinvi, L., Monwanou, A., and Orou, J. C. Non-linear dynamics of a ϕ_6 - modified Duffing oscillator: resonant oscillations and transition to chaos. *Nonlinear dynamics*, 88:97–113, 2016.

Mohamad, M. A. and Sapsis, T. P. Sequential sampling strategy for extreme event statistics in nonlinear dynamical systems. volume 115. Proceedings of the National Academy of Sciences of the United States of America, October 2018.

Naess, A. Prediction of extreme response of nonlinear oscillators subjected to random loading using the path integral technique. *Journal of Research of the National Institute of Standards and Technology*, 99(4), July-August 1994.

Namachchivaya, N. S. Stochastic bifurcation. *Applied Mathematics and Computation*, 39(3), 1990.

Ochi, M. Prediction of occurence and severity of ship slamming at sea. Fifth Symposium on Naval Hydrodynamics, 1964.

Ochi, M. K. *Applied Probability and Stochastic Processes*. Wiley, 1990a.

Ochi, M. K. *Applied Probability and Stochastic Processes in Engineering and Physical Sciences*. Wiley series in probability and mathematical sciences, 1990b.

Pipiras, V. Pitfalls of data-driven peaks-over-threshold analysis: Perspectives from extreme ship motions. *Probabilistic Engineering Mechanics*, 60, 2020.

Razola, M., Olausson, K., Garme, K., and Rosén, A. On high-speed craft acceleration statistics. *Ocean Engineering*, 114, 2016.

Rice, S. Mathematical analysis of random noise. *The Bell System Technical Journal*, 23(3):282–332, 1944.

Roberts, J. and Spanos, P. *Random Vibration and Statistical Linearization*. John Wiley and Sons Inc., 1990.

Santo, H., Taylor, P., Moreno, E. C., Stansby, P., Taylor, R. E., Sun, L., and Zang, J. Extreme motion and response statistics for survival of the three-float wave energy converter m4 in intermediate water depth. *Journal of Fluid Mechanics*, 813, 2017.

Seyffert, H. C. *Extreme Design Events due to Combined, Non-Gaussian Loading*. PhD thesis, University of Michigan, 2018.

Sterk, A. Extreme amplitudes of a periodically forced Duffing oscillator. *Indagationes Mathematicae*, 27(5), December 2016.

Taylor, P., Jonathan, P., and Harland, L. Time domain simulation of jack-up dynamics with the extremes of a gaussian process. *Journal of Vibration and Acoustics*, 119, 1997.

Tromans, P., Anaturk, A., and Hagemeijer, P. A new model for the kinematics of large ocean waves - applications as a design wave. In *Proceedings of the First International Offshore and Polar Engineering Conference*, 1991.

Welch, P. D. The use of fast fourier transform for the estimation of power spectra: A method based on time averaging over short, modified periodograms. *IEEE Transactions on Audio and Electroacoustics*, AU-15(2), 1967.

Zhang, Y. and Spanos, P. D. A linearization scheme for vibrations due to combined deterministic and stochastic loads. *Probabilistic Engineering Mechanics*, 60, 2020.